



**MARMARA UNIVERSITY**  
**INSTITUTE FOR GRADUATE STUDIES**  
**IN PURE AND APPLIED SCIENCES**



**ADSORPTION OF ENDOCRINE  
DISRUPTING COMPOUNDS BY MAGNETIC  
NANOPARTICLES**

---

GÜL GÜLENAY HACIOSMANOĞLU

**Ph.D. THESIS**

Department of Environmental Engineering

**Thesis Supervisor**

Prof. Dr. Zehra Semra CAN

ISTANBUL, 2019



**MARMARA UNIVERSITY  
INSTITUTE FOR GRADUATE STUDIES  
IN PURE AND APPLIED SCIENCES**



**ADSORPTION OF ENDOCRINE  
DISRUPTING COMPOUNDS BY MAGNETIC  
NANOPARTICLES**

---

**GÜL GÜLENAY HACIOSMANOĞLU  
(724311702)**

**Ph.D. THESIS**

Department of Environmental Engineering

**Thesis Supervisor**

Prof. Dr. Zehra Semra CAN

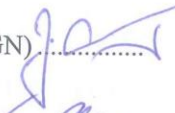
**ISTANBUL, 2019**


---

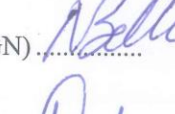
**MARMARA UNIVERSITY**  
**INSTITUTE FOR GRADUATE STUDIES IN PURE AND APPLIED**  
**SCIENCES**


Gül Gülenay HACIOSMANOĞLU, a Doctor of Philosophy student of Marmara University Institute for Graduate Studies in Pure and Applied Sciences, defended her thesis entitled “Adsorption of Endocrine Disrupting Compounds by Magnetic Nanoparticles”, on April 25, 2019 and has been found to be satisfactory by the jury members.


**Jury Members**

Prof. Dr. Zehra Semra CAN (Advisor)  
Marmara University ..... (SIGN) 

Prof. Dr. Güleda ENİN (Jury Member)  
Yıldız Technical University ..... (SIGN) 

Prof. Dr. Nihal BEKTAŞ (Jury Member)  
Gebze Technical University ..... (SIGN) 

Assoc. Prof. Dr. Neslihan SEMERCI (Jury Member)  
Marmara University ..... (SIGN) 

Assist. Prof. Seval GENÇ (Jury Member)  
Marmara University ..... (SIGN) 

**APPROVAL**

Marmara University Institute for Graduate Studies in Pure and Applied Sciences Executive Committee approves that Gül Gülenay HACIOSMANOĞLU be granted the degree of Doctor of Philosophy in Department of Environmental Engineering, Environmental Engineering Program on 08/05/2019. (Resolution no: 2019/10-02)

Director of the Institute Prof.

Dr.  Bülent EKİCİ



## **ACKNOWLEDGEMENTS**

First and foremost, I am deeply grateful to my thesis's supervisor, Prof. Dr. Zehra Semra CAN who guided me to discover her interesting research field where I gained a lot of knowledge and experience. I greatly appreciate the opportunity that she provided me to study with her. I am grateful for her guidance, support, patience, encouragement and immense knowledge. It was a pleasure to work with her.

I gratefully acknowledge to members of thesis committee, Assist. Prof. Dr. Seval GENÇ, Prof. Dr. Güleda ENGİN, Assoc. Prof. Dr. Neslihan SEMERCİ and Prof. Dr. Nihal BEKTAŞ for their valuable contributions.

I would express my special thanks to Prof. Dr. Ebru TOKSOY ÖNER and Tuğçe DOĞRUDEL for the production of levan biopolymer. I am also grateful to Assist. Prof. Dr. Seval GENÇ for her support and help in the production and characterization of the magnetic nanoparticles. I would like to thank Prof. Dr. Sinan KESKİN and Burcu Nilgün ÇETİNER from Marmara University XRD laboratory for XRD analysis. I also thank to Middle East Technical University Central Laboratory and Ege University Application and Research Center for Testing and Analysis Laboratory for conducting the XPS analyses. Thanks also go to Marmara University Biomedical Imaging Systems Laboratory for SEM and FTIR analyses.

I would like to acknowledge the financial support provided by Marmara University through BAPKO project FEN- FEN-C-DRP-110117-0022.

I would like to express my sincere thanks to all my friends for their helps and support whenever I needed.

I want to express my deepest gratitude to my family members: Mehmet Çetin HACIOSMANOĞLU, Serap HACIOSMANOĞLU and Esenay HACIOSMANOĞLU. This thesis is dedicated to my family for their support and love.

Finally, I would like to thank other people not mentioned here, but in my sincerest mind and heart.

**April 2019**

**Gül Gülenay HACIOSMANOĞLU**

# TABLE OF CONTENTS

ACKNOWLEDGEMENTS.....	i
ÖZET .....	v
ABSTRACT.....	vii
CLAIM FOR ORIGINALITY .....	viii
SYMBOLS.....	ix
ABBREVIATIONS .....	xi
LIST OF FIGURES .....	xiv
LIST OF TABLES .....	xvi
1. INTRODUCTION .....	1
1.1. Endocrine disrupting compounds .....	1
1.1.1. Environmental significance of EDCs .....	1
1.1.2. Bisphenol A (BPA).....	4
1.1.3. 17 $\alpha$ -Ethinylestradiol (EE2).....	8
1.2. Measurement methods for EDCs.....	10
1.3. Treatment methods for EDCs .....	12
1.4. Adsorption .....	17
1.4.1. Fundamentals of adsorption process.....	17
1.4.2. EDC removal by adsorption .....	20
1.5. Magnetic nanoparticles (MNPs).....	21
1.5.1. Surface modification of MNPs .....	22
1.6. Use of surface modified MNPs for the adsorption of EDCs .....	24
1.7. Objective and scope of the study .....	29
2. MATERIALS AND METHODS .....	30
2.1. Materials .....	30
2.2. Methods .....	30
2.2.1. Production of the adsorbents .....	30
2.2.2. Material characterization .....	33
2.2.3. Adsorption experiments.....	34
2.2.4. Desorption and reuse experiments.....	37
2.2.5. Analytical methods .....	37
2.2.6. Validation of kinetic and isotherm models.....	38
3. RESULTS AND DISCUSSION.....	40
3.1. Characterization of the adsorbents.....	40

3.1.1. SEM Results .....	40
3.1.2. FTIR Results.....	44
3.1.3. XRD Results .....	50
3.2. Analysis of BPA and EE2.....	51
3.3. Adsorption studies .....	53
3.3.1. Adsorption equilibrium .....	53
3.3.1.1. Adsorption equilibrium for BPA .....	53
3.3.1.2. Adsorption equilibrium for EE2 .....	62
3.3.2. Comparison of the adsorption amounts of BPA and EE2 .....	68
3.3.3. Adsorption kinetics.....	72
3.3.3.1. Adsorption kinetics for BPA .....	74
3.3.3.2. Adsorption kinetics for EE2 .....	75
3.3.4. Adsorption mechanism .....	76
3.3.5. Desorption and reuse studies .....	90
4. CONCLUSIONS .....	93
REFERENCES .....	95
APPENDIX A. Comparison of FTIR results for PhHL and pure levan.....	112
APPENDIX B. XPS spectra of P2p .....	113
ÖZGEÇMİŞ.....	114

# ÖZET

## ENDOKRİN BOZUCU MADDELERİN MANYETİK NANOPARÇACIKLAR İLE ADSORPSİYONU

Endokrin bozucu maddeler (EDC'ler) çevrede yaygın olarak bulunmaları ve insan/çevre sağlığı üzerindeki olası olumsuz etkileri nedeniyle önemli kirletici maddeler olarak değerlendirilmektedir. EDC'lerin geleneksel su ve atıksu arıtma prosesleri kullanılarak tamamen bertaraf edilemediği bilinmektedir. Bu durumun sonucu olarak EDC'ler, arıtma tesislerinin çıkış sularında, yüzey sularında, sediment ve arıtma çamurlarında bulunur.

Son yıllarda, EDC'lerin sulu çözeltilerden uzaklaştırılması için yeni yöntemlerin geliştirilmesi üzerine çalışmalar yapılmaktadır. Bu yöntemler arasında yer alan adsorpsiyon prosesi, etkin olması ve uygulamadaki basitliğinin yanı sıra başlangıç maliyetinin düşük olması gibi avantajlara sahiptir.

Bu çalışma, sucul ortamlarda en çok rastlanan EDC'ler arasında yer alan Bisfenol A (BPA) ve 17 $\alpha$ -Ethinylestradiol'ün (EE2) adsorpsiyon yoluyla giderimini araştırmaktadır. Kullanılan adsorban malzemeler saf manyetik nanoparçacıklar (MNP), saf biyopolimerler (kitosan ve fosfonatlanmış levan (PhHL)) ve MNP-biyopolimer kompozitleridir.

Bu malzemelerin karakterizasyonu SEM, FTIR ve XRD analizleriyle yapılmıştır. Daha sonra bu malzemeler kullanılarak sulu çözeltilerden BPA ve EE2 giderimi amacıyla kesikli adsorpsiyon deneyleri yapılmıştır. Denge adsorpsiyon çalışmalarına göre, hem BPA hem de EE2 adsorpsiyonu için PhHL'nin performansının diğer malzemelerden çok daha yüksek olduğu tespit edilmiştir. PhHL'nin maksimum adsorpsiyon kapasitesi BPA için 126.6 mg/g iken EE2 için 18.13 mg/g olarak tespit edilmiştir. Bu adsorban malzeme (PhHL) kullanılarak yapılan deneyler için izoterm ve kinetik modeller uygulanmıştır. Adsorpsiyon mekanizması ve yeniden kullanılabilirlik de değerlendirilmiştir. FTIR ve XPS analizleri adsorpsiyon mekanizmasının OH-pi and CH-pi etkileşimlerini içerdiğini göstermiştir.

Elde edilen sonuçlar, BPA ve EE2 gibi EDC'lerin, adsorpsiyon yoluyla sulu çözeltilerden

etkili bir şekilde giderilebileceğini ve bu konuda özellikle PhHL biyopolimerinin, incelenen diğer malzemelerden daha etkili olduğunu göstermiştir.

**Anahtar sözcükler:** Endokrin bozucu maddeler, Adsorpsiyon, Manyetik nanoparçacıklar, Pi etkileşimleri, Biyopolimer, Kompozit maddeler, Kitosan, Fosfonatlı levan





## ABSTRACT

### ADSORPTION OF ENDOCRINE DISRUPTING COMPOUNDS BY MAGNETIC NANOPARTICLES

Endocrine disrupting compounds (EDCs) are important emerging contaminants since they are found widespread and may have adverse effects on human health and the environment. Since EDCs are not completely removed by conventional treatment processes, they are found in treatment plant effluents, surface waters, sediments and sewage sludge.

Currently, novel methods are evaluated for removal of EDCs from aqueous solutions. Among these methods, adsorption has some advantages such as being effective and simple with low initial cost.

This study investigates adsorptive removal of bisphenol A (BPA) and 17 $\alpha$ -ethinyloestradiol (EE2) which are well-known EDCs. The evaluated adsorbent materials are magnetic nanoparticles (MNPs), biopolymers including chitosan and phosphonated levan (PhHL), and MNP-biopolymer composites.

Characterization of these materials was performed by SEM, FTIR and XRD analyses. Batch adsorption experiments were conducted by using these materials for the removal of BPA and EE2 from aqueous solutions. The performance of PhHL for both BPA and EE2 adsorption was better than that of other adsorbents evaluated. The maximum adsorption capacity of PhHL was determined as 126.6 and 18.13 mg/g, for BPA and EE2, respectively. Using this adsorbent, isotherm and kinetic models were assessed for the description of BPA and EE2 adsorption. The adsorption mechanism and reusability were also evaluated. FTIR and XPS analyses revealed that the adsorption mechanisms included OH- $\pi$  and CH- $\pi$  interactions.

The results demonstrate that EDCs like BPA and EE2 can be effectively removed from aqueous solution by adsorption, especially with PhHL, which has the highest adsorption capacity among the materials evaluated in this study.

**Keywords:** Endocrine disrupting compounds, Adsorption, Magnetic nanoparticles, Pi interactions, Biopolymers, Composite materials, Chitosan, Phosphonated levan

## **CLAIM FOR ORIGINALITY**

Endocrine disrupting compounds (EDCs) in water and wastewater streams are a significant problem because of their potential impacts on human health and the environment. Since complete elimination of EDCs is not possible by conventional treatment processes, recent studies are focused on innovative and effective methods for their removal from aqueous solutions.

This study investigates the effectiveness of different materials including magnetic nanoparticles (MNP), chitosan, phosphonated levan (PhHL), chitosan-MNP composite and PhHL-MNP composite for the adsorptive removal of bisphenol A (BPA) and 17 $\alpha$ -ethinyloestradiol (EE2) which are selected to represent EDCs from industrial sources and synthetic hormones, respectively.

No prior study has examined the removal of EDCs by PhHL or PhHL-MNP composite. Although there are few studies investigating BPA removal by magnetite and chitosan, these studies did not include EE2 adsorption. There is also a study using chitosan-Fe<sub>3</sub>O<sub>4</sub> nanocomposite based material as an electrochemical sensor for bisphenol A but that study did not include adsorption experiments.

Among different adsorbent materials evaluated in this study, PhHL showed the highest adsorption capacity both for BPA and EE2. Thus, its adsorption properties including adsorption kinetics, mechanism of adsorption and reuse potential was further investigated.

This is the first study in the literature evaluating the PhHL as an adsorbent material. Moreover, determination of the adsorption mechanism by means of FTIR and XPS analyses is a relatively new research area. In this study, FTIR and XPS analyses were conducted for PhHL both before and after adsorption, as well as for pure BPA and EE2, for comparative purposes. The FTIR and XPS results revealed that the adsorption mechanisms included OH- $\pi$  interaction and CH- $\pi$  interaction.

The obtained results can serve as a basis for the development of novel adsorption systems to remove EDCs from aqueous solutions.

**Gül Gülenay HACIOSMANOĞLU**

**Prof. Dr. Zehra Semra CAN**

## SYMBOLS

$\alpha$	: Initial sorption rate (mg/(g min))
$\beta$	: Elovich constant (g/mg)
$\beta$	: Line broadening at half maximum, FWHM (Radians)
$C_e$	: Equilibrium concentration (mg/L)
$C_i$	: Initial concentration (mg/L)
$C_s$	: Aqueous solubility (mg/L)
$C_t$	: Concentration at time, t (mg/L)
$\chi^2$	: Chi square
$K$	: Scherrer constant
$K_{DA}$	: Constant related to the sorption energy ((mol/J) <sup>n<sub>DA</sub></sup> )
$K_F$	: Freundlich constant ((mg/g)/(mg/L) <sup>n</sup> )
$K_L$	: Langmuir constant(L/mg)
$K_S$	: Sips constant(mg/L) <sup>(-1/n<sub>S</sub>)</sup>
$k_1$	: Rate constant of pseudo-first order equation (1/min)
$k_2$	: Rate constant of pseudo-second order equation (g/(mg×min))
$K_{OC}$	: Organic carbon/water partition coefficient
$K_{OW}$	: Octanol/water partition coefficient
$\lambda$	: X-ray wavelength (Å)
$m$	: Mass (g)
$n$	: Freundlich intensity parameter
$n_{DA}$	: Heterogeneity factor of Dubinin-Astakhov isotherm
<b>NRMSE</b>	: Normalized root mean square error
$q_{calc}$	: Calculated amount of adsorbate uptake (mg/g)
$q_{DA(max)}$	: Maximum adsorption capacity estimated from D-A model (mg/g)
$q_e$	: Amount of adsorbate uptake at equilibrium (mg/g)
$q_{exp}$	: Amount of adsorbate uptake, experimental (mg/g)
$q_{exp,max}$	: Maximum amount of adsorbate uptake, experimental (mg/g)
$q_{exp,mean}$	: Mean amount of adsorbate uptake, experimental (mg/g)
$q_{exp,min}$	: Minimum amount of adsorbate uptake, experimental (mg/g)
$Q_{max}$	: Maximum adsorption capacity calculated from Langmuir model (mg/g)
$q_e$	: Amount of adsorbate uptake at equilibrium (mg/g)

- $q_t$**  : Amount of adsorbate uptake at time,  $t$  (mg/g)  
 **$q_m^S$**  : Maximum adsorption capacity calculated from Sips model (mg/g)  
 **$R^2$**  : Correlation coefficient  
 **$t$**  : Time (min)  
 **$\theta$**  : Diffraction angle ( $^\circ$ )  
 **$\tau$**  : Size of the crystalline domains (nm)  
 **$V$**  : Volume (L)



## **ABBREVIATIONS**

<b>AC</b>	: Activated Carbon
<b>AOPs</b>	: Advanced Oxidation Processes
<b>APEs</b>	: Alkylphenol Polyethoxylates
<b>AS</b>	: Activated Sludge
<b>B</b>	: Biodegradation
<b>BAC</b>	: Biological Activated Carbon
<b>BPA</b>	: Bisphenol A
<b>CAS</b>	: Chemical Abstracts Service
<b>CBZ</b>	: Carbamazepine
<b>CEC</b>	: Contaminants of emerging concern
<b>CI</b>	: Chemical Ionization
<b>CNMs</b>	: Carbon nanomaterials
<b>CNTs</b>	: Carbon Nanotubes
<b>CTAB</b>	: Cetyltrimethyl Amonium Bromide
<b>D-A</b>	: Dubinin-Astakhov
<b>DDT</b>	: Dichloro Diphenyl Trichloroethane
<b>DES</b>	: Diethylstilbestrol
<b>DETA</b>	: Diethylenetriamine
<b>D-R</b>	: Dubinin-Radushkevich
<b>DTZ</b>	: Diatrizoate
<b>E1</b>	: Estrone
<b>E2</b>	: 17 $\beta$ -estradiol
<b>E3</b>	: Estriol
<b>ECD</b>	: Electron Cloud Density
<b>EDA</b>	: Ethylenediamine
<b>EDC</b>	: Endocrine Disrupting Compounds
<b>EE2</b>	: 17 $\alpha$ -Ethinylestradiol

<b>EI</b>	: Electron Impact
<b>EPA</b>	: Environmental Protection Agency
<b>FTIR</b>	: Fourier Transform Infrared Spectroscopy
<b>FWHM</b>	: Full Width at Half Maximum
<b>GAC</b>	: Granular Activated Carbon
<b>GC</b>	: Gas Chromatography
<b>HL</b>	: <i>Halomonas</i> Levan
<b>HPLC</b>	: High Performance Liquid Chromatography
<b>IONPAC</b>	: Iron Oxide Nanoparticles/Powdered Activated Carbon
<b>IUPAC</b>	: International Union of Pure and Applied Chemistry
<b>JCPDS</b>	: Joint Committee on Powder Diffraction Standards
<b>K<sub>OC</sub></b>	: Organic/Carbon Partition Coefficient
<b>K<sub>OW</sub></b>	: Octanol/Water Partition Coefficient
<b>LC</b>	: Liquid Chromatography
<b>m/z</b>	: Mass-to-Charge Ratio
<b>MF</b>	: Microfiltration
<b>MGO</b>	: Magnetic Graphene Oxide
<b>MN 250</b>	: Hypersol Macronet Polymer
<b>MNPs</b>	: Magnetic Nanoparticles
<b>MNPs@PDA</b>	: Polydopamine-Coated Magnetic Nanoparticles
<b>MNPs@PPy</b>	: Polypyrrole-Coated Magnetic Nanoparticles
<b>MS</b>	: Mass Spectrometry
<b>MWCNTs</b>	: Multi-Walled Carbon Nanotubes
<b>NAA</b>	: Naphthalene Acetic Acid
<b>NAP</b>	: Naproxen
<b>NF</b>	: Nanofiltration
<b>NMR</b>	: Nuclear Magnetic Resonance
<b>NOM</b>	: Natural Organic Matter
<b>NPs</b>	: Nanoparticles

<b>P</b>	: Photodegradation
<b>PA612</b>	: Aliphatic Polyamide
<b>PAC</b>	: Powdered Activated Carbons
<b>PAMAM</b>	: Polyamidoamine Dendrimer
<b>PCBs</b>	: Polychlorinated Biphenyls
<b>PFO</b>	: Pseudo-First Order
<b>PhHL</b>	: Phosphonated <i>Halomonas</i> Levan
<b>PNP</b>	: p-Nitrophenol
<b>PSO</b>	: Pseudo-Second Order
<b>PTBP</b>	: p-tert-Butylphenol
<b>PTFE</b>	: Polytetrafluoroethylene
<b>PVC</b>	: Polyvinyl Chloride
<b>QS</b>	: Quinine Sulfate
<b>rGOs</b>	: Magnetic Reduced Graphene Oxides
<b>RO</b>	: Reverse Osmosis
<b>SEM</b>	: Scanning Electron Microscopy
<b>STPs</b>	: Sewage Treatment Plants
<b>SWCNT</b>	: Single-Walled Carbon Nanotube
<b>TBBPA</b>	: Tetrabromobisphenol
<b>TC</b>	: Triclosan
<b>TEPA</b>	: Tetraethylenepentamine
<b>TETA</b>	: Triethylenetetramine
<b>UF</b>	: Ultrafiltration
<b>UV</b>	: Ultra Violet
<b>VOCs</b>	: Volatile Organic Compounds
<b>XPS</b>	: X-ray Photoelectron Spectroscopy
<b>XRD</b>	: X-ray Diffraction

## LIST OF FIGURES

<b>Figure 1. 1.</b> Simplified diagram of routes of contamination of water bodies by EDCs ..	3
<b>Figure 1. 2.</b> Chemical structure of BPA .....	5
<b>Figure 1. 3.</b> Chemical structure of EE2 .....	8
<b>Figure 1. 4.</b> Schematic representation of EI ionization .....	11
<b>Figure 1. 5.</b> Transport processes during adsorption.....	19
<b>Figure 1. 6.</b> Chemical structure of magnetite .....	22
<b>Figure 1. 7.</b> Chemical structure of chitosan.....	23
<b>Figure 1. 8.</b> Chemical structure of levan .....	23
<b>Figure 1. 9.</b> Chemical structure of PhHL.....	24
<b>Figure 2. 1.</b> Biopolymers used for the surface modification of MNPs.....	31
<b>Figure 2. 2.</b> MNP production process .....	33
<b>Figure 2. 3.</b> Magnetic separation process .....	36
<b>Figure 3. 1.</b> SEM images pure MNP (a) 15K magnification.....	40
<b>Figure 3. 2.</b> SEM images of chitosan and chitosan-MNP composite .....	41
<b>Figure 3. 3.</b> SEM images of PhHL and PhHL-MNP composite.....	42
<b>Figure 3. 4.</b> FTIR results for pure levan (a) and PhHL (b).....	45
<b>Figure 3. 5.</b> FTIR results for PhHL (a) PhHL-MNP composite (b) pure MNP (c) .....	47
<b>Figure 3. 6.</b> FTIR results for chitosan (a) chitosan-MNP composite (b) pure MNP (c) .....	49
<b>Figure 3. 7.</b> X-ray diffraction pattern of PhHL-MNP composite .....	50
<b>Figure 3. 8.</b> Mass Chromatogram and Fragment Spectrum for BPA .....	51
<b>Figure 3. 9.</b> Mass Chromatogram and Fragment Spectrum for EE2 .....	52
<b>Figure 3. 10.</b> Mass Chromatogram and Fragment Spectrum for anthracene-d10 .....	52
<b>Figure 3. 11.</b> Equilibrium data for BPA using different adsorbents.....	54
<b>Figure 3. 12.</b> Sips isotherm model for BPA adsorption by PhHL .....	58
<b>Figure 3. 13.</b> Equilibrium data for EE2 using different adsorbents.....	62
<b>Figure 3. 14.</b> Sips isotherm model for EE2 adsorption by PhHL .....	64
<b>Figure 3. 15.</b> Adsorption isotherms of PhHL for BPA and EE2 .....	68
<b>Figure 3. 16.</b> Comparison of BPA (a) and EE2 (b) molecules .....	69
<b>Figure 3. 17.</b> Kinetic data and PSO model fit for BPA adsorption by PhHL.....	74
<b>Figure 3. 18.</b> Kinetic data and PSO model fit for EE2 adsorption by PhHL.....	75
<b>Figure 3. 19.</b> FTIR Results of pure PhHL (a), PhHL after BPA adsorption (b), pure BPA (c).....	79
<b>Figure 3. 20.</b> XPS spectra of C1s for BPA (a) PhHL before adsorption (b) PhHL after BPA adsorption (c) .....	82
<b>Figure 3. 21.</b> XPS spectra of O1s for BPA (a) PhHL before adsorption (b) PhHL after BPA adsorption (c) .....	83
<b>Figure 3. 22.</b> FTIR Results of pure PhHL (a) PhHL after EE2 adsorption (b) pure EE2 (c).....	85



<b>Figure 3. 23.</b> XPS spectra of C1s for EE2 (a) PhHL before adsorption (b) PhHL after EE2 adsorption (c).....	87
<b>Figure 3. 24.</b> XPS spectra of O1s for EE2 (a) PhHL before adsorption (b) PhHL after EE2 adsorption (c).....	88
<b>Figure 3. 25.</b> Illustration of the pi interaction.....	89
<b>Figure 3. 26.</b> Results of reuse studies for BPA adsorption by PhHL .....	91
<b>Figure 3. 27.</b> Results of reuse studies for EE2 adsorption by PhHL .....	91
<b>Figure A. 1.</b> Comparison of FTIR results for PhHL and pure levan .....	111
<b>Figure B. 1.</b> XPS spectra of P2p .....	112



## LIST OF TABLES

<b>Table 1.1.</b> Some known and suspected endocrine disrupting chemicals.....	2
<b>Table 1.2.</b> Physicochemical properties of BPA.....	6
<b>Table 1.3.</b> Physicochemical properties of EE2.....	9
<b>Table 1.4.</b> Comparison of the efficiencies of different treatment methods for EDC removal.....	15
<b>Table 1.5.</b> Comparison of physisorption and chemisorption.....	17
<b>Table 2.1.</b> Detailed GC-MS parameters.....	38
<b>Table 2.2.</b> Validation parameters used for model evaluation.....	39
<b>Table 3.1.</b> IUPAC classification of porous solids.....	43
<b>Table 3.2.</b> Isotherm models evaluated for the adsorption of BPA on PhHL.....	57
<b>Table 3.3.</b> Comparison of BPA adsorption on PhHL with other biopolymer based materials.....	60
<b>Table 3.4.</b> Isotherm models evaluated for the adsorption of EE2 on PhHL.....	63
<b>Table 3.5.</b> Comparison of EE2 adsorption on PhHL with other materials.....	65
<b>Table 3.6.</b> Mobility classification based on $K_{OC}$ values.....	71
<b>Table 3.7.</b> Evaluation of kinetic models for BPA adsorption by PhHL.....	75
<b>Table 3.8.</b> Evaluation of kinetic models for EE2 adsorption by PhHL.....	76

# **1. INTRODUCTION**

## **1.1. Endocrine disrupting compounds**

Endocrine disrupting compounds (EDCs) are an important class of environmental contaminants because of their health and environmental impacts. US Environmental Protection Agency definition for EDCs is given as “exogenous agents that interfere with the synthesis, secretion, transport, binding, action, or elimination of natural hormones in the body that are responsible for the maintenance of homeostasis, reproduction, development, and/or behaviour” (Agency, 1997). EDCs can interfere with tissue and organ development and function, which may increase the susceptibility to different types of diseases (Bergman et al., 2013). Therefore EDCs are considered as a global threat which needs to be resolved.

EDCs include pesticides, herbicides, insecticides, industrial chemicals (e.g. heat stabilizers, chemical catalysts, plastic contaminants), pharmaceuticals and personal care products. There are a large number of substances proven to be EDC or suspected of being EDC. The most important groups of these compounds were summarized in a previous study (Phillips and Harrison, 1999) and are given in Table 1.1.

### **1.1.1. Environmental significance of EDCs**

EDCs are classified among the contaminants of emerging concern (CEC) which are the chemicals for which new concerns (occurrence, fate, adverse effects on human health and the environment) raised in recent years (Focazio et al., 2008). Contaminants of emerging concern have environmental significance because they pose different problems. An important problem related to these compounds is that they are not routinely monitored in most cases although they can enter the environment from a variety of sources. It is found worrying that widespread use of these compounds and their environmental diffusion leads to increase in the possible exposure of humans (Careghini et al., 2015).

Another problem related to EDCs is the lack of enough knowledge on the environmental behaviour for most of them e.g. diffusion, fate, toxicity and biological effects. EDCs are released to the environment in a continuous manner. This can lead to

their accumulation in the ecosystem because their high loading rate can exceed their transformation and removal rate (Careghini et al., 2015).

**Table 1.1.** Some known and suspected endocrine disrupting chemicals

(Source: Phillips and Harrison, 1999)

<b>EDC Group</b>	<b>Explanations</b>
Natural and synthetic hormones	Natural hormones, augmented by hormonal drugs such those used as oral contraceptives, are excreted by humans and animals and occur in sewage.
Phytoestrogens	Natural constituents of many foodstuffs including beans, sprouts, cabbage, spinach, soybean, grains and hops. The major classes are lignans and isoflavones (e.g. daidzein and genistein).
Mycotoxins	Produced by fungi which can contaminate crops. Some, such as zearalenone, are estrogenic.
Organochlorine pesticides	DDT, lindane and beta-HCH are common, persistent environmental pollutants.
Polychlorinated biphenyls (PCBs)	Widespread, persistent environmental pollutants
Alkylphenol polyethoxylates (APEs)	Non-ionic surfactants used in detergents, paints, herbicides, pesticides and plastics. Breakdown products, such as nonylphenol and octylphenol, are found in sewage and industrial effluents.
Dioxins	Products of combustion of many materials
Phthalate esters	Widely used as plasticisers for PVC. Common environmental pollutants
Bisphenol A	A component of polycarbonate plastics and epoxy resins used to line food cans

EDCs find their way to water and wastewater streams by several different pathways including domestic wastes, industrial discharges, landfill leachates and stormwater runoff. Conventional water and wastewater treatment plants are not capable of completely destroying or removing these compounds since they are not designed for this purpose (Can et al., 2014; Snyder et al., 2003; Ternes et al., 1999). As a result, these compounds can reach to fresh water sources. A schematic diagram describing the routes of contamination of water bodies by EDCs is adapted from previous studies (Paula Alves da Silva et al., 2018; Velicu and Suri, 2009; Wise et al., 2010) and given in Figure 1.1.

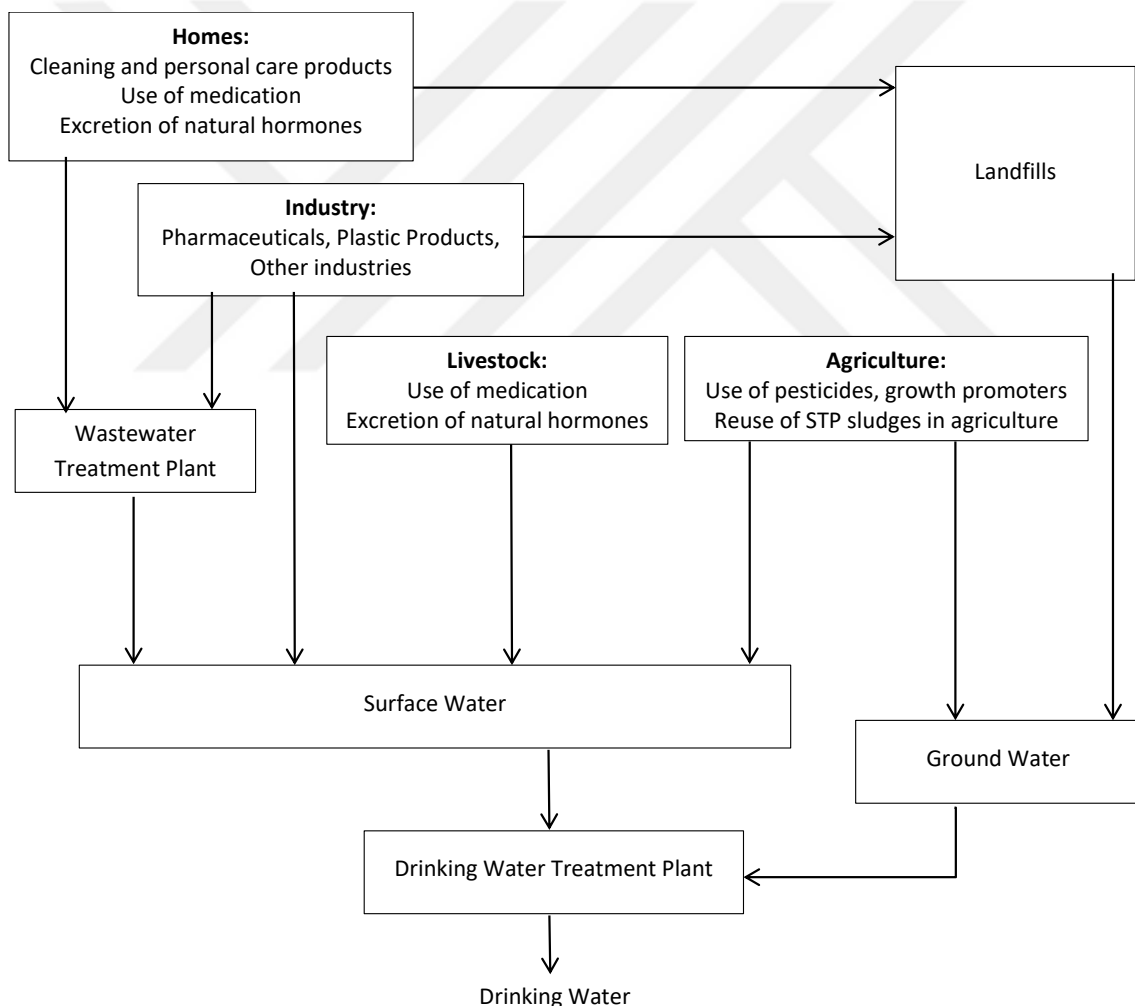


**Figure 1. 1.** Simplified diagram of routes of contamination of water bodies by EDCs (Adapted from Paula Alves da Silva et al., 2018; Velicu and Suri, 2009; Wise et al., 2010)

The accumulation of EDCs in water streams, soil and sediments can cause negative impacts on human health and environment. Many health effects are linked to EDCs e.g. teratogenicity, infertility, carcinogenicity and mutagenicity (Choi et al., 2004). Moreover, EDCs have been discovered in various surface and ground waters, and some of them are linked to adverse ecological impacts, even at trace concentrations (Pickering and Sumpter, 2003; Snyder et al., 2003).

Damstra et al. (2002) stated that there is sufficient evidence to conclude that adverse endocrine-mediated effects have occurred in some wildlife species (Damstra et al., 2002). Although the endocrine disruption effects of chemicals on wildlife is more clearly demonstrated, revealing the potential human health impacts are inherently more complex and difficult to deal with (Ying et al., 2004). Moreover the bioaccumulation factor and synergistic effects of different EDCs in the organisms make the risk assessment more complex.

Street et al. (2018) reviewed the studies on the effects of EDCs related to animal and human biology. They stated that many of the reviewed studies related to the health effects of EDCs had significant limitations, including lack of replication, limited sample sizes, retrospective design, publication biases, inadequate matching of cases and controls, and the use of non-standardized tools to diagnose conditions (Street et al., 2018). Despite of these limitations, the health risks of EDCs are of great concern (Gore et al., 2015; Lee and Pak, 2018).

In this study, two EDCs from different classes, bisphenol A (BPA) which is a plastic monomer used in industrial applications and  $17\alpha$ -ethinylestradiol (EE2) which is a pharmaceutical estrogen are selected as target pollutants. These EDCs are selected since they are widely used and they are found in aqueous streams from different sources. The properties of these compounds are explained in detail, in the following sections.

### **1.1.2. Bisphenol A (BPA)**

BPA or 4,4'-(propane-2,2-diyl)diphenol is a monomer of polycarbonate plastics and it is one of the highest volume chemicals produced worldwide (Rubin, 2011). It is found in several different consumer products, and its exposure to human and wildlife is widespread (Miyagawa et al., 2016). Global BPA production rate is estimated to exceed

6.4 billion lb/year (29 million tons/year) (vom Saal and Hughes, 2005). Application areas of BPA include polycarbonate plastics in automotive, electrical construction, packaging and medical materials. It is also used to coat the inner surfaces of metallic cans by food and beverage to inhibit the polymerization in polyvinyl chloride, and in thermal paper.

#### 1.1.2.1. Properties of BPA

BPA consists of two phenolic rings connected by a single carbon carrying two methyl groups. Its chemical structure is given in Figure 1.2.

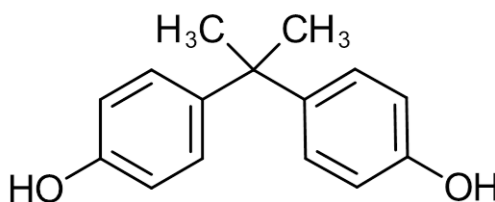


**Figure 1. 2.** Chemical structure of BPA

BPA is classified among EDCs since it exhibits estrogenic activity (Kitamura et al., 2005; Perez et al., 1998; Steinmetz et al., 1997). The reported EC50 (half maximal effective concentration) and LC50 (lethal Concentration 50%) values for BPA range between 1.0-10 mg/L and it is considered as moderately to slightly toxic to the fish and invertebrates tested (Alexander et al., 1988).

The physicochemical properties of BPA are given in Table 1.2. These physicochemical parameters are important for the determination of environmental fate and transport of EDCs, as well as their adsorption properties, which will be discussed together with the experimental results in the Results and Discussion part of this study.

**Table 1.2.** Physicochemical properties of BPA

<b>IUPAC name</b>	4,4'-(propane-2,2-diyl)diphenol
<b>Synonyms</b>	Bisphenol A 2,2-Bis(4-hydroxyphenyl)propane
<b>Molecular formula</b>	C <sub>15</sub> H <sub>16</sub> O <sub>2</sub>
<b>CAS No</b>	80-05-7
<b>Molecular weight (g/mol)</b>	228.29
<b>Boiling point (°C)</b>	220 <sup>a</sup> 360.5 <sup>b</sup>
<b>Melting point (°C)</b>	156 <sup>a</sup>
<b>Water solubility at 25 °C (mg/L)</b>	200 <sup>a</sup> 300 <sup>c</sup> 120 <sup>d</sup>
<b>Log K<sub>ow</sub></b>	3.32 <sup>e</sup>
<b>K<sub>oc</sub> (ml/g)</b>	314-1524 (calculated) <sup>f</sup> 778 for aquifer material <sup>g</sup>
<b>Vapor pressure (mm Hg)</b>	4 x 10 <sup>-8</sup> <sup>f</sup>
<b>pK<sub>a</sub></b>	9.59 (pK <sub>a1</sub> ) <sup>f</sup> 10.2 (pK <sub>a2</sub> ) <sup>f</sup>

<sup>a</sup> (Michałowicz, 2014)<sup>b</sup> (Buysch, 1999)<sup>c</sup> (Shareef et al., 2006)<sup>d</sup> (Dorn et al., 1987)<sup>e</sup> (Hansch et al., 1995)<sup>f</sup> (Staples et al., 1998)<sup>g</sup> (Ying et al., 2003)



### **1.1.2.2. Occurrence of BPA in the environment**

BPA contamination in the aquatic environment is primarily linked to effluent from wastewater treatment plants and landfill leachates (Kang et al., 2007). It doesn't have high concentration in surface water. The concentration of BPA in surface water was reported between 4.7 ng/L-12 µg/L (Ghijsen and Hoogenboezem, 2000; Kolpin et al., 2002; Kuch and Ballschmiter, 2001).

Depending on spatial and temporal effects, a wide range of BPA concentration is observed for the wastewater treatment plant influents (3-1550 ng/L) and effluents (0.26-125 ng/L) (Ballesteros-Gomez et al., 2007; Can et al., 2014; Clara et al., 2005; Mauricio et al., 2006). In addition to wastewater treatment plant influents and effluents, BPA is reported to be present in sediments, sewage sludge and surface water (Belfroid et al., 2002; Corrales et al., 2015; Fromme et al., 2002; Sharma et al., 2009; Staples et al., 1998). Moreover, very high BPA concentrations are reported in leachates from industrial waste and municipal waste disposal sites e.g. 26-8400 µg/L (Urase and Miyashita, 2003) and in wastewater effluents from waste paper recycling plants e.g. 196-10300 µg/L (Fukazawa et al., 2002).

### **1.1.2.3. Ecological and health effects of BPA**

There is a debate in the literature related to the health risks of BPA. Based on a review of 19 studies, Harvard Center for Risk Analysis, stated that evidence for low-dose effects of BPA is weak (Gray et al., 2004). On the other hand, a comprehensive review of the literature suggested that the opposite is true (vom Saal and Hughes, 2005). On the basis of publications with vertebrate and invertebrate animals, vom Saal and Hughes, (2005) stated that significant effects occurred below the predicted "safe" or reference dose of 50 µg/kg/day BPA. Moreover, it is noted that, an estrogenic mode of action of BPA is confirmed by *in vitro* experiments, which describe disruption of cell function at  $10^{-12}$  M or 0.23 ppt.

BPA is reported to have the capacity to bind DNA after metabolic activation and has estrogenic activity at low concentrations (Marwick, 1999). It is stated that the presence of BPA in water affects the growth, reproduction and development of aquatic organisms (Kang et al., 2007).

### 1.1.3. 17 $\alpha$ -Ethinylestradiol (EE2)

An important sub-group of EDCs is natural and synthetic hormones since they are found to accumulate in aquatic species and adversely affect their endocrine functions (Chen et al., 2010; Kuster et al., 2004; Purdom et al., 1994; Ying et al., 2002). This class of EDCs include mainly, natural steroid hormones e.g. estrone (E1), 17 $\beta$ -estradiol (E2), estriol (E3) and 17 $\alpha$ -estradiol (17 $\alpha$ ); synthetic nonsteroidal estrogens e.g. diethylstilbestrol (DES) and synthetic steroidal estrogens e.g. 17 $\alpha$ -ethinylestradiol (EE2) and mestranol.

In this study, synthetic estrogen, EE2 is selected as a target pollutant since it is a widely used contraceptive agent. Due to its ability to act as an endocrine disruptor at low levels in waters, it has become a major problem for the environment (Larcher et al., 2012).

#### 1.1.3.1. Properties of EE2

EE2 is an alkylated estradiol with a 17-alpha-ethinyl substitution. It contains 18 carbon atoms forming three hexagonal rings and one pentagonal ring. The addition of an ethinyl group at C-17 results in a hormone that is more resistant to biodegradation than natural ones. The chemical structure of EE2 is presented in Figure 1.3.

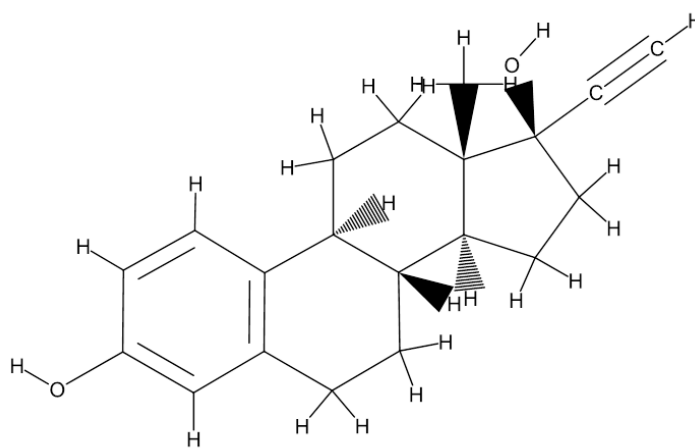


**Figure 1. 3.** Chemical structure of EE2

Some important physicochemical properties of EE2 are given in Table 1.3.

**Table 1.3.** Physicochemical properties of EE2

<b>IUPAC name</b>	(8R,9S,14S,17S)-17-ethynyl-13-methyl-7,8,9,11,12,14,15,16-octahydro-6H-cyclopenta[a] phenanthrene-3,17-diol
<b>Synonyms</b>	17-alpha-ethinylestradiol
<b>Molecular formula</b>	C <sub>20</sub> H <sub>24</sub> O <sub>2</sub>
<b>CAS No</b>	57-63-6
<b>Molecular weight (g/mol)</b>	296.41 g/mol
<b>Melting Point (°C)</b>	184.9 <sup>a</sup>
<b>Water solubility at 25 °C (mg/L)</b>	9.20 <sup>b</sup>
<b>Log K<sub>ow</sub></b>	3.67 <sup>c</sup> 4.15 <sup>d</sup>
<b>K<sub>oc</sub> (ml/g)</b>	<b>Log K<sub>oc</sub>: 3.45 - 3.85<sup>e</sup> for soil and sediment</b> <b>K<sub>oc</sub>: 4840<sup>f</sup> for aquifer material</b>
<b>Vapor pressure (Pa)</b>	6 x 10 <sup>-9</sup> <sup>e</sup>
<b>pK<sub>a</sub></b>	10.7 <sup>g</sup> 10.4 <sup>h</sup>

<sup>a</sup> (Schulz et al., 2011)<sup>b</sup> (Shareef et al., 2006)<sup>c</sup> (Kuster et al., 2004)<sup>d</sup> (Lai et al., 2000)<sup>e</sup> (Yu et al., 2004)<sup>f</sup> (Ying et al., 2003)<sup>g</sup> (Clara et al., 2004)<sup>h</sup> (Hurwitz and Liu T, 1977)

### **1.1.3.2. Occurrence of EE2 in the environment**

The source of EE2 in the aqueous streams is mainly due to the discharge from sewage treatment plants (STPs). The measured ranges of EE2 concentration is between 0.4 - 70 ng/L for the treatment plant influents, while it is between 0.15 - 178 ng/L for the effluents (Baronti et al., 2000; Can et al., 2014; Fernandez et al., 2007; Pickering and Sumpter, 2003; Thorpe et al., 2005) . EE2 is also found in activated sludge, digested sludge and sediments in different concentration ranges including 0.9 - 17 ng/g (Ternes et al., 2002).

### **1.1.3.3. Ecological and health effects of EE2**

Hormones, natural or synthetic origin, are reported to cause adverse health effects in aquatic organisms even at very low concentrations of 0.1-0.5 ng/L (Länge et al., 2001). Exposure to steroid hormones is known to influence developmental and reproductive patterns in fish populations (Piferrer and Donaldson, 1992).

Aris et al., (2014) reviewed the effects of EE2 on the exposed biota in the environment. They indicated that EE2 has become an environmental problem because of its high resistance to degradation, as well as its tendency to be absorbed by organic matter, to accumulate in sediment and to concentrate in biota (Aris et al., 2014). EE2 is shown to alter sex determination, delay sexual maturity, and decrease the secondary sexual characteristics of exposed organisms even at a low concentration (ng/L) by mimicking its natural analogue, 17 $\beta$ -estradiol (E2). EE2 is reported to be far more persistent compared to E1 and E2, and has estrogenic effect *in vitro* about 2-3 fold higher compared to E2 (De Mes et al., 2005).

## **1.2. Measurement methods for EDCs**

Measurement of EDCs in aqueous solutions is a challenging process because of their low concentrations and matrix effects depending on the source of solution. Due to recent advances in the analytical techniques, different methods are developed for sample concentration, purification and measurement of EDCs in aqueous solutions. These methods include sample preparation techniques such as solid phase extraction and liquid-liquid extraction; and analytical techniques such as high performance liquid

chromatography (HPLC), gas chromatography-mass spectrometry (GC-MS), gas chromatography tandem-mass spectrometry (GC-MS/MS), liquid chromatography-mass spectrometry (LC-MS), liquid chromatography tandem-mass spectrometry (LC-MS/MS) and liquid chromatography /time-of-flight/mass spectrometry (LC/TOF/MS). In this study, gas chromatography-mass spectrometry is used for EDC measurements and this technique is briefly described in the following part.

### Gas chromatography-mass spectrometry

Gas chromatography-mass spectrometry (GC-MS) is one of the most accurate tools for analysing environmental contaminants. It can be used to separate pharmaceuticals, volatile organic compounds (VOCs) and pesticides. During the GC-MS analysis, the gas chromatography (GC) component separates chemical mixtures and the mass spectrometry (MS) component identifies the components at a molecular level.

The basic principle of GC is that a mixture is separated into individual substances when it is heated. The samples to be analysed are first volatilized at high temperature and then pass through a column. The components in the mixture have different tendencies to adsorb onto the column thus they are separated as they pass through the column. The separated substances leaving the column flow into the MS detector.

In the MS part, the samples are ionized by different methods, e.g. electron impact (EI) and/or chemical ionization (CI). A schematic representation of the ion generation process by EI ionization is given in Figure 1.4.

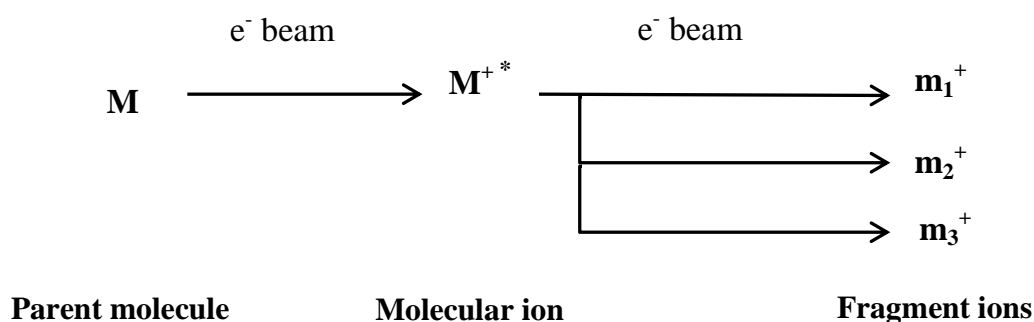


**Figure 1. 4.** Schematic representation of EI ionization

The generated ions are passed through a magnetic field and separated according to their mass-to-charge ratio ( $m/z$ ). These ions are detected in proportion to their abundance. Mass spectrometry can be used for qualitative and quantitative analysis of components in a mixture, as well as structural characterization, molecular weight determination and gas phase reactivity studies. It is considered as the only definitive analytical detector (Verma et al., 2015).

### **1.3. Treatment methods for EDCs**

The conventional water and wastewater treatment processes are not sufficient to completely eliminate EDCs (Can et al., 2014; Clara et al., 2005; Deblonde et al., 2011; Gómez et al., 2007; Larcher et al., 2012; Lee and Peart, 2000; Stackelberg et al., 2007). Moreover, some relatively high reduction in the concentration of these substances in the final effluents of wastewater treatment plants may be attributed to their accumulation in sludge phase (Gómez et al., 2007; Lee and Peart, 2000). As a result, novel treatment methods are currently being evaluated for the removal of EDCs from aqueous streams.

The applicable treatment options to remove EDCs from water include advanced separation processes (e.g. adsorption and membrane filtration), biological and chemical conversion processes (Chang et al., 2009). These treatment processes have some advantages and disadvantages, which are briefly discussed below.

Biological conversion processes are usually considered as environmentally friendly but they have shown limited EDCs removal (Chang et al., 2009; Janex-Habibi et al., 2009; Joss et al., 2005). Membrane bioreactor is a relatively new biological treatment process and it has higher removal efficiencies for micropollutants when compared to conventional aerobic biological treatment methods. On the other hand, membrane bioreactors are not effective in removing some micropollutants such as organic molecules with long, highly branched side chains, saturated/polycyclic compounds, and those having electron receptive functional groups or sulphate and halogen (Lee et al., 2009). Another problem related to the biological processes is the high amounts of biological sludge produced by these processes. Moreover the microbial community is sensitive and they are subject to the toxicity of some recalcitrant substances (De Cazes et al., 2014).

Another treatment alternative for EDCs is the application of advanced oxidation processes (AOPs) such as photo-oxidation with UV light, ozonation and ozone related processes (O<sub>3</sub>/H<sub>2</sub>O<sub>2</sub>, UV/O<sub>3</sub>), Fenton oxidation, sonolysis and photocatalysis are effective in reducing the concentrations of different classes of EDCs. For example, UV/H<sub>2</sub>O<sub>2</sub> treatment is shown to be effective in removal of atrazine, N-nitrosodimethylamine, tert-butyl ether, dioxane, bisphenol A, microcystine, diclofenac and ibuprofen up to 80 % (Kruithof et al., 2007). On the other hand advanced oxidation processes necessitate high power consumption and they have high operation cost. Moreover they may cause to the production of toxic intermediate by-products (Jardim et al., 1997; Rivera-Utrilla et al., 2018).

Membrane filtration processes include microfiltration (MF), ultrafiltration (UF), nanofiltration (NF) and reverse osmosis (RO). The removal mechanism by membrane processes includes filtration and adsorption on the membrane. Among different methods, RO has the smallest membrane pore sizes and it is the most effective membrane process to remove micropollutants such as diclofenac, carbamazepine, fenoprop, metronidazole and trimethoprim (Hai et al., 2011). However membrane processes are less sensitive to neutral compounds e.g. Bisphenol A, nonylphenol, N-nitrosodimethylamine, 17 $\beta$ -estradiol, and caffeine (Lee et al., 2009). As a result, membrane applications combined with different processes recommended to get a better performance (Bui et al., 2016). Moreover membrane processes have some drawbacks including high cost of equipment, cleaning and regeneration processes, and possible operational problems. These operational problems include short membrane life-time and membrane fouling. Membrane fouling is a major problem caused by dissolved matter, particulate matter, salt precipitates and microorganisms. As a result pretreatment of the feed stream is required to reduce the potential for membrane fouling (Cartinella et al., 2006).

Compared to other treatment methods, adsorption process has some advantages such as high-efficiency and simple operation design. Moreover, it has low initial cost for implementation and it doesn't lead to the formation of toxic intermediate products. Since this study is based on the adsorption process, it is described in more detail in Section 1.4.

A comparative view of the efficiencies of different treatment methods for EDC removal is adapted from previous studies and given in Table 1.4 (Jung et al., 2015; Snyder et al., 2003).





**Table 1.4.** Comparison of the efficiencies of different treatment methods for EDC removal

(Adapted from Jung et al., 2015; Snyder et al., 2003)

EDCs	AC	BAC	CNT	O <sub>3</sub> / AOPs	UV	Cl <sub>2</sub> / ClO <sub>2</sub>	Coagulation/ flocculation	Softening/ metal oxides	NF	RO	Degradation {B/P/AS}
Pesticides	E	E	G-E	L-E	E	P-E	P	G	G	E	E {P}
Industrial chemicals	E	E	F-E	F-G	E	P	P-L	P-L	E	E	G-E {B}
Steroids	E	E	G-E	E	E	E	P	P-L	G	E	L-E {B}
Metals	G	G	F-G	P	P	P	F-G	F-G	G	E	P {B} E {AS}
Inorganics	P-L	F	P-L	P	P	P	P	G	G	E	P-L

AC: activated carbon; BAC: biological activated carbon; AOPs: advanced oxidation processes; UV: ultraviolet; NF: nanofiltration; RO: reverse osmosis; B: biodegradation; P: photodegradation (solar); AS: activated sludge  
E: excellent (>90%), G: good (70–90%), F: fair (40–70%), L: low (20–40%), P: poor (<20%)

When Table 1.4 is examined, it is observed that activated carbon and biological activated carbon showed excellent performance for most EDCs (e.g. pesticides, industrial chemicals and steroids) but their performance were lower for metals and inorganics. On the other hand carbon nanotubes and ozone/advanced oxidation processes showed different performance ranges from poor to excellent for most of the EDCs. Similarly,  $Cl_2/ClO_2$  applications had poor performance for most EDC groups with some exceptions. UV application is found excellent for pesticides, industrial chemicals and steroids but poor for metals and inorganics. Coagulation/ flocculation and softening applications had poor to low efficiencies for most cases. Reverse osmosis had an excellent performance for each kind of EDCs. But nanofiltration is found to be less effective when compared to reverse osmosis. Photodegradation was found effective for pesticides. The effectiveness of biodegradation for industrial chemicals and steroids was ranged between low to excellent. For metals, activated sludge process was found to be highly effective.

In a more recent study, multicriteria assessment of advanced treatment technologies for micropollutants removal by full-scale and pilot-scale studies was carried out (Bui et al., 2016). In this study adsorption, oxidation and advanced oxidation processes, membrane processes and membrane bioreactors were evaluated using different criteria i.e. the range of treated pollutants, treatment efficiency, environmental considerations, technological considerations, economic assessment and social aspects.

Based on their review, Bui et al., (2016) stated that one single treatment technology was incapable to control all types of micropollutants because of the diversity in nature of these substances. They indicated that each treatment method had its drawbacks to be resolved. As a result, Bui et al. (2016) suggested that the combination of different advanced methods is an interesting research topic.

According to specific case studies, Bui et al. (2016) concluded that ozonation and activated carbon adsorption were technically feasible and cost-effective; and they had acceptable removal performance. However Bui et al. (2016) indicated that the other methods were also promising and worth to be studied thoroughly.

## 1.4. Adsorption

### 1.4.1. Fundamentals of adsorption process

Adsorption is a phase transfer process defined as the accumulation of one substance on the surface of the other substance. The substance that gets adsorbed on the surface is known as adsorbate and the surface on which adsorption occurs is known as adsorbent.

Depending on the kind of forces involved in the adsorption process, it is classified as physical adsorption (physisorption) or chemical adsorption (chemisorption). The main differences in these two phenomenon can be stated as follows (Ruthven, 1984): physisorption is nonspecific but chemisorption is highly specific. While physisorption is rapid and reversible, chemisorption may be slow and irreversible. For physisorption adsorption may take place as monolayer or multilayer but for chemisorption it is monolayer. Physisorption usually involves low heat of adsorption while chemisorption involves high heat of adsorption.

Based on the explanations given in previous studies (Patel and Vashi, 2015; Rouquerol et al., 2013; Ruthven, 1984) a table is prepared for the comparison of physical and chemical adsorption (Table 1.5).

**Table 1.5.** Comparison of physisorption and chemisorption

<b>Physisorption</b>	<b>Chemisorption</b>
Physisorption is a general phenomenon with a relatively low degree of specificity.	Chemisorption is specific to the nature of adsorbent and adsorbate, and it is dependent on their reactivity.
Involves relatively weak intermolecular forces.	Involves essentially the formation of a chemical bond between the sorbent molecule and the surface of the adsorbent.
At high relative pressures, physisorption generally occurs as a multilayer.	Chemisorbed molecules are linked to reactive parts of the surface and the adsorption is necessarily confined to a monolayer.

(Table 1.5. Continued)

<b>Physisorption</b>	<b>Chemisorption</b>
A physisorbed molecule keeps its identity and on desorption returns to the fluid phase in its original form.	If a chemisorbed molecule undergoes reaction or dissociation, it loses its identity and cannot be recovered by desorption.
Physisorption is always exothermic; the energy involved is generally not much larger than the energy of condensation of the adsorbate. However, it is enhanced when physisorption takes place in very narrow pores.	The energy of chemisorption is the same order of magnitude as energy change in a comparable chemical reaction.
Physisorption requires no activation energy. The system generally attains equilibrium very rapidly, but equilibration may be slow if the transport process is rate-determining.	Activation energy is often involved in chemisorption, and at low temperature, the system may not have sufficient thermal energy to attain thermodynamic equilibrium.
No electron transfer occurs for physisorption although polarization of the sorbate might occur.	Electron transfer leading to bond formation between sorbate and surface occurs during chemisorption.

The adsorption process usually involves four main steps, i.e. bulk transport, film transport, intraparticle transport and adsorption of the solutes on the active sites. These steps are evaluated in previous studies (Aharoni and Sparks, 1991; Weber and Morris, 1963; Weber and Smith, 1987; Zogorski et al., 1976) and they are explained below:

**Bulk transport:** Transport of solute in the bulk solution phase. This step is usually fast due to mixing and convective flow.

**Film transport:** Diffusion of the solute through a liquid film (or hydrodynamic boundary layer) at the particle-liquid interface. Although the diffusion is intrinsically slow process, the film thickness can be reduced by increasing the intensity of agitation. As a result, this step might be rapid or slow depending on the mixing intensity.

**Intraparticle transport:** Internal diffusion of solute into the pores of the sorbent. In general, this step is considered as the rate limiting step for the adsorption on porous solid adsorbent from aqueous solution.

**Adsorption of the solutes on the active sites:** When the adsorbates reach an available site, the adsorption bond is formed between the adsorbate and adsorbent. This is considered as an equilibrium reaction and it is usually every rapid process.

A schematic diagram describing the adsorption steps is given in Figure 1.5.

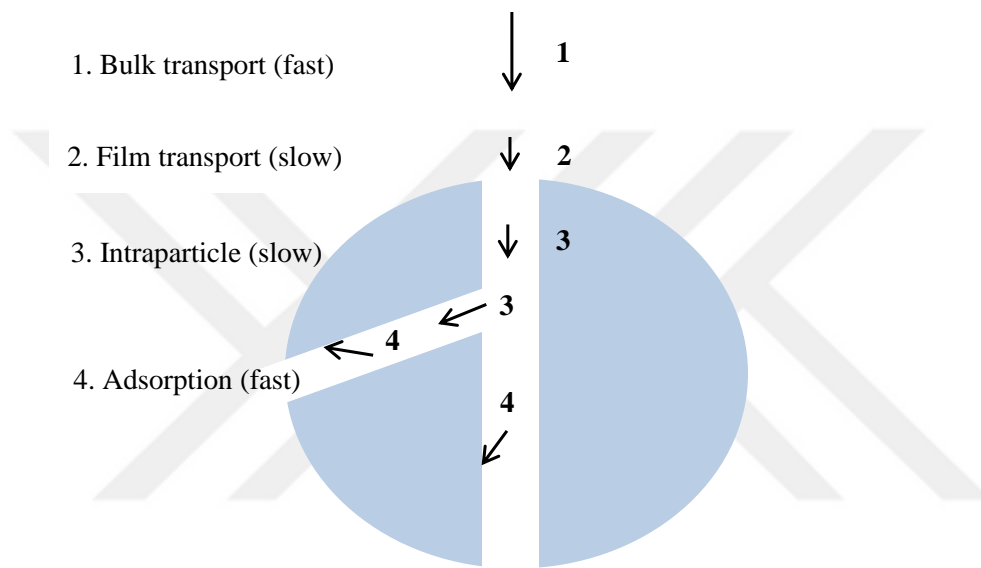


**Figure 1. 5.** Transport processes during adsorption  
(Redrawn after Weber and Smith, 1987)

The mechanism of adsorption is influenced by several different factors. These include the adsorbent properties i.e. surface area, surface functional groups, pore size and distribution; and the adsorbate properties i.e. functional groups, branching, polarity, hydrophobicity, dipole moment, molecular weight and size, and aqueous solubility. For example, LaGrega et al. (2010) explained that less polar organic molecules are more easily adsorbed by carbon, compared to polar organics. Similarly, less soluble compounds are adsorbed to a greater extent than more soluble compounds. Generally, molecules with larger molecular weight are more easily adsorbed than smaller molecules but for the adsorption processes involving pore diffusion, the opposite is true. The branched-chain organics are more easily adsorbed by carbon, compared to straight-

chain organics. It is also noted that unsaturated (double or triple-carbon bond) organic molecules are more easily adsorbed than saturated (single-carbon bond) organic molecules (LaGrega et al., 2010).

The mechanism of adsorption for a physisorption process is usually hydrogen bond interactions and van der Waals type attraction i.e. dipolar and dispersion forces between molecules of adsorbent and adsorbate. These are weak forces of attraction and the process can be easily reversed. For the chemisorption process, the mechanism involves ion exchange, electrostatic attraction and chelating formation (Liu et al., 2018). Since the forces of attraction between the adsorbate and the adsorbent are very strong for chemisorption, it can't be easily reversed.

#### **1.4.2. EDC removal by adsorption**

Several different adsorbents are evaluated for the removal of EDCs from aqueous solutions such as natural inorganic materials, bio-based sorbents, carbon and graphene based adsorbents, molecularly imprinted polymers, nanomaterials, composite materials and waste based adsorbents.

Delgado et al. (2012) reviewed the scientific research on the removal of trace level contaminants and EDCs by activated carbon (AC) in drinking water treatment. The evaluated EDCs included atrazine, bisphenol A, nonylphenol and 17- $\beta$ -estradiol and they concluded that AC adsorption has proven to be an effective removal process for EDCs (Delgado et al., 2012).

In another study, Jung et al. (2015) reviewed use of carbon nanotubes (CNTs) for the removal of EDCs, pharmaceuticals and personal care products in water. It was concluded that CNTs have high potential adsorption capacities for the removal of a diverse range of EDCs including bisphenols, hormones, pesticides and herbicides (Jung et al., 2015).

Although some adsorbents are proven to be effective in EDC removal, depending on the situation, these adsorbents may not always be the most preferable alternatives because of economic or availability considerations. As a result, novel adsorbents for the removal of EDCs are currently being evaluated by different studies. Such studies also serve to gain insights on the interaction between materials which would help to design more

efficient adsorbents. Among these novel adsorbents, magnetic nanoparticles have a great potential due to their specific properties, which are described in the following part.

### **1.5. Magnetic nanoparticles (MNPs)**

In recent years, nanotechnology has gained attention in various scientific areas such as biomedicine, materials science, energy and environmental applications. Nanoparticles are defined as the particulate dispersions or solid particles with a size between 10-100 nm (Zhang et al., 2001). On the other hand, definitions including particle sizes of up to 1  $\mu\text{m}$  are also reported (Zhang et al., 2001). These materials represent an important research field because of their distinctive characteristics which are mainly small size and high surface area to volume ratios.

Magnetic nanoparticles are nanomaterials that can be manipulated using magnetic fields. MNPs can be produced by different materials with a general formula of  $\text{MFe}_2\text{O}_4$  (where M is Fe, Co, Cu, Mn etc.). Examples of MNPs include magnetite ( $\text{Fe}_3\text{O}_4$ ), maghemite ( $\gamma\text{-Fe}_2\text{O}_3$ ) and cobalt oxide ( $\text{Co}_3\text{O}_4$ ). Important properties of MNPs which are biocompatibility, ease of synthesis, paramagnetic property, large surface area, coating and functionalization provide various opportunities for the application for MNPs in different research areas. Some examples are data storage, catalysis, biosensing, microfluidics, nanofluids, optical filters, magnetic particle imaging, environmental remediation and medical applications including magnetic resonance imaging, hyperthermia therapy and drug delivery (Boyer et al., 2010; Corchero and Villaverde, 2009; Elliott and Zhang, 2001; Hyeon, 2003; Pankhurst et al., 2009; Philip et al., 2008; Vangijzegem et al., 2019).

In this study, magnetite ( $\text{Fe}_3\text{O}_4$ ) nanoparticles are synthesized and evaluated as an adsorbent because the production of this material is simple and cost-effective. Magnetite is a ferrimagnetic material which allows its separation from water by applying an external magnetic field, easily. Moreover, its toxicity is low (Asad, 2018; Wu et al., 2015) compared to most other MNPs. The chemical structure of magnetite is given in Figure 1.6.

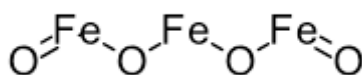


**Figure 1. 6.** Chemical structure of magnetite

### **1.5.1. Surface modification of MNPs**

It is common to apply surface modification to MNPs by using a variety of materials. One of the reasons of this application is to add different functional groups on the surface of the MNPs. Moreover, bare metallic nanoparticles are chemically active due to their nanoscale dimensions, and they are easily oxidized when exposed to air. Surface modification of MNPs helps to obtain chemically stabilized solutions. This application also helps to avoid the agglomeration of MNPs.

Different materials used for the surface modification of MNPs include surfactants, polymers, silica or carbon based materials. MNPs with surface modified by organic materials have different surface functional groups. MNPs modified with an organic layer show increased the adsorption capacity, selectivity, reactivity and reusability (Kraus et al., 2009; Mousavi et al., 2019).

In this study, pure  $\text{Fe}_3\text{O}_4$  MNP, MNP-biopolymer composites and pure biopolymers will be evaluated as adsorbents for EDCs. For this purpose, two biopolymers, chitosan and phosphonated levan will be used. These biopolymers are briefly described below.

#### **1.5.1.1. Chitosan**

Chitosan is the major derivative of chitin. Chitin is obtained from the exoskeletons of shrimp and crab; and chitosan is produced by alkaline deacetylation of chitin. Chitosan is a non-toxic, biodegradable polysaccharide with the main characteristics including hydrophilicity, biocompatibility and capability to adsorb different materials.

Chitosan consists of  $\beta$  (1–4)-linked 2-amino-2-deoxy-D-glucose (D-glucosamine) and 2-acetamido-2-deoxy-D-glucose (N-acetyl-D-glucosamine) units. The chemical structure of chitosan is given in Figure 1.7. As seen in this figure, the polymer structure of chitosan contains reactive functional groups including amino ( $-\text{NH}_2$ ) and hydroxyl



groups (-OH). Depending on the extent of chitin deacetylation, different grades of chitosan are available with a nitrogen content varying between 5% and 8%.

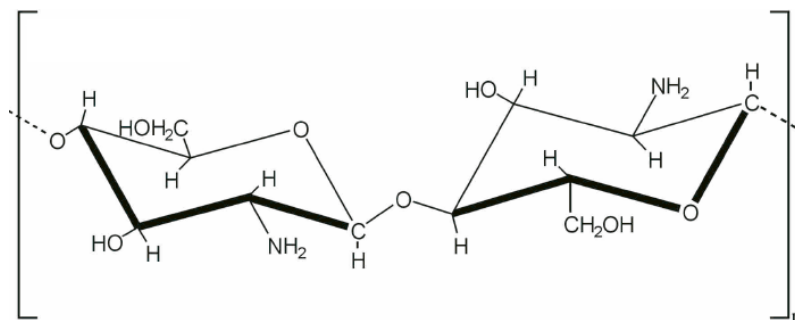


**Figure 1. 7.** Chemical structure of chitosan

The functional groups of chitosan enable this polymer to interact with different materials. As a result, chitosan and composite materials containing chitosan are widely used in different applications such as pharmaceuticals, food science, catalysis and materials science (Guibal, 2005; Rao et al., 2010; Sinha et al., 2004; Velmurugan et al., 2009).

#### 1.5.1.2. Phosphonated levan:

The other biopolymer used in this study is phosphonated levan, which is derived from levan biopolymer. Levan is a homopolymer of D-fructose units linked by β-(2-6) glycosidic bonds. The chemical structure of levan biopolymer is shown in Figure 1.8.

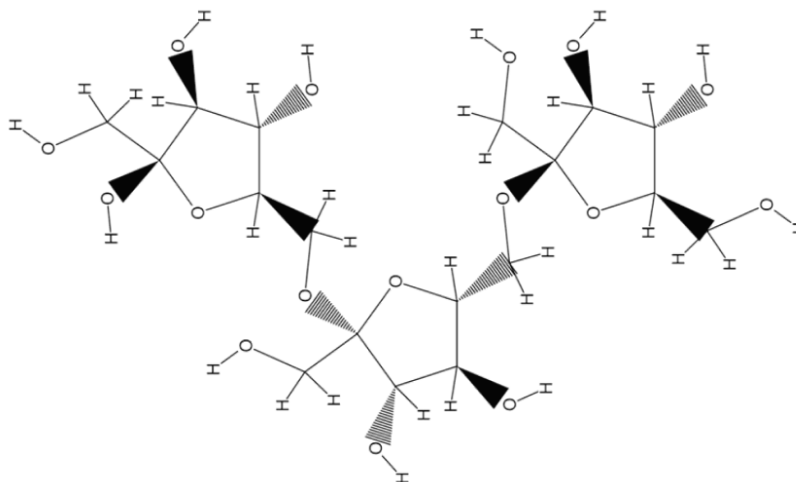


**Figure 1. 8.** Chemical structure of levan

Levan is a natural polysaccharide which can be obtained from microorganisms and plants. Recently, levan obtained from *Halomonas smyrnensis* AAD6<sup>T</sup>, *Halomonas* Levan, is produced at high yields from low cost substrates (Erkorkmaz et al., 2018). Due to its very low intrinsic viscosity, strong interaction with biological membranes, adhesivity and its ability to form self-assembled spherical colloids, levan biopolymer is used for various applications in food, chemical, pharmaceutical, water treatment, cosmetic and other industries (Avsar et al., 2018; Gomes et al., 2018; Öner et al., 2016; Sam et al., 2011).

The furanose rings in levan structure makes levan a good candidate for molecular interaction with EDCs. On the other hand, levan is water soluble (Han, 1990; Manandhar et al., 2009) making its separation from aqueous solutions ineffective. The use of its phosphonated derivative which is insoluble in water (below pH 13) could lead to more effective separation from aqueous solutions after its use as an adsorbent for EDCs. As a result, in this study, phosphonated *Halomonas* Levan (PhHL) is used and its chemical structure is given in Figure 1.9. To the best of our knowledge, there is no study on the use of PhHL as an adsorbent for EDCs.

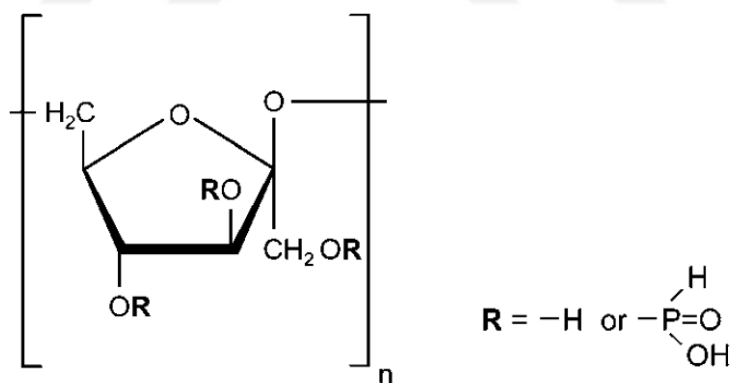


**Figure 1. 9.** Chemical structure of PhHL

### 1.6. Use of surface modified MNPs for the adsorption of EDCs

Pure and surface modified MNPs can be used for several environmental applications including air clean-up and carbon sequestration, water disinfection, flocculation as well as adsorptive removal of organic and inorganic contaminants (Mohammed et al., 2017;

Sherlala et al., 2018; Su, 2017). Although these materials hold a great potential, there are only a limited number of studies evaluating the use of MNPs for adsorption of organic micropollutants. The main studies related to this topic found in the literature, are summarized below.

In a recent study, Khatibikamal et al. (2019) synthesized different generations of magnetic iron oxide nanoparticles coated with poly(amidoamine) (Khatibikamal et al., 2019). Then produced material was modified with 4-aminophenol and used for the adsorption of nonylphenol from water. The maximum adsorption capacity obtained by Langmuir model was 7.86 mg/g. Based on the obtained results, it was concluded that the synthesized material can be used for the removal of nonylphenol.

In another study, organic/inorganic core-shell magnetic composites were used for the removal of diltiazem hydrochloride and sodium naproxen (Fierascu et al., 2018). The tested adsorbents were copper ferrite, copper ferrite/chitosan composite, nickel ferrite and nickel ferrite composite. The results showed that nickel ferrite/chitosan composite had the highest affinity towards the adsorption of sodium naproxen (52.78 mg/g), while the best results for the adsorption of diltiazem hydrochloride were obtained for the copper ferrite/chitosan composite (33.65 mg/g).

Zhang et al. (2018) investigated magnetic iron oxide/graphene oxide (MGO) nanocomposites for the removal of p-tert-butylphenol (PTBP) (Zhang et al., 2018). According to the results, the adsorption capacity of MGO was 59.18 mg/g for PTBP. It was shown that MGO can be applied as a promising adsorbent to achieve the efficient removal of aromatic pollutants and separation from aqueous solution.

Ghoochian et al. (2018) synthesized  $\text{Fe}_3\text{O}_4$  nanoparticles coated by  $\text{SiO}_2$  shell and modified them with 3-(trimethoxysilyl)-1-propanethiol. Then, they grafted them with polyamidoamine dendrimer (PAMAM). After immobilization of chitosan on the prepared nanoparticles, removal of tamoxifen from aqueous solutions was studied. The results indicated that the Freundlich model could best describe the equilibrium data and the maximum adsorption capacity of the prepared adsorbents for tamoxifen was found to be 20.5 mg/g (Ghoochian et al., 2018).

Nethaji and Sivasamy (2017) prepared graphene oxide coated with porous iron oxide ribbons for the removal of 2, 4-Dichlorophenoxyacetic acid (2,4-D). According to the

results, the maximum monolayer capacity from Langmuir isotherm was found as 67.26 mg/g (Nethaji and Sivasamy, 2017).

Superparamagnetic iron oxide nanoparticles and those coated with methacrylic acid, Al(OH)<sub>3</sub> and SiO<sub>2</sub> were tested for the adsorptive removal of carbamazepine (CBZ) and diatrizoate (DTZ) (Yoon et al., 2016). The maximum adsorption capacities based on Freundlich isotherm were obtained by using methacrylic acid coated NPs, which were determined as 112.46 mg/g and 77.30 mg/g, for DTZ and CBZ respectively.

Guo et al. (2016) evaluated iron oxide MNPs functionalized with four types of organic acid (oleic, undecenoic, caprylic or hexanoic acid) for the removal of tetracycline from aqueous solution. The authors reported that undecenoic acid-coated MNPs exhibited the highest adsorption efficiency while it can be easily retrieved with a low-gradient magnetic separator (Guo et al., 2016). Langmuir isotherm was found to best fit the experimental data with a maximum adsorption capacity of 222.2 mg/g (318 K).

The adsorption behaviour of diquat on the surface of graphene oxide nanocomposite (GO-Fe<sub>3</sub>O<sub>4</sub>) was investigated (Hao et al., 2015). The Langmuir adsorption isotherm model was found applicable for describing the adsorption of diquat onto GO-Fe<sub>3</sub>O<sub>4</sub>, with a maximum adsorption capacity of 74.85 mg/g, at room temperature.

Core-shell superparamagnetic iron oxide  $\beta$ -cyclodextrin composites were evaluated for the adsorption of two different PCBs, that are PCB52 and PCB28 (Wang et al., 2015). Based on Langmuir model, the absorptive capacities calculated were 30.32 and 40.01 mmol/kg for PCB52 and PCB28, respectively. The produced nanomaterial was reported as an ideal candidate for various applications, including the recognition and removal of environmental contaminants.

Powdered activated carbons (PAC) impregnated with iron oxide nanoparticles (IONPACs) were fabricated and used for the simultaneous removal of BPA and natural organic matter (NOM) (Park et al., 2015). It was found that IONPAC adsorbents had considerably greater sorption capabilities for BPA and NOM compared to bare PAC particles. The Freundlich adsorption coefficients of BPA and NOM were in the following order: bare PAC < hematite/PAC < magnetite/PAC < ferrihydrite/PAC.

Alginate beads with encapsulated magnetic nanoparticles were used for the adsorption of p-nitrophenol (PNP) (Obeid et al., 2015). The effect of a cationic surfactant,

cetylpyridinium chloride on the adsorption process was also evaluated. The study showed that the presence of surfactant significantly enhanced the adsorption of PNP and the maximum adsorption capacity was 140 mg/g.

Adsorption of 4-n-nonylphenol (4-n-NP) and bisphenol A (BPA) on magnetic reduced graphene oxides (rGOs) were investigated (Jin et al., 2015). The maximum adsorption capacities of magnetic rGOs were 63.96 and 48.74 mg/g (at 293 K) for 4-n-NP and BPA, respectively. The results were found to be significantly higher than that of activated carbon.

Molecularly imprinted amino-functionalized nano-Fe<sub>3</sub>O<sub>4</sub>-polymer magnetic composite was synthesized and used for highly selective adsorption of 2,4,6-trichlorophenol (Shen et al., 2015). Four different amines, i.e., ethylenediamine (EDA), diethylenetriamine (DETA), triethylenetetramine (TETA) and tetraethylenepentamine (TEPA) were used for surface grafting. The results showed specific selectivity and remarkable adsorption capacity of the produced adsorbent. The highest adsorption capacity was found as 898.7 mg/g for the magnetic polymer microspheres grafted with TEPA.

Miah et al. (2015) synthesized polydopamine-coated magnetic nanoparticles (MNPs@PDA) and polypyrrole-coated magnetic nanoparticles (MNPs@PPy). They determined the binding efficiencies of the synthesized materials with BPA, metformin (MF), naphthalene acetic acid (NAA), phenformin (PF), quinine sulfate (QS), and triclosan (TC) in water. Their results showed that MNPs@PDA binded 65 % BPA, 14 % MF, 21 % NAA, 99 % PF, 92 % TC and 94 % QS whereas MNPs@PPy binded 99 % BPA, 34 % MF, 39 % NAA, 99 % PF, 99 % TC, and 98 % QS (Miah et al., 2015).

Zhou et al. (2014) synthesized multi-walled carbon nanotubes (MWCNTs) coated with magnetic amino-modified CoFe<sub>2</sub>O<sub>4</sub>(CoFe<sub>2</sub>O<sub>4</sub>-NH<sub>2</sub>) nanoparticles and functionalized this composite material with chitosan. The obtained hybrid materials were tested as adsorbents for tetrabromobisphenol A (TBBPA). The adsorption of TBBPA was well represented by the Freundlich isotherm and the maximum adsorption capacity was 42.48 mg/g (Zhou et al., 2014).

Bogdan (2013) evaluated commercial magnetite (Fe<sub>3</sub>O<sub>4</sub>) and hematite (Fe<sub>2</sub>O<sub>3</sub>) for the adsorptive removal of BPA. The results indicated that hematite had the highest adsorption capacity at pH 2 where the maximum adsorption capacity was 0.395 mg/g

(Langmuir model). It was noted that magnetite had a lower adsorption capacity than hematite (Bogdan, 2013).

In another study, the use of Fe<sub>3</sub>O<sub>4</sub> MNPs, carbon nanotubes (CNTs) and CNTs/Fe<sub>3</sub>O<sub>4</sub> magnetic nanocomposites as adsorbents to remove bisphenol A was investigated. The maximum adsorption capacities obtained by Langmuir model for Fe<sub>3</sub>O<sub>4</sub> MNPs, CNTs and CNTs/Fe<sub>3</sub>O<sub>4</sub> magnetic nanocomposites were determined as 5.08, 46.18 and 45.31, respectively (Li et al., 2015).

Sinha and Jana (2013) produced graphene-based composites with  $\gamma$ -Fe<sub>2</sub>O<sub>3</sub> nanoparticle for the removal of EDCs from water (Sinha and Jana, 2013). They used BPA, atrazine, 1-naphthol, and dibutylphthalate as target EDC samples. Based on Langmuir model, the maximum adsorption capacities of BPA and 1-naphthol were 360 mg/g and 680 mg/g, respectively. The measured maximum adsorption capacities for atrazine and dibutylphthalate were 200 and 200 mg/g, respectively. The authors stated that the magnetic iron-oxide component offers easier magnetic separation of adsorbed EDC. They concluded that these composite materials showed excellent removal efficiency of EDCs from water.

Superparamagnetic Fe<sub>3</sub>O<sub>4</sub> nanoparticles bearing aminated  $\beta$ -cyclodextrin was synthesized and used for the adsorption of naproxen (NAP), carbamazepine (CBZ) and BPA (Ghosh et al., 2013). The authors noted that aminated  $\beta$ -cyclodextrin provided the ability to adsorb organic pollutants through inclusive host-guest interactions, while Fe<sub>3</sub>O<sub>4</sub> nanoparticles served as magnetic separators. It was also shown that physicochemical properties of each organic pollutant were important factors in adsorption process i.e. BPA with logK<sub>ow</sub> value of 3.3 was least adsorbed, whereas carbamazepine with logK<sub>ow</sub> value of 2.45 was most adsorbable.

### **1.7. Objective and scope of the study**

The objective of this thesis study is to evaluate magnetic nanoparticles (MNPs) for the adsorptive removal of endocrine disrupting compounds (EDCs) from aqueous solutions.

For this purpose, two widely used EDCs, bisphenol A (BPA) as a representative of EDCs from industrial sources and 17 $\alpha$ -ethinylestradiol (EE2) as a representative of synthetic hormones, are selected as target contaminants.

The evaluated adsorbents are iron oxide MNPs and MNP-biopolymer composites prepared by chitosan and phosphonated levan (PhHL). For comparison, pure biopolymers (chitosan and PhHL) are also evaluated as adsorbents.

The scope of this study is divided into six main parts, which are described below.

- Optimization of GCMS analysis methods for determination of BPA and EE2.
- Preparation and characterization of the adsorbents.
- Determination of the adsorbent with highest adsorption capacity for BPA and EE2 by batch equilibrium adsorption studies.
- Conducting kinetic studies to determine the rates of adsorption reactions.
- Determination of the adsorption mechanisms by FTIR and XPS studies.
- Desorption and reuse studies.

## **2. MATERIALS AND METHODS**

### **2.1. Materials**

Certified standards of BPA (99.8 % purity) and EE2 (99.5 % purity) were purchased from Dr. Ehrenstorfer GmbH (Germany). Primary standards were prepared by dissolving these standards in GC-MS grade methanol (Merck, Germany). Calibration standards were prepared by diluting the primary standards in methanol. Working solutions to be used in the adsorption experiments were prepared by diluting these standard solutions with ultrapure water produced by a Sartorius Arium 611UV Ultrapure Water System (Germany).

Anthracene-d10 (CAS RN: 1719-06-8; 99.5 % purity) was purchased from Dr. Ehrenstorfer GmbH (Germany) and used as a surrogate to ensure the analytical quality.

Magnetic nano-particles were prepared as described in the methodology part. For this purpose, iron (II) chloride (98 % purity) and iron (III) chloride (97 % purity) were purchased from Sigma-Aldrich (Germany).

Chitosan with medium molecular weight was purchased from Sigma-Aldrich (USA). Other materials used in this study i.e. ethanol, acetone hexane and dichloromethane were GC-MS grade and purchased from Merck, Germany.

### **2.2. Methods**

#### **2.2.1. Production of the adsorbents**

##### **2.2.1.1. Production of microbial levan**

*Halomonas* levan (HL) was microbially produced in Marmara University Bioengineering Department. In the production process, *Halomonas smyrnensis* cultures are used based on a recently developed cost-effective process and then purified as described before (Erkorkmaz et al., 2018). Briefly, bioreactor cultures at steady state were centrifuged to remove cellular biomass and levan in the supernatant was precipitated with an equal volume of ice-cold ethanol. After centrifugation, polymer pellets were redissolved in water, dialyzed and then air dried in a laboratory oven.



Phosphonated HL derivatives (PhHL) were prepared by following a previously optimized method where levan is reacted with  $\text{PCl}_3$  in pyridine, recovered by aqueous extraction and then purified by dialysis (Costa et al., 2013). The produced PhHL is shown in Figure 2.1 (a) together with chitosan, the other biopolymer used in this study (Figure 2.1 (b)).

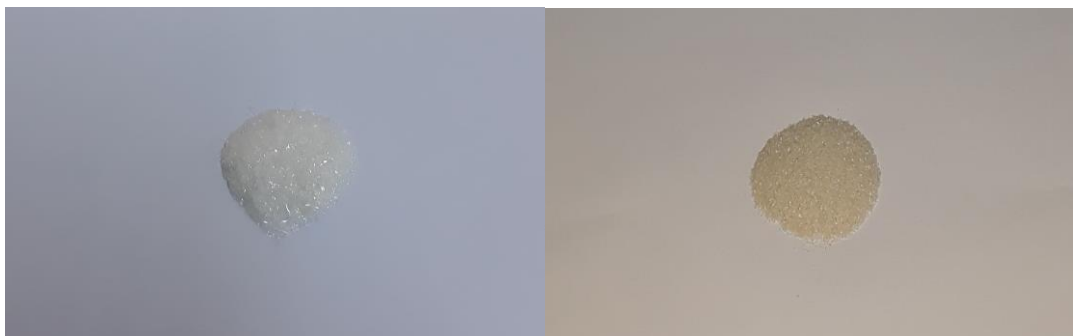
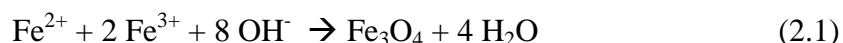


**Figure 2. 1.** Biopolymers used for the surface modification of MNPs  
PhHL (a) Chitosan (b)

#### 2.2.1.2. Production of $\text{Fe}_3\text{O}_4$ MNP

$\text{Fe}_3\text{O}_4$  MNP was produced by chemical co-precipitation method which is based on the precipitation of  $\text{Fe}^{2+}$  and  $\text{Fe}^{3+}$  salts under alkaline and inert condition (Shamim et al., 2007). The reaction taking place is given in the Equation 2.1.



MNP production process is shown in Figure 2.2. Briefly, 150 ml of 0.5 M  $\text{FeCl}_3$  solution and 100 ml of 0.5 M  $\text{FeCl}_2$  (0.5 M) solution are prepared. These solutions were mixed and stirred at 550 rpm with a mechanical stirrer for 5 minutes. The temperature of the mixture was adjusted to 70 °C. Then, 4 M ammonia solution is added to the solution until pH 10 was reached. Mixing was continued at 500 rpm while nitrogen gas bubbles were introduced in order to strip air from the solution. At the end of 2 hours, the prepared solution was taken and the supernatant was separated from the formed iron oxide particles by applying external magnetic field.

The separated particles were washed with distilled water and ethanol to remove any other contaminants. The obtained iron oxide particles were vacuum dried at 70 °C for

24 hours. Then beat-beater homogenizer was used to grind the iron oxide particles, thus MNPs were obtained.

### **2.2.1.3. Production of MNP-biopolymer composites**

MNP-biopolymer composites were prepared using chitosan or PhHL. For this purpose, a similar method described for MNP production was used. In this case, the 2.5 g biopolymer (chitosan or PhHL) was first dissolved in an appropriate solvent. Chitosan was dissolved in 100 mL of 0.05 M acetic acid solution and PhHL was dissolved in 100 mL of 0.01 M ammonia solution. The prepared biopolymer solutions were added into the mixture of  $\text{FeCl}_3$  and  $\text{FeCl}_2$ , while mixing is continued at 500 rpm. The remaining steps of MNP production was applied as described for the MNP production process.

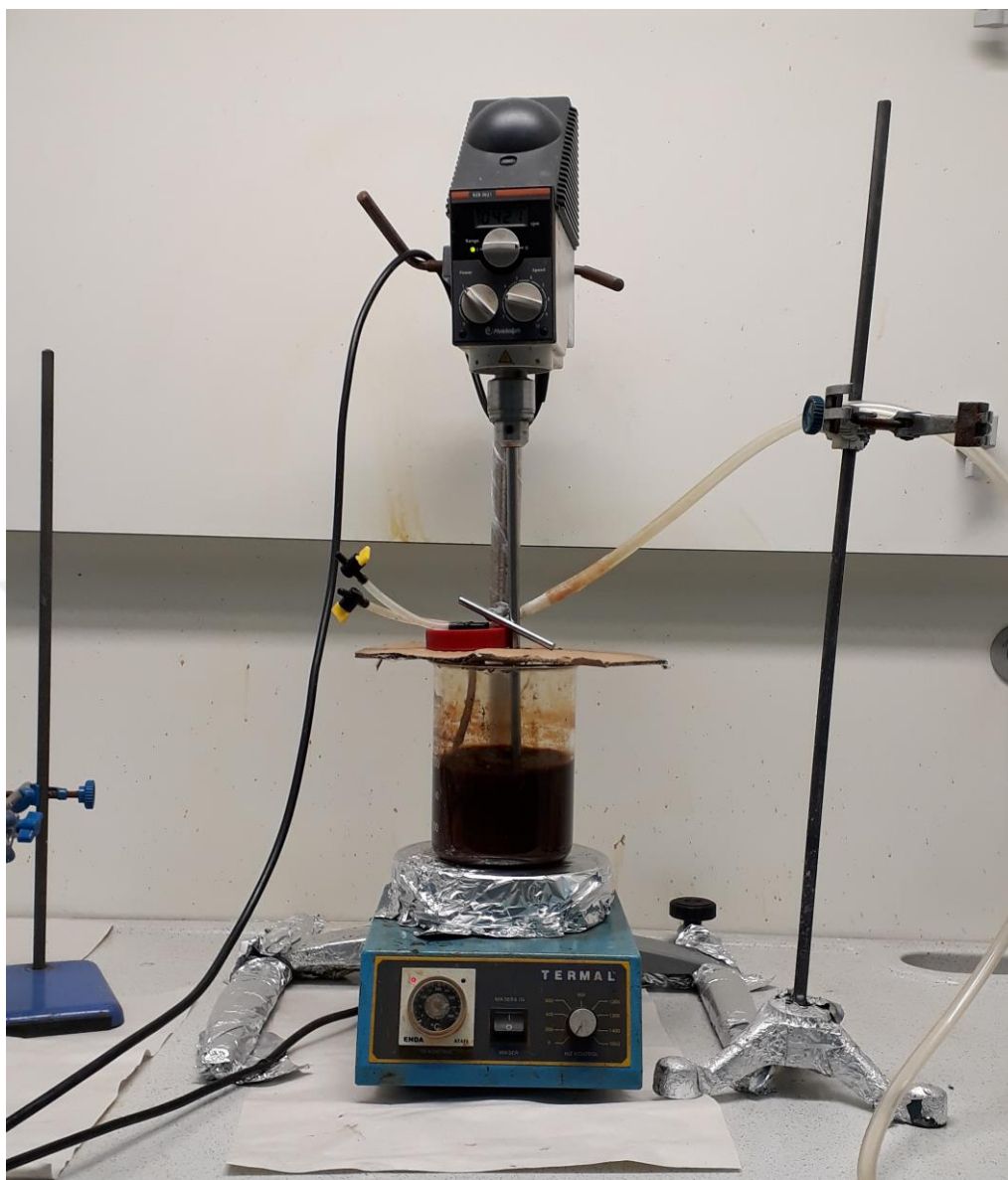


**Figure 2. 2.** MNP production process

### **2.2.2. Material characterization**

Scanning electron microscopy (SEM) was used to observe the surface morphology of PhHL samples. SEM analyses were performed using a Zeiss Evo 10 electron microscope (Germany).

Fourier transform infrared (FTIR) spectroscopy was used to assess the characteristic functional groups of the PhHL before and after adsorption. FTIR analysis of pure BPA and EE2 were also performed for comparison. In order to remove any impurities, the

samples were purified by washing them three times with deionized water and dried prior to the analysis. FTIR spectra were measured with a Jasco FT/IR-4700 spectrometer (Jasco, Japan) in the spectral range of 4000-450 cm<sup>-1</sup>.

X-ray diffraction (XRD) analysis is used to characterize crystalline materials and reveal their structural parameters e.g. average grain size, crystallinity, strain and crystal defects. For this purpose XRD analyses were conducted at Marmara University Metallurgical and Materials Engineering Department using Rigaku XRD apparatus (Rigaku Ltd., Japan). The samples were scanned in the 2θ range of 5°– 105°.

X-ray photoelectron spectroscopy (XPS) measurements were conducted to analyze the chemical states of PhHL (before and after adsorption), pure BPA and pure EE2. The XPS studies were carried out at Middle East Technical University Central Laboratory and Ege University Application and Research Center for Testing and Analysis Laboratory. Peak deconvolution for the XPS results were performed with the trial version of OriginPro software (OriginLab, USA).

### 2.2.3. Adsorption experiments

Adsorption experiments were carried out in batch mode using a temperature controlled shaker (IKA, Germany) at a constant speed of 200 rpm. 10 ml aqueous BPA or EE2 samples were prepared in 40 ml glass vials with screw caps. The adsorbent dose was 0.5 g/L, unless otherwise stated. Temperature was adjusted to 25 °C in each experiment.

For the isotherm studies, selection of a wide range of initial adsorbate concentrations is important to observe the complete adsorption isotherm, (Tran et al., 2017). Regarding this concern and solubility limits given in Table 1.2 and Table 1.3, initial concentrations between 1-280 mg/L and 1-9 mg/L were selected for BPA and EE2, respectively.

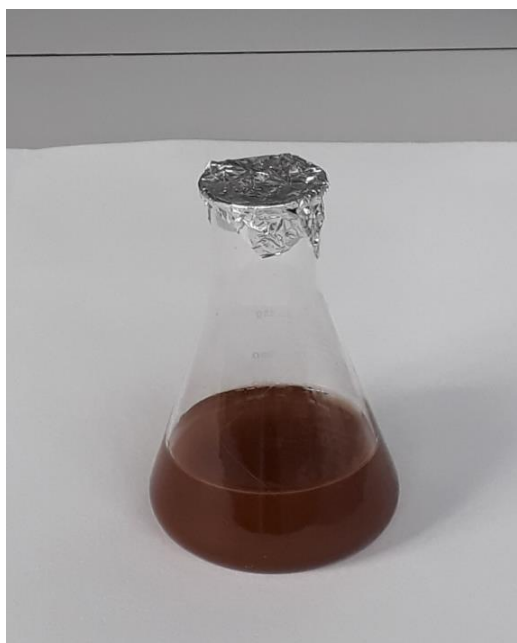
For kinetic studies, different contact times between 1 min to 25 hour were evaluated. Initial BPA and EE2 concentrations were 10 and 9 mg/L, respectively. The amount of target pollutant adsorbed on unit weight of adsorbent at any time, *t*, is calculated using the Equation 2.2.

$$q_t = \frac{(C_0 - C_t)V}{m} \quad (2.2)$$

where  $q_t$  is the amount of pollutant adsorbed (mg/g) at time  $t$ ;  $C_0$  is the initial pollutant concentration (mg/L);  $C_t$  is the pollutant concentration at time  $t$  (mg/L);  $V$  is the volume of the solution (L) and  $m$  is the weight of the adsorbent (g).

After the adsorption process, the samples were prepared for GC-MS analysis, as described in Analytical Methods section. For the samples containing MNPs (Figure 2.3 (a)), magnetic separation was applied just after the adsorption process. Permanent magnet was used for the magnetic separation process as demonstrated in Figure 2.3 (b). Then the supernatant was taken and filtrated. The resulting solution (Figure 2.3 (c)) was prepared for GC-MS analysis.

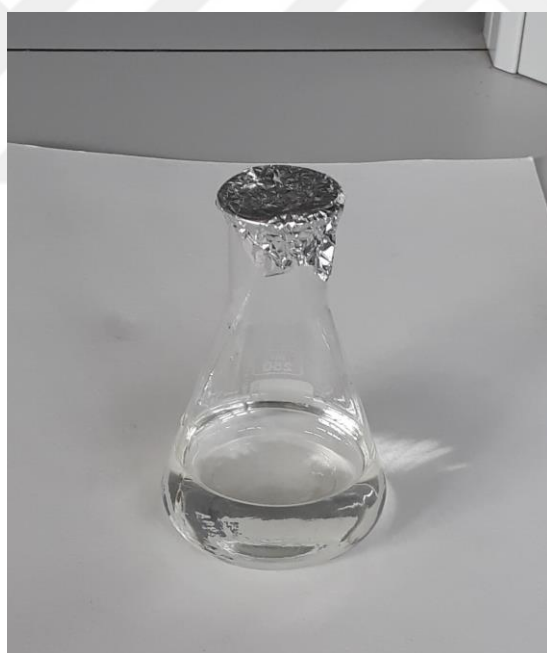




(a)



(b)



(c)

**Figure 2. 3.** Magnetic separation process

(a) MNP containing samples before magnetic separation (b) after magnetic separation

(c) after filtration process

#### **2.2.4. Desorption and reuse experiments**

In this study, desorption and reuse experiments were conducted with 10 ml aqueous BPA or EE2 samples with an initial concentration of 10 and 9 mg/L, respectively. The adsorbent dose was 0.5 g/L. After the initial use, centrifugation was applied to separate the adsorbent material from aqueous phase and the supernatant was discarded. Then ethanol/water mixture in a volumetric ratio of 4:1 was added to the adsorbent and sonicated for 5 minutes to solubilize BPA or EE2 residuals. Finally, centrifugation was applied again, the supernatant was discarded and the collected adsorbents were vacuum dried at 60 °C for 24 hours.

#### **2.2.5. Analytical methods**

BPA or EE2 concentrations in the samples before and after adsorption studies were measured by a gas chromatograph-mass spectrometer (GCMS-QP2010, Shimadzu, Japan). Prior to GC-MS analysis, the samples were first filtered by passing them through 0.2 µm syringe filters to remove impurities. In this study, the filter material was selected as PTFE with reference to Godby and Conklin (2017) since it is demonstrated that phenolic compounds adsorb less to the PTFE filter, compared to other syringe filter materials (Godby and Conklin, 2017).

After the filtration process, 0.5 ml of samples was taken and added into GC-MS vials. They are spiked with 100 µL surrogate (anthracene-d10). Then, the samples were dried at 60 °C, for 48 hours to remove the water content. Finally, the samples were reconstituted with 100 µL GC-MS grade acetone prior to GC-MS analysis.

The GC-MS analyses of the samples were conducted by a modification to the method described by Can et al. (2014). The analytes were chromatographically separated by injecting a 1 µL of sample onto a Trb-5ms capillary GC column. The mass spectrometer was set to selectively monitor for mass ions ( $m/z$ ) 213, 296 and 188  $m/z$ , corresponding to BPA, EE2 and anthracene-d10, respectively. The optimized GC-MS parameters are provided in Table 2.1.

**Table 2.1.** Detailed GC-MS parameters

GC	Column:	TRB-5MS (30 m x 0,25 mm x 0,25 $\mu$ m)
	Injection temperature:	280 °C
	Injection mode:	Splitless
	Helium gas flow rate:	1.0 ml/min
	Sample volume:	1 $\mu$ l
	Control mode:	Linear (37.5 cm/s)
	Oven temperature program for BPA	120 °C (1 min) $\rightarrow$ (10 °C /min) $\rightarrow$ 190 °C (1 min) $\rightarrow$ (5 °C /min) $\rightarrow$ 250 °C $\rightarrow$ (20 °C /min) $\rightarrow$ 290 °C (15 min)
	Oven temperature program for EE2	120 °C (1 min) $\rightarrow$ (10 °C /min) $\rightarrow$ 190 °C (1 min) $\rightarrow$ (5 °C /min) $\rightarrow$ 250 °C (10 min) $\rightarrow$ (20 °C /min) $\rightarrow$ 290 °C (10 min)
	Injection unit:	250 kPa (1 min)
MS	Ion source temperature:	250 °C
	Interface temperature:	280 °C
	Measurement mode for BPA:	5.00-6.50 min: Scan (0.50 s) 6.50-22.00 min: Scan (0.30 s) 6.50-22.00 min: SIM (0.20 s) m/z: 119; 188; 213; 228 22.00-24.00 min: Scan (0.50 s)
	Measurement mode for EE2:	5.00-6.50 min: Scan (0.50 s) 6.50-22.00 min: Scan (0.30 s) 6.50-22.00 min: SIM (0.20 s) m/z: 145; 160; 188; 213; 296 22.00-24.00 min: Scan (0.50 s)

### 2.2.6. Validation of kinetic and isotherm models

The parameters for isotherm and kinetic models were determined by nonlinear optimization technique using Microsoft Office Excel software (Microsoft Corp., USA) as described by a previous study (Tran et al., 2017).

The obtained models were evaluated according to Chi square ( $\chi^2$ ), correlation coefficient ( $R^2$ ) and normalized root mean square error (NRMSE). The equations used



to calculate these parameters are given in Table 2.2.

**Table 2.2.** Validation parameters used for model evaluation

Parameter	Equation
Chi square	$\chi^2 = \sum_{i=1}^n \frac{(q_{\text{exp}} - q_{\text{calc}})^2}{q_{\text{calc}}}$
Correlation coefficient	$R^2 = 1 - \frac{\sum_{i=1}^n (q_{\text{exp}} - q_{\text{calc}})^2}{\sum_{i=1}^n (q_{\text{exp}} - q_{\text{exp,mean}})^2}$
Normalized root mean square error	$\text{NRMSE} = \frac{\sqrt{\frac{\sum_{i=1}^n (q_{\text{exp}} - q_{\text{calc}})^2}{n}}}{q_{\text{exp,max}} - q_{\text{exp,min}}}$

Where  $n$  is the number of data points;  $q_{\text{exp}}$  and  $q_{\text{calc}}$  are the quantities adsorbed determined experimentally and the quantities adsorbed calculated by the models, respectively;  $q_{\text{exp,max}}$  and  $q_{\text{exp,min}}$ ,  $q_{\text{exp,mean}}$  are the maximum, minimum and mean values of the quantities adsorbed determined experimentally, respectively.

$\chi^2$  close to zero,  $R^2$  close to unity and NRMSE close to zero demonstrate that the model is effective at estimating the experimental results.

### 3. RESULTS AND DISCUSSION

#### 3.1. Characterization of the adsorbents

The adsorbent materials (i.e. pure  $\text{Fe}_3\text{O}_4$  MNP, chitosan-MNP composite, PhHL-MNP composite, chitosan and PhHL) were characterized by scanning electron microscopy (SEM), Fourier transform infrared (FTIR) spectroscopy and X-ray diffraction (XRD) analyses.

##### 3.1.1. SEM Results

SEM images of the prepared MNP samples without polymer coating (pure MNP) are shown in Figure 3.1.

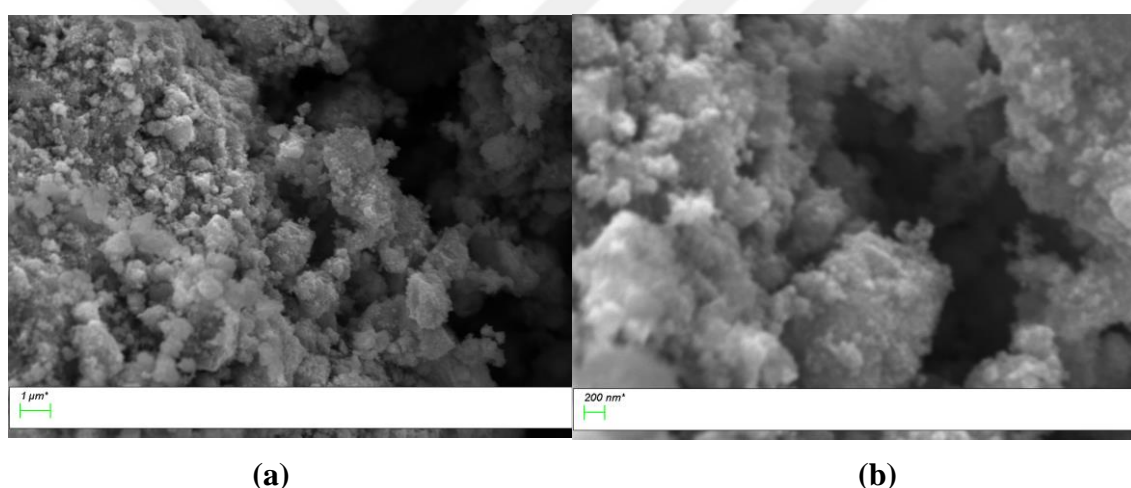


**Figure 3. 1.** SEM images pure MNP (a) 15K magnification  
(b) 50K magnification

The SEM images of pure chitosan and chitosan-MNP composite are given together in Figure 3.2, for comparison purposes. Similarly, SEM images of pure PhHL and PhHL-MNP composite are given in Figure 3.3.

The results of SEM images are evaluated by using International Union of Pure and Applied Chemistry (IUPAC) classification of porous solids (Everett, 1972), which is presented in Table 3.1.

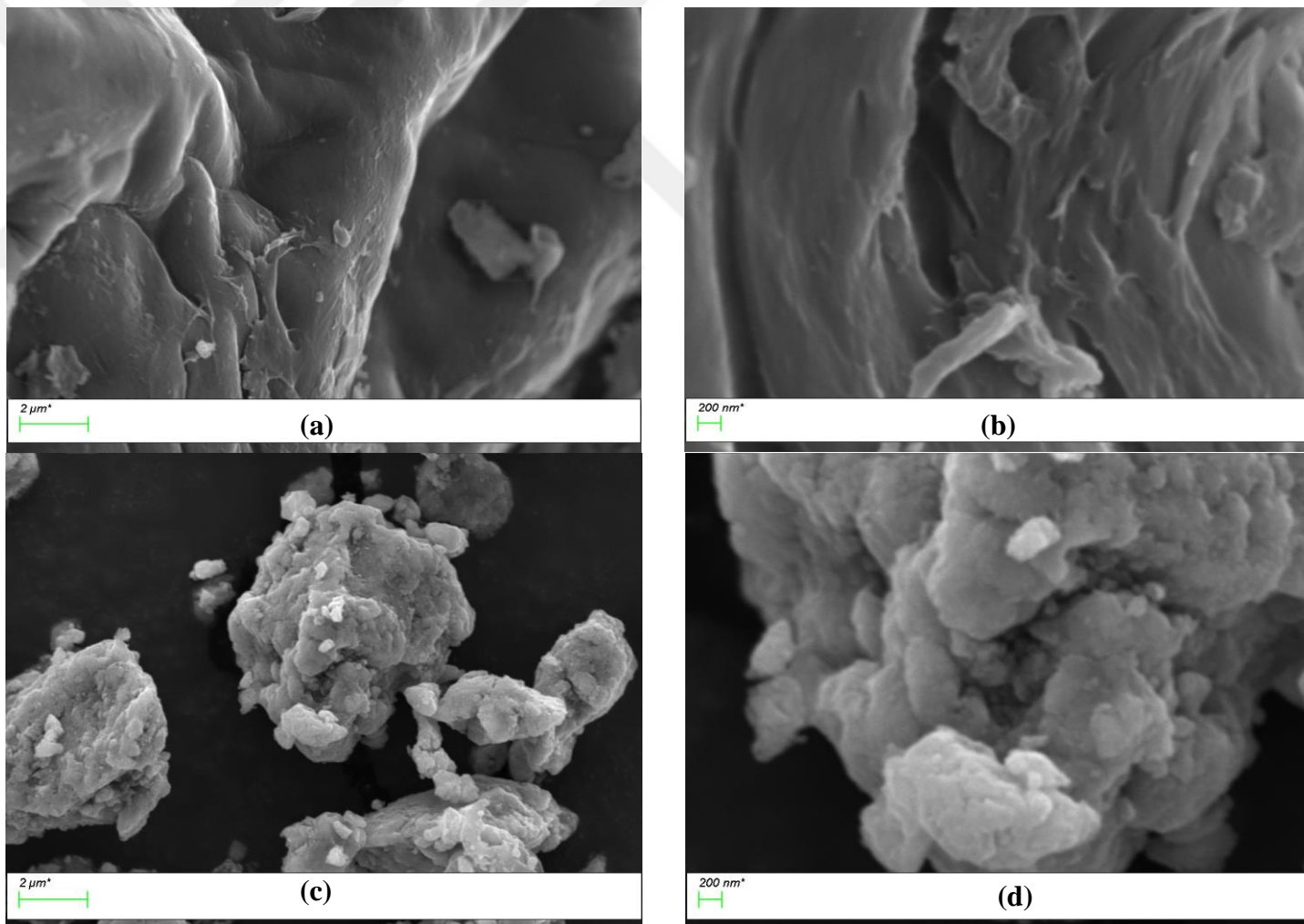


**Figure 3. 2.** SEM images of chitosan and chitosan-MNP composite

- (a) Pure chitosan with 15K magnification (b) Pure chitosan with 50K magnification (c) Chitosan-MNP composite with 15K magnification  
(d) Chitosan-MNP composite with 50K magnification

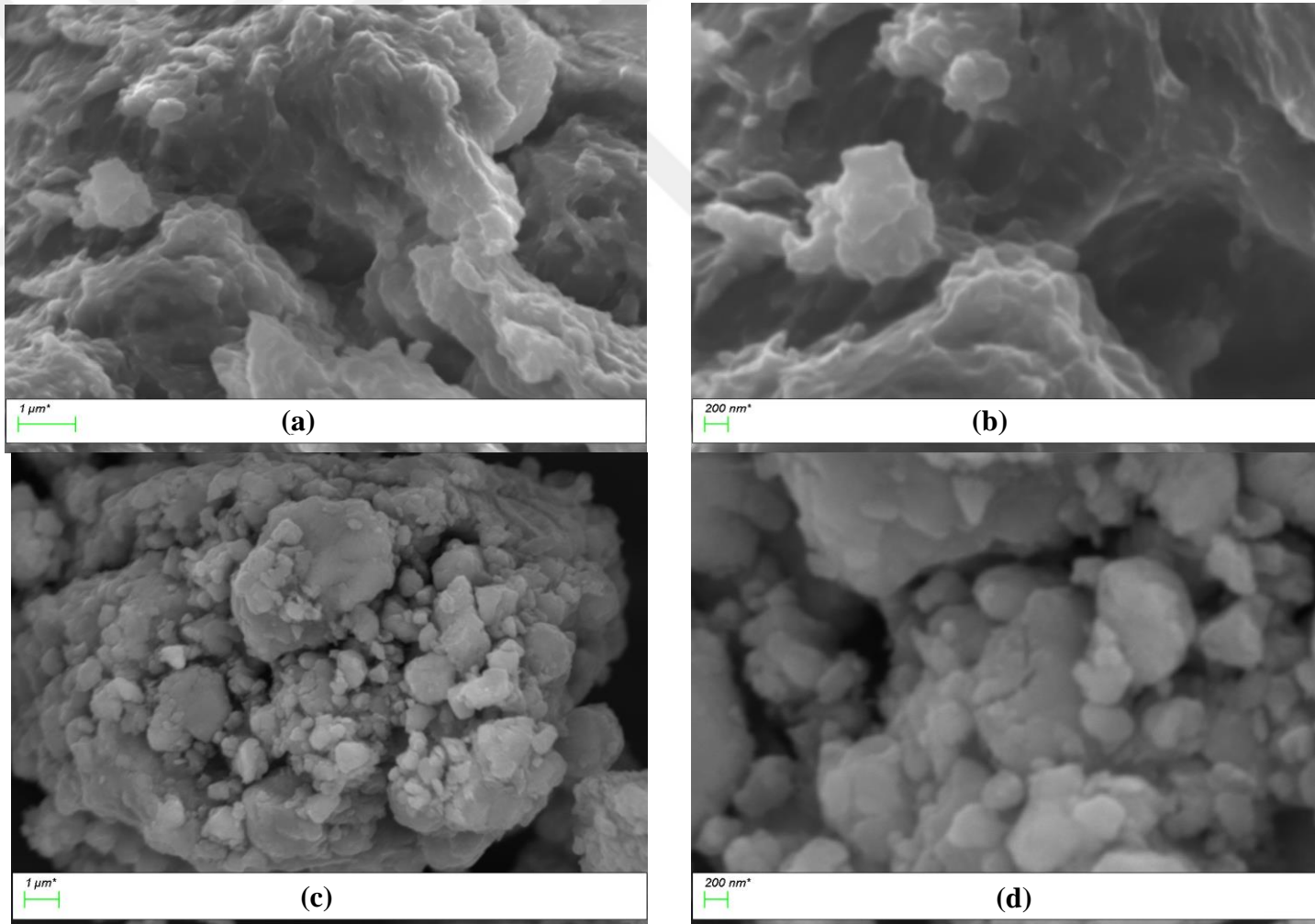


**Figure 3. 3.** SEM images of PhHL and PhHL-MNP composite  
(a) Pure PhHL with 15K magnification (b) Pure PhHL with 50K magnification (c) PhHL-MNP composite with 15K magnification (d) PhHL-MNP composite with 50K magnification

**Table 3.1.** IUPAC classification of porous solids

<b>Pore diameter</b>	<b>Solid Classification</b>
< 2 nm	Microporous
2-50 nm	Mesoporous
> 50 nm	Macroporous

SEM images of chitosan and PhHL are shown in Figure 3.2 (a, b) and 3.3 (a, b), respectively. When these images are examined, it is noted that pure biopolymers do not have discrete particles. On the other hand, MNP-biopolymer composites (Figure 3.2 (c, d) and 3.3 (c, d)) contain small discrete particles. These small discrete particles can be preferable since better dispersion in aqueous solutions is expected for these particles and also better adsorption due to larger surface area.

When Figure 3.1, 3.2 and 3.3 are evaluated, it can be seen that the samples have an irregular and clumpy morphology. Regarding IUPAC classification, all samples have highly porous structure while most of the pores have diameters higher than 50 nm, indicating that macropores dominate these structures. In all samples, there are also a few number of pores with diameters between 2 and 50 nm, which shows the existence of mesopores. The porous structure of the samples is expected to promote their adsorptive capacities.

Another observation in the SEM images of all the samples is that they are agglomerated. The agglomeration of adsorbents can result in lower adsorption capacities for the materials used. Moreover, agglomeration causes to decrease in reproducibility of the adsorption studies, which was observed at the beginning of the studies. In order to avoid these drawbacks, sonication is applied for five minutes prior to the adsorption studies which supply better dispersion of the adsorbents in aqueous solution and prevent agglomeration.

### 3.1.2. FTIR Results

FTIR analysis is important to identify the functional groups present on the surface of the adsorbent materials. The FTIR spectrum of pure levan is presented in Figure 3.4 (a). The results were interpreted according to previous studies (Barone and Medynets, 2007; Jathore et al., 2012; Yu et al., 2016). In Figure 3.4, the broad band with a peak at  $3273.6\text{ cm}^{-1}$  indicating O–H stretching vibration and the band at  $2933.2\text{ cm}^{-1}$  related to C–H stretching vibration are the evidences for the existence of polysaccharide. The band at  $1638.2\text{ cm}^{-1}$  is due to deformation vibration of the absorbed water molecules. The peak at around  $1418.4\text{ cm}^{-1}$  is associated with C–H bending. The fingerprint region ( $1200\text{--}900\text{ cm}^{-1}$ ) includes the vibrations of C–C and C–O bonds.

The FTIR spectrum of PhHL is given in Figure 3.4 (b) and it is compared with that of pure levan. In this figure, it is observed that O–H stretching vibration corresponds to the absorption band at  $3240.8\text{ cm}^{-1}$ , which is slightly different to that of pure levan ( $3273.6\text{ cm}^{-1}$ ). Similarly, bending vibration of the absorbed water molecules occurs at  $1644.0\text{ cm}^{-1}$  and C–H bending vibrations occurs at  $1453.1\text{ cm}^{-1}$ . The absorption band at  $2933.2\text{ cm}^{-1}$  corresponding to C–H stretching vibration is the same as that of pure levan. The fingerprint regions ( $1200\text{--}900\text{ cm}^{-1}$ ) are also similar for PhHL and pure levan.

The effect of phosphonate modification on levan biopolymer is evaluated using the information given by Costa et al. (2013). For PhHL, an absorbance band occurs at  $2370\text{ cm}^{-1}$  which is different from pure levan and it is attributed to the P–H bond. Another band is observed at around  $1195\text{ cm}^{-1}$  corresponding to the P=O bond. The shoulder at  $1050\text{ cm}^{-1}$  is assigned to the P–OH bond. The bands around  $875\text{ cm}^{-1}$  corresponds to the P–O–C bonds (Costa et al., 2013). These bands are shown encircled in Figure 3.4. These results demonstrate that PhHL was successfully produced. In order to better visualize the differences in pure levan and PhHL, absorbance is plotted on the y-axis (instead of transmittance) and the resulting graph is given in Figure A1 (Appendix A).

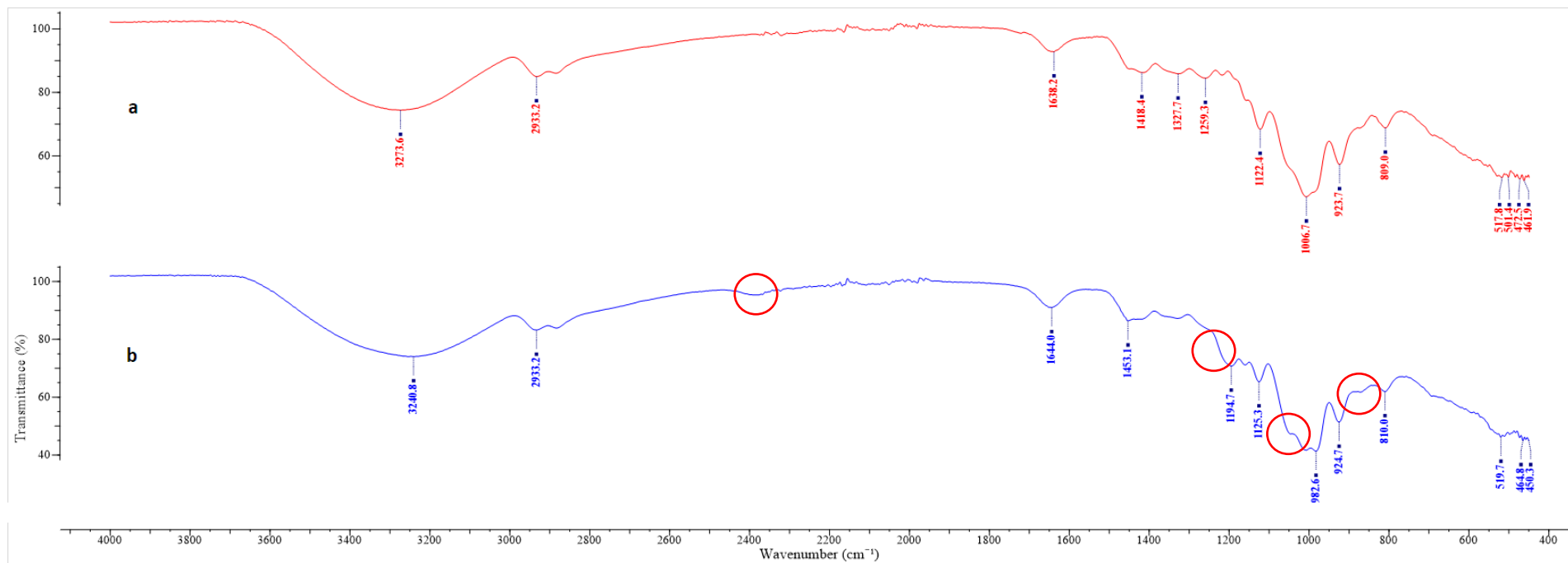


**Figure 3. 4.** FTIR results for pure levans (a) and PhHL (b)

The FTIR analysis results for PhHL, PhHL-MNP composite and pure Fe<sub>3</sub>O<sub>4</sub> MNP are given in Figure 3.5. The FTIR spectrum of PhHL (Figure 3.5.a) is previously explained.

FTIR spectrum of pure Fe<sub>3</sub>O<sub>4</sub> MNP (Figure 3.5.c) is also investigated. The absorption bands at 3366.1 cm<sup>-1</sup> and 1542.8 cm<sup>-1</sup> are attributed to the adsorbed water on the surface of iron oxide nanoparticles due to O–H stretching and H–O–H bending modes of vibration (Ternes et al., 2002). The two intense peaks at 538.0 cm<sup>-1</sup> and 450.3 cm<sup>-1</sup> are due to the stretching vibration mode associated to the metal-oxygen absorption band i.e. Fe–O bonds in the crystalline lattice of Fe<sub>3</sub>O<sub>4</sub> (Ahn et al., 2003). This occurs due to the contributions from the stretching vibrations related to metal in the octahedral and tetrahedral sites of the oxide structure (Lopez et al., 2010).

FTIR spectrum of PhHL-MNP composite (Figure 3.5.b) is evaluated and compared with the FTIR results from pure Fe<sub>3</sub>O<sub>4</sub> MNP and pure PhHL. For PhHL-MNP composite, the absorption band in 2914.9 is due to stretching vibration of C–H bond band. This bond is also observed in PhHL with a band in 2933.2 cm<sup>-1</sup> corresponding to the stretching vibration of C–H bond. Similarly, the band at 1013.4 cm<sup>-1</sup> for PhHL-MNP composite corresponds to stretching vibrations of the glycosidic linkage contributions of C–O–C and C–O–H (Costa et al., 2013) and it is also observed at around 982.6 for PhHL. These bands indicate the presence of polysaccharide structure.

The characteristic absorption bands of the Fe–O bond of magnetite were in 538.0 cm<sup>-1</sup> and 450.3 cm<sup>-1</sup>. For PhHL-MNP composite these bands are shifted to 551.5 and 453.2 cm<sup>-1</sup>, respectively, and they are split into smaller fractions. These differences may indicate that the interactions between PhHL and MNP are of intermolecular origin (Maciel et al., 2012).



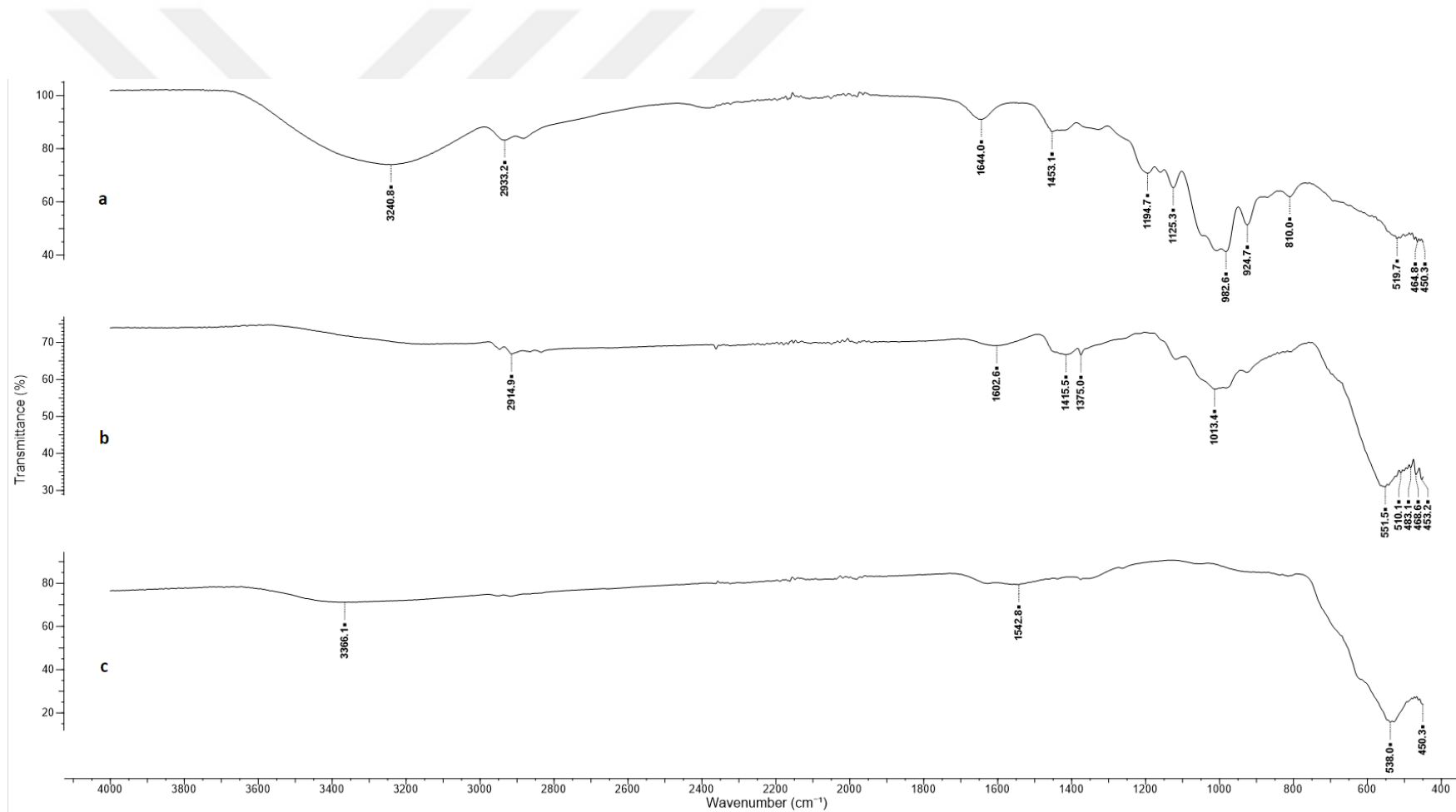


**Figure 3. 5.** FTIR results for PhHL (a) PhHL-MNP composite (b) pure MNP (c)

The FTIR analysis results for pure Fe<sub>3</sub>O<sub>4</sub> MNP, pure chitosan and chitosan-MNP composite are given in Figure 3.6.

In the FTIR spectrum of pure chitosan (Figure 3.6.a), the band at 3290.9 cm<sup>-1</sup> is explained by the stretching vibrations of OH<sup>-</sup> groups. The absorption peak at 2866.7 cm<sup>-1</sup> results from the C-H stretching vibration of the polymer backbone in the chitosan structure. The characteristic absorption bands at 1654.6 cm<sup>-1</sup> and 1561.1 cm<sup>-1</sup> are due to amide I (C=O stretching) and amide II (N-H angular deformation), respectively. The peak at 1420.3 cm<sup>-1</sup> is attributed to -C-O stretching of primary alcohol group in chitosan (Yadav et al., 2014). Other peaks are CH<sub>3</sub> symmetrical angular deformation at 1373.1 cm<sup>-1</sup> and C-N amino groups axial deformation at 1310.4 cm<sup>-1</sup> (Monier et al., 2010). Two characteristic polysaccharide bands at 1020.2 cm<sup>-1</sup> and 1149.4 cm<sup>-1</sup> are ascribed to the C-O stretching from glycosidic bonds (Lopez et al., 2010).

FTIR spectrum of pure Fe<sub>3</sub>O<sub>4</sub> MNP given in Figure 3.6.c is previously discussed for the interpretation of Figure 3.5.

FTIR spectrum of chitosan-MNP composite (Figure 3.6.b) is compared with the FTIR results from pure Fe<sub>3</sub>O<sub>4</sub> MNP and pure chitosan. The 1654.6 cm<sup>-1</sup> peak of amide I for the pure chitosan was shifted to 1634.4 cm<sup>-1</sup> and the 1561.1 cm<sup>-1</sup> peak of amide II was shifted to about 1550 cm<sup>-1</sup> in the FTIR spectrum of chitosan-MNP composite. The C-H stretching vibration peak (2866.7 cm<sup>-1</sup>) of the polymer backbone in the FTIR results from chitosan was reduced in intensity and shifted to 2914.9 cm<sup>-1</sup> in the FTIR results from chitosan-MNP composite. These changes can be explained by successful production of chitosan-MNP composite (Yadav et al., 2014). Moreover the C-O stretching band at 1020.2 cm<sup>-1</sup> was shifted to 1027.9 cm<sup>-1</sup> confirming the chitosan-MNP interaction. A strong band in the low-frequency region about 1000-500 cm<sup>-1</sup> can be associated to the iron oxide skeleton (Yadav et al., 2014).

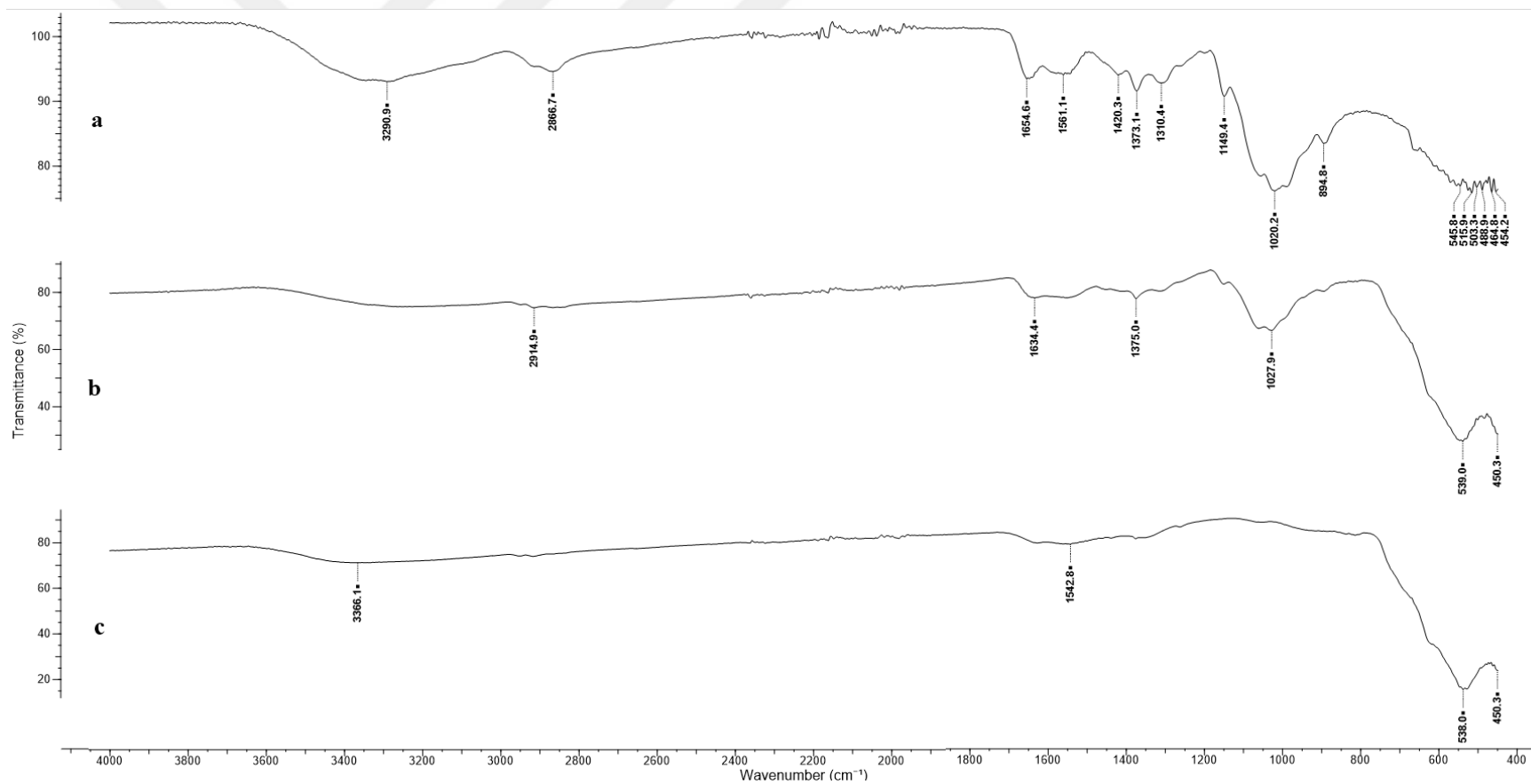


**Figure 3. 6.** FTIR results for chitosan (a) chitosan-MNP composite (b) pure MNP (c)

### 3.1.3. XRD Results

XRD analysis was used to verify the synthesizing process of  $\text{Fe}_3\text{O}_4$  MNPs. In this study, XRD analysis was done for PhHL-MNP composite and the results are given in Figure 3.7. Since pure MNP and chitosan-MNP composite were synthesized by using the same procedure that is used for PhHL-MNP composite, the XRD analysis was not repeated for pure MNP and chitosan-MNP composite.

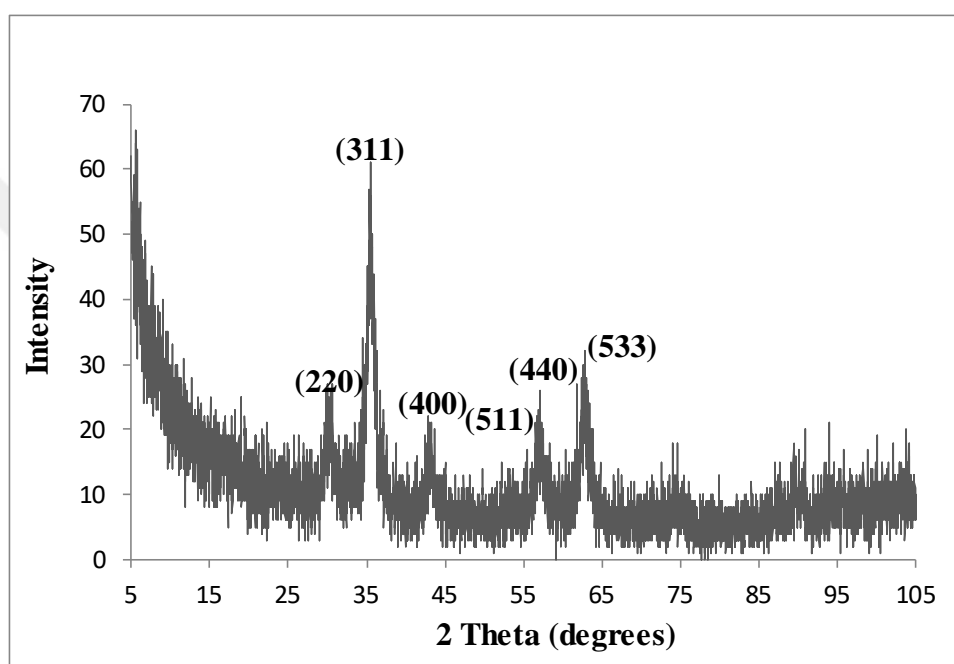


**Figure 3. 7.** X-ray diffraction pattern of PhHL-MNP composite

In Figure 3.7, the numbers in parenthesis indicate Miller indices (hkl) which show that the related peak is due to X-ray diffraction from (hkl) planes of the sample.

When the XRD pattern is examined, the major diffraction peaks (220, 311, 400, 511, 440 and 533) are found to be characteristic for  $\text{Fe}_3\text{O}_4$  crystal phase which are consistent with the Joint Committee on Powder Diffraction Standards (JCPDS) database (file no: 01-1111). This result indicates that  $\text{Fe}_3\text{O}_4$  is the dominant phase in the synthesized PhHL-MNP composite.

All the peaks observed in the XRD pattern are broad. Since the X-ray scattering from amorphous materials show broad bands (Jerden Jr and Sinha, 2006), this can indicate the presence of PhHL in the produced magnetic particles. As a result, it can be

concluded that PhHL-MNP composite was successfully synthesized.

XRD analysis results can also be used to calculate the crystallite size of the sample based on Scherrer equation (Scherrer, 1918) given below:

$$\tau = \frac{K\lambda}{\beta \cos\theta} \quad (3.1)$$

where  $\tau$  is the mean size of the crystalline domains (nm),  $K$  is Scherrer constant (0.9),  $\lambda$  is the X-ray wavelength ( $\text{\AA}$ ),  $\beta$  is the line broadening at half maximum (FWHM), and  $\theta$  is the diffraction angle ( $^\circ$ ).

Using Scherrer equation with 0.154 nm wavelength for Cu-K $\alpha$  radiation, the estimated crystallite size of synthesized PhHL-MNP composite was found as 13.90 nm.

### 3.2. Analysis of BPA and EE2

GCMS conditions were optimized for the analysis of BPA, EE2 and surrogate (anthracene-d10). The obtained chromatogram and mass spectrums for BPA, EE2 and anthracene-d10 are given in Figure 3.8, 3.9 and 3.10, respectively.

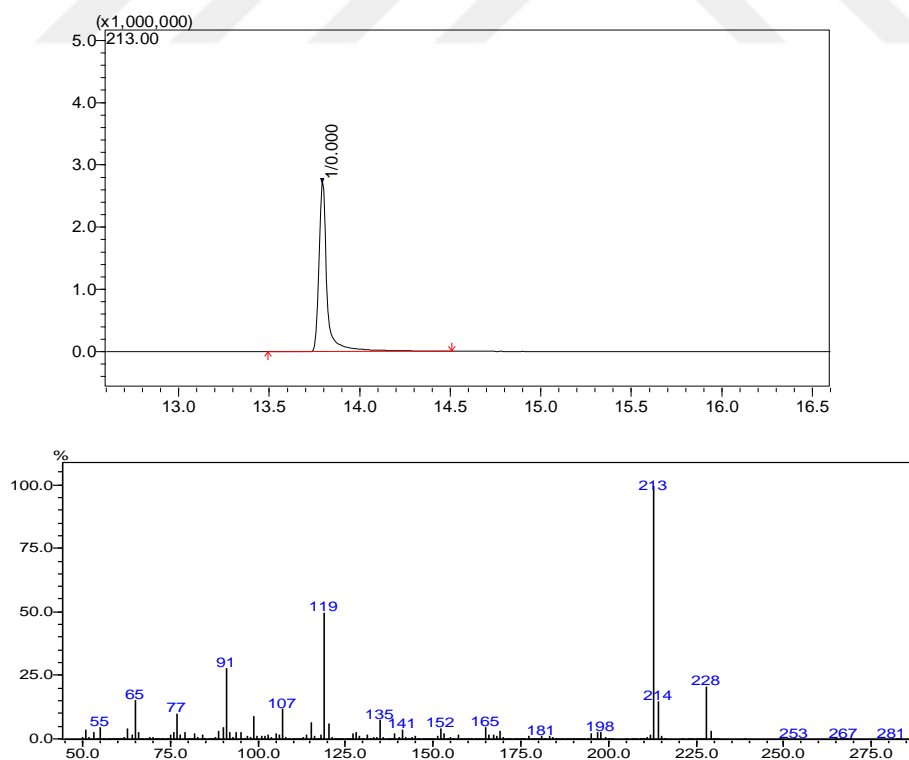


**Figure 3. 8.** Mass Chromatogram and Fragment Spectrum for BPA  
(Concentration: 10 ng injected; Retention time: 13.6 minutes; m/z: 213)

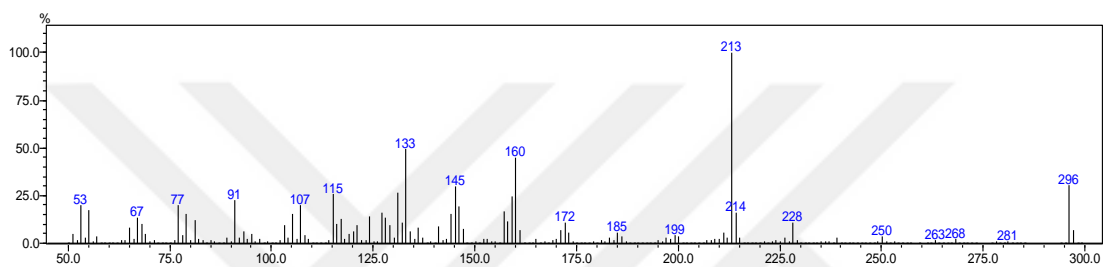
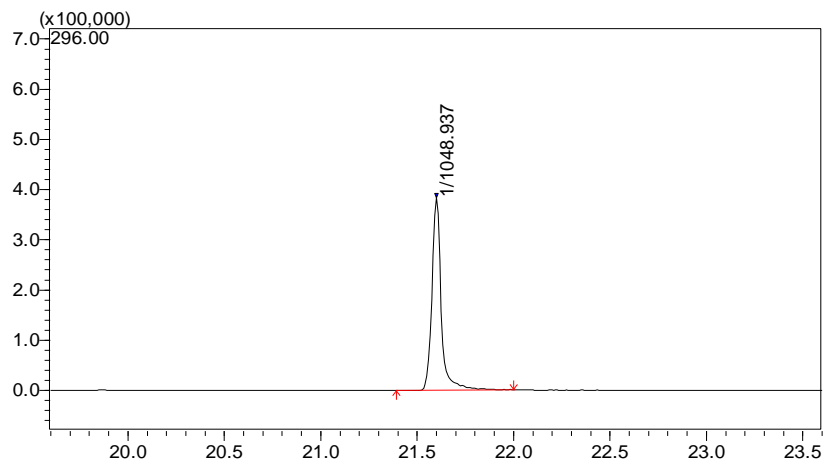


**Figure 3. 9.** Mass Chromatogram and Fragment Spectrum for EE2  
(Concentration: 10 ng injected; Retention time: 21.6 minutes; m/z: 296)

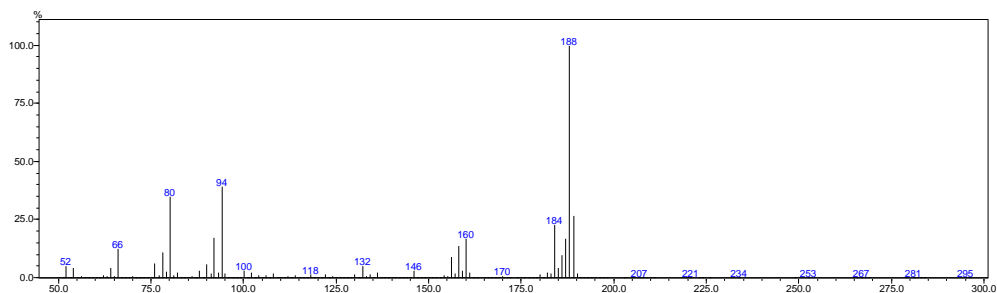
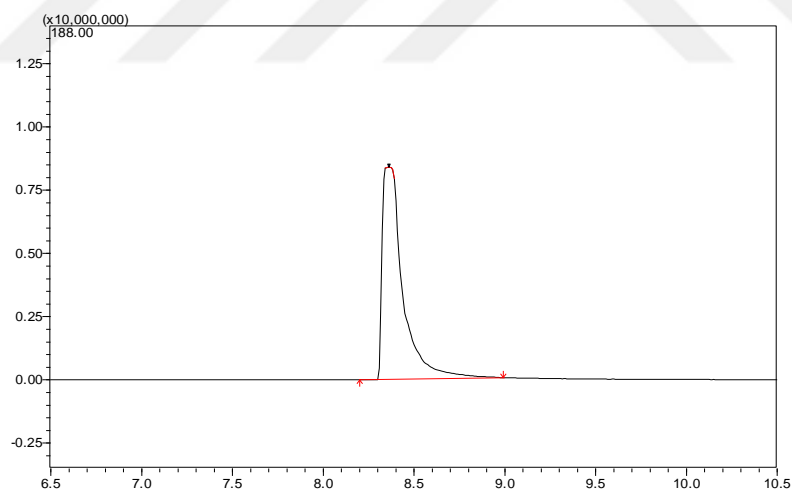


**Figure 3. 10.** Mass Chromatogram and Fragment Spectrum for anthracene-d10  
(Concentration: 10 ng injected; Retention time: 8.4 minutes; m/z: 188)

During GCMS analyses, reproducibility problems were encountered from time to time. Moreover, it was determined that the GCMS injector was frequently blocked. To avoid these problems, before each assay set, the syringe was cleaned with acetone in a sonication bath. Different syringe cleaning solvents were evaluated for the analyses and methanol was found to be the best option. On the other hand, methanol residuals can interfere with the results. To avoid this side effect, the syringe is washed with the sample three times before each injection.

The blockage in the GCMS column was another problem which was solved by the injection of different solvents before the analysis of each sample. The order of solvents was as follows: acetone, dichloromethane and hexane; so that the most polar solvent was injected first and the least polar solvent is injected last.

Although solvent cleaning applications improved the column performance; it posed another problem: MS detector was quickly contaminated because of the impurities continuously transported by these solvents. This problem was solved by changing the GCMS method during solvent analysis so that solvents do not accumulate in the MS detector. These applications solved the problems encountered during the GCMS analyses.

### **3.3. Adsorption studies**

#### **3.3.1. Adsorption equilibrium**

##### **3.3.1.1. Adsorption equilibrium for BPA**

Equilibrium studies were conducted at 25 °C by using pure MNP (magnetite), PhHL-MNP composite, chitosan-MNP composite, PhHL and chitosan for the removal of BPA. The obtained results are given in Figure 3.11.

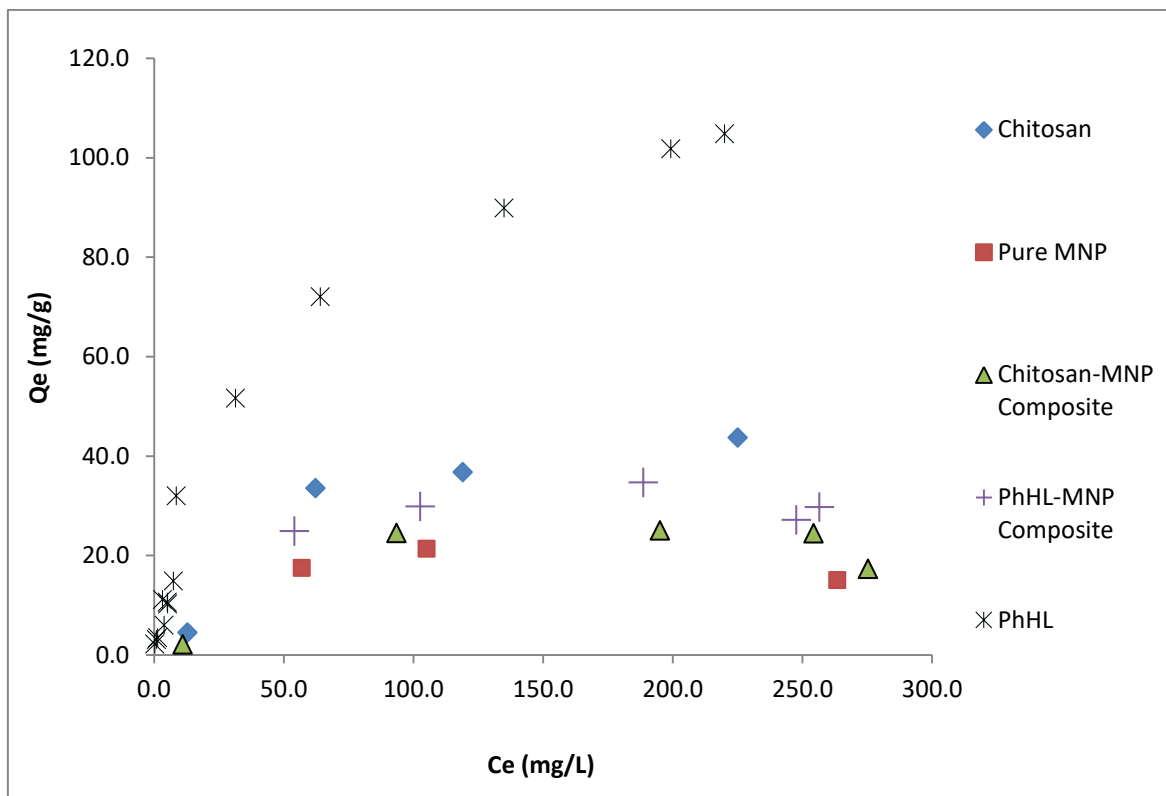


**Figure 3. 11.** Equilibrium data for BPA using different adsorbents

When the results given in Figure 3.11 are examined, it can be seen that the performances of the evaluated materials for BPA adsorption are in the following order:

PhHL >> Chitosan > PhHL-MNP composite > Chitosan-MNP composite > Pure MNP

The results obtained for different adsorbent materials and possible adsorption mechanisms are briefly described below:

The performance of PhHL for BPA adsorption was far better than the other adsorbents used in this study. The maximum amount of BPA adsorbed on unit weight of PhHL was 104.8 mg/g. The adsorption mechanism might involve interactions of -CH and -OH groups which are present in the PhHL structure with the functional groups of BPA molecule. This will be further investigated in detail in Section 3.3.4.

According to Figure 3.11, pure chitosan has the second highest adsorption potential (43.67 mg/g). It can be expected that hydroxyl and amino groups in chitosan polymeric chains which can serve as coordination and reaction sites, are effective in the adsorption



process (Inoue et al., 1993; Wu et al., 2001).

In this study, the maximum adsorption amounts obtained for PhHL-MNP composite and chitosan-MNP composite were 34.69 and 25.02 mg/g, respectively. These results obtained for composite materials are lower than that of pure biopolymers (i.e. PhHL and chitosan). This can be explained by the composition of the adsorbents. Since the amounts of biopolymers are lower in the composite materials, their effectiveness in the adsorption is low.

Among the evaluated materials, pure MNP has the lowest adsorption potential (21.34 mg/g). The adsorption mechanism of metal ions in aqueous systems by metal oxides (i.e. magnetite, maghemite, goethite and hematite) involves the exchange of metal ions, hydrolysis and electrostatic bonds between the metal ions and the oxide surfaces. On the other hand, inner-sphere complexation (Rakshit et al., 2013) may be the main adsorption mechanism for the adsorption of organic molecules by magnetite.

Since PhHL showed the highest adsorption potential among the other materials used in this study, its adsorption properties are further evaluated in the following sections.

### **Evaluation of isotherm models for BPA adsorption by PhHL**

In order to model the equilibrium data obtained for the adsorption of BPA by PhHL, two parameter isotherms (Langmuir, Freundlich) and three parameter isotherms (Sips and Dubinin-Astakhov) were evaluated which are among the most commonly used isotherms in the aqueous phase adsorption studies. Such models can be used to obtain useful information related to the surface characteristics, adsorbate-adsorbent affinity, adsorption capacity and favourability of the sorption process. The isotherm models used in this study are summarized in Table 3.2.

Langmuir isotherm model (Langmuir, 1918) describes monolayer adsorption onto homogeneous surface. This model is based on the assumptions of a surface containing a finite number of accessible sites with uniform energy of adsorption, reversible adsorption process and no interaction between adsorbed species.

Freundlich isotherm model (Freundlich, 1907) is widely used in heterogeneous surfaces with a non-uniform energetic distribution of active sites accompanied by interaction between adsorbed molecules. It is not limited to monolayer adsorption, and can be used

for multilayer adsorption. It suggests that sorption energy exponentially decreases upon the completion of adsorption process.

Sips isotherm (Sips, 1948) is an empirical model incorporating the properties of Langmuir and Freundlich isotherms. According to this model, the surface of the adsorbent can be homogeneous or heterogeneous. At low concentrations of adsorbate, Sips equation relatively reduces to Freundlich equation and at high concentration it predicts a monolayer adsorption capacity, characteristic of the Langmuir isotherm (Bergmann and Machado, 2015).

Dubinin-Radushkevich and Dubinin-Astakhov isotherms are among the most extensively used models for the adsorption processes in aqueous solutions. Dubinin-Radushkevich (D-R) is only a special case of Dubinin-Astakhov (D-A) model and it is not applicable for the systems described with a heterogeneity factor different than 2 (Inglezakis, 2007). As a result, in this study, D-A model was preferred over D-R model. D-A model was first developed for the adsorption of gases and vapours by microporous adsorbents (Dubinin and Astakhov, 1971). While there are different formulations for the application of D-A model in aqueous phase adsorption studies, the solubility-normalized form (Inglezakis, 2007; Kleineidam et al., 2002) is used in this study (Table 3.2).

The isotherm models applied to the experimental data along with the calculated parameters are presented in Table 3.2. Among the applied models, Langmuir, Sips and Dubinin-Astakhov showed good performance with high  $R^2$  but Sips isotherm had a slightly better fit to the experimental data with smaller values of  $\chi^2$  and NRMSE. The experimental data fitted with Sips model are given in Figure 3.12. The maximum adsorption capacity calculated by Sips model was found to be 126.6 mg/g (at 298 K).

**Table 3.2.** Isotherm models evaluated for the adsorption of BPA on PhHL

Model	Equation	Model Parameters	Goodness of fit measures
Langmuir	$q_e = \frac{Q_{max}^o K_L C_e}{1 + K_L C_e}$	$Q_{max}$ (mg/g) = 122.6 $K_L$ (L/mg) = 0.023	$R^2 = 0.990$ $\chi^2 = 12.552$ NRMSE = 0.0369
Freundlich	$q_e = K_F C_e^n$	$K_F$ ((mg/g)/(mg/L) <sup>n</sup> ) = 7.630 n = 0.496	$R^2 = 0.968$ $\chi^2 = 29.293$ NRMSE = 0.066
Sips	$q_e = \frac{q_m^S K_S C_e^{1/n_S}}{1 + K_S C_e^{1/n_S}}$	$q_m^S$ (mg/g) = 126.6 $K_S$ (mg/L) <sup>-1/n<sub>S</sub></sup> = 0.025 1/n <sub>S</sub> = 0.957	$R^2 = 0.990$ $\chi^2 = 12.045$ NRMSE = 0.0367
Dubinin-Astakhov	$q_e = q_{DA(max)} \cdot \exp \left\{ -K_{DA} \left[ RT \ln \left( \frac{C_S}{C_e} \right) \right]^{n_{DA}} \right\}$	$q_{DA(max)}$ (mg/g) = 104.987 $K_{DA}$ ((mol/kJ) <sup>n<sub>DA</sub></sup> ) = 0.001 n <sub>DA</sub> = 1.756	$R^2 = 0.990$ $\chi^2 = 14.256$ NRMSE = 0.0371

where  $q_e$  (mg/g) is the amount of BPA uptake at equilibrium;  $C_e$  (mg/L) is the equilibrium concentration of BPA;  $Q_{max}$  (mg/g) is the maximum adsorption capacity calculated from Langmuir model;  $K_L$  (L/mg) is the Langmuir constant;  $K_F$  ((mg/g)/(mg/L)<sup>n</sup>) is the Freundlich constant; n (dimensionless) is the Freundlich intensity parameter;  $q_m^S$  (mg/g) is the maximum adsorption capacity calculated from Sips model;  $K_S$  is the Sips equilibrium constant (mg/L)<sup>-1/n<sub>S</sub></sup>, 1/n<sub>S</sub> is the Sips heterogeneity constant;  $q_{DA(max)}$  (mg/g) is the maximum adsorption capacity estimated from Dubinin-Astakhov model;  $K_{DA}$  (mol/J)<sup>n<sub>DA</sub></sup> a constant related to the sorption energy;  $C_S$  (mg/L) is the aqueous solubility of BPA at the given temperature; n<sub>DA</sub> is the heterogeneity factor of Dubinin-Astakhov isotherm.

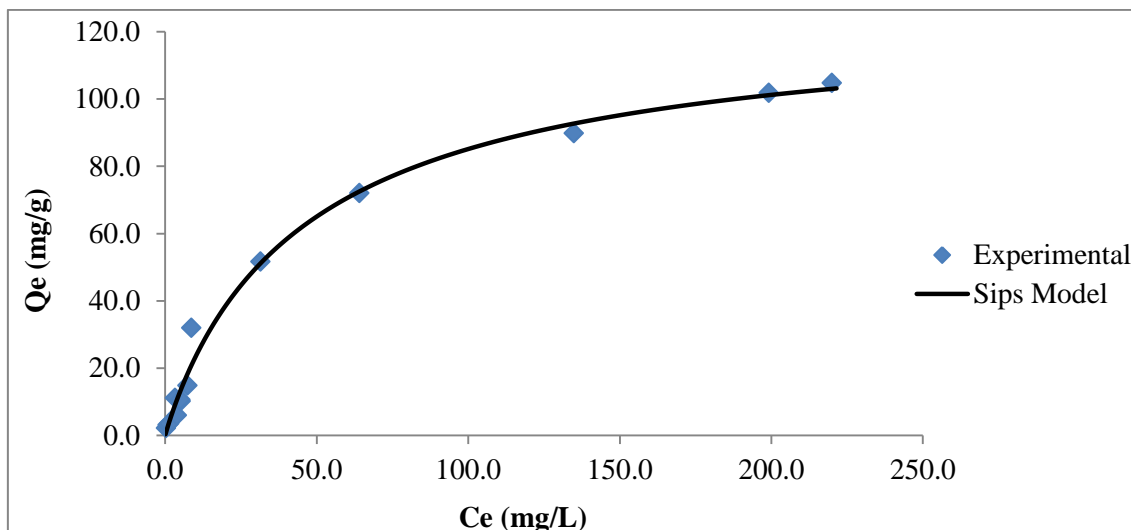


**Figure 3. 12.** Sips isotherm model for BPA adsorption by PhHL

In this study, the highest BPA adsorption amount was obtained by PhHL, where  $q_e$  was 104.8 mg/g (experimental) and 126.6 mg/g (Sips model). In order to compare these results, the other adsorbents used for the adsorption of BPA in the literature are evaluated.

There are many different adsorbents used for the removal of BPA from aqueous solutions which are reviewed recently (Bhatnagar and Anastopoulos, 2017). Among different adsorbents, some materials are shown to have very high adsorption capacity for BPA, such as powdered activated carbon (PAC) and CoFe<sub>2</sub>O<sub>4</sub>/PAC composite (Li et al., 2014), where the maximum adsorption capacities were determined as 771.2 and 727.2 mg/g, respectively. In another study, commercial carbon modified by thermal treatment (Liu et al., 2009) is used and its maximum adsorption capacity was found as 430.33 mg/g. Libbrecht et al. (2015) evaluated mesoporous carbon (hard templated) for BPA adsorption and showed that its maximum adsorption capacity was 447 mg/g (Libbrecht et al., 2015). Activated carbon prepared from potato peels was also effective in BPA removal with a maximum adsorption capacity of 454.62 mg/g (Arampatzidou and Deliyanni, 2016). The maximum adsorption capacity of hydrophobic mesoporous molecular sieves was 416.7 mg/g (Liu et al., 2016) while that of mesostructured metal-organic framework MIL-53(Al) was 472.7 mg/g (Zhou et al., 2013).

The adsorption capacities of the materials mentioned above are higher than that of obtained in this study.

However, those materials may not always be economically feasible or easily accessible. In this study, the highest adsorption capacity is obtained for a biopolymer, PhHL. Therefore, the adsorption capacity of PhHL is compared with other biopolymers used for BPA removal in the literature. When comparing the results of different studies, it is important to consider experimental conditions applied in each study. For this reason, a detailed comparison table is prepared (Table 3.3).

**Table 3.3.** Comparison of BPA adsorption on PhHL with other biopolymer based materials

Material Used	Maximum adsorption amount (mg/g)	Conditions	Ref.
Phosphonated levan	104.8 (Experimental) 126.6 (Sips model)	T = 298 K; pH = 6.6 (solution pH was not adjusted) Adsorbent dose = 0.5 g/L; Ci_BPA = 1-300 mg/L	<b>This study</b>
Chitosan	34.48 for laboratory synthesized chitosan 27.02 for commercial chitosan (Langmuir model)	Ambient temperature; pH = 5 Adsorbent dose = 0.06 g/L ; Ci_BPA = 0.1 g/L	(Dehghani et al., 2016)
Lignin	237.07 (Langmuir model)	T = 296 K; pH = 6.0 Adsorbent dose = 33-10,000 mg/L; Ci_BPA = 0.33-300 mg/L	(W. Han et al., 2012)
Porous $\beta$ -cyclodextrin polymer	22 (Experimental) 88 (Langmuir model)	Ambient temperature; pH = neutral pH Adsorbent dose = 1 g/L; Ci_BPA= 0.1 mM	(Alsaiee et al., 2016)
$\beta$ -cyclodextrin hydroxypropyl methylcellulose hydrogels	14.6 (Dubinin-Radushkevitch model)	T = 298 K; pH = 5.5 Adsorbent dose = 10 g/L; Ci_BPA = 4.57 - 99.54 mg/L	(de Souza and Petri, 2018)
Graphene oxide- $\beta$ -cyclodextrin nanocomposite	373.4 (Langmuir model)	T = 298 - 328 K; pH = 9 Adsorbent dose = 0.4 – 1 g/L; Ci_BPA = 100 mg/L	(Gupta et al., 2017)
Citric acid-crosslinked $\beta$ -cyclodextrin	83 (0.3636 mmol/g) (Langmuir model)	T = 298 K; pH = 6.3 Adsorbent dose = 1 g/ L; Ci_BPA = 10 - 400 mg/L	(Huang et al., 2018)
$\beta$ -cyclodextrin–carboxymethylcellulose-based hydrogels	38.12 (Langmuir model)	T = 298 K; pH = not adjusted Adsorbent dose = 1 g/L; Ci_BPA = 0.05- 0.25 mmol/L	(Kono et al., 2013)

(Table 3.3. Continued)

Material Used	Maximum adsorption amount (mg/g)	Conditions	Ref.
Magnetic iron oxide-guar gum ester nanocomposite	111.11 (Langmuir model)	T = 298 K; pH = 3 Adsorbent dose = 1 g/L; Ci_BPA = 20 - 400 mg/L	(Abdullah et al., 2016)
Polyacrylamide-lignin composite	55.358 mg/g (Langmuir model)	T = 298 K; pH = 1-12 Adsorbent dose = 10 g/L; Ci_BPA = 0.44–4.4 mmol/L	(Şimşek and Ulusoy, 2018)
Molecularly imprinted polymer based on $\beta$ -cyclodextrin modified magnetic chitosan	105.5 mg/g (Langmuir model)	T = 298 K; pH = 6 Adsorbent dose = 0.4 g/L; Ci_BPA = 10 – 600 mg/L	(Huang et al., 2017)
Amphoteric $\beta$ -cyclodextrin-based adsorbent	79 mg/g (Experimental) 94.1 mg/g (Langmuir model)	T = 298 K; pH = 6.5 Adsorbent dose = 1 g/L; Ci_BPA = 25 – 250 mg/L	(Zhou et al., 2018)
$\beta$ -cyclodextrin functionalized mesoporous magnetic clusters	52.7 mg/g (Langmuir model)	T = 303 K; pH = 6.5–7.0 Adsorbent dose = 1 g/L; Ci_BPA = 4-130 mg/L	(Lee and Kwak, 2018)
Hyper-crosslinked $\beta$ -cyclodextrin porous polymer	278 mg/g (Langmuir model)	T = 298 K; pH: not adjusted Adsorbent dose = 0.25 g/L; Ci_BPA = 5 – 150 mg/L	(X. Li et al., 2018)
$\beta$ -cyclodextrin capped graphene-magnetite nanocomposite	59.6 (Experimental) 66 mg/g (Langmuir model)	T = 298 K; pH = 6 Adsorbent dose = 0.5 g/L; Ci_BPA = 10-200 mg/L	(Ragavan and Rastogi, 2017)

T: Temperature

Ci\_BPA : initial BPA concentration

According to Table 3.3, among different biosorbents, lignin, graphene oxide- $\beta$ -cyclodextrin nanocomposite and hyper-crosslinked  $\beta$ -cyclodextrin porous polymer showed high adsorption capacities which were obtained by Langmuir model as 237.07 mg/g, 373.4 mg/g and 278 mg/g, respectively. The fourth highest adsorption capacity was obtained for PhHL (this study) with the maximum adsorption capacity obtained by Sips model as 126.6 mg/g. When compared with other bio-based sorbents, it can be concluded that PhHL has a relatively high adsorption capacity for BPA. These results demonstrate that PhHL holds a high potential for the application as an adsorbent for BPA.

### 3.3.1.2. Adsorption equilibrium for EE2

The results of the equilibrium studies for EE2 adsorption using pure MNP, PhHL-MNP composite, chitosan-MNP composite, PhHL and chitosan are given in Figure 3.13.

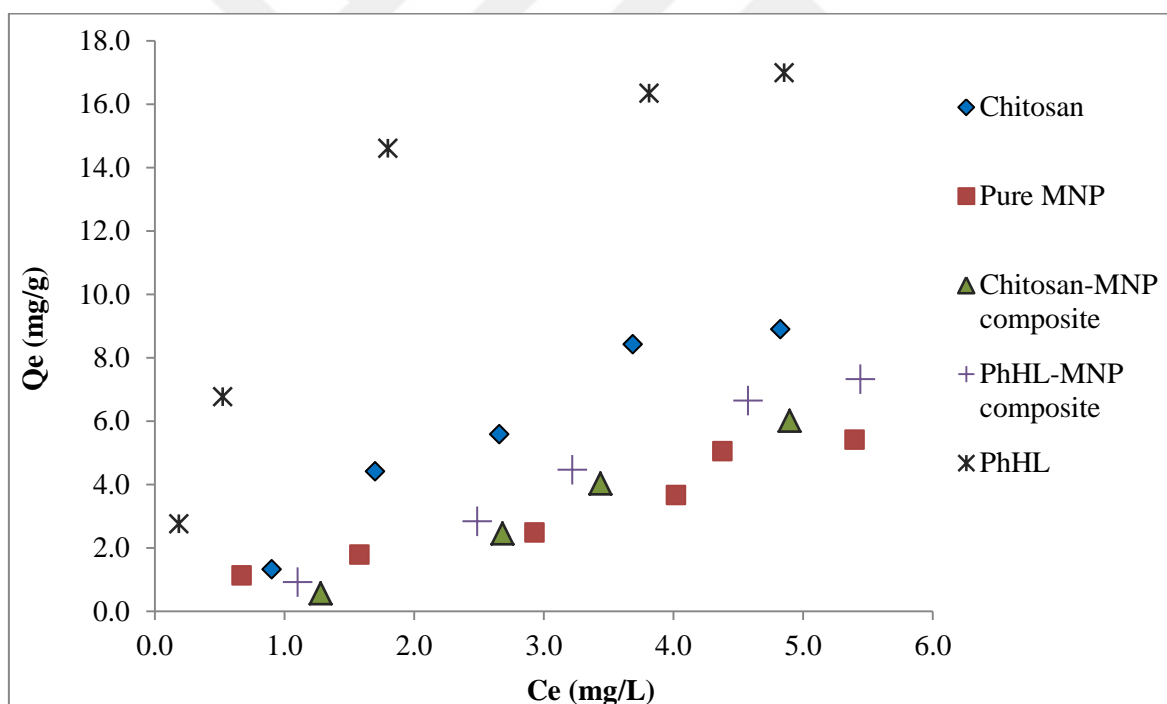


**Figure 3. 13.** Equilibrium data for EE2 using different adsorbents

From Figure 3.13 it can be seen that PhHL has the highest adsorption capacity (16.98 mg/g) for the removal of EE2. The second highest adsorption capacity was obtained for pure chitosan (8.89 mg/g). The results for the other adsorbent materials i.e. pure MNP, PhHL-MNP composite and chitosan-MNP composite were very close to each other but



PhHL-MNP composite had slightly higher adsorption capacity. The maximum amount of EE2 adsorbed per unit weight of PhHL-MNP composite was 7.32 mg/g while that of chitosan-MNP composite and pure MNP were 6.01 and 5.41 mg/g, respectively.

Similar to the results obtained for BPA, the results for EE2 adsorption was highest when PhHL was used as adsorbent. Thus, the adsorption properties of PhHL for EE2 were further investigated in the following sections.

### Evaluation of isotherm models for EE2 adsorption by PhHL

Langmuir, Freundlich, Sips and Dubinin-Astakhov isotherms were applied to model the adsorption of EE2 by PhHL and the obtained results are given in Table 3.4.

**Table 3.4.** Isotherm models evaluated for the adsorption of EE2 on PhHL

Model	Model Parameters	Goodness of fit measures
Langmuir	$Q_{\max}$ (mg/g) = 20.94 $K_L$ (L/mg) = 0.998	$R^2 = 0.988$ $\chi^2 = 0.226$ NRMSE = 0.027
Freundlich	$K_F$ ((mg/g)/(mg/L) <sup>n</sup> ) = 9.28 n = 0.424	$R^2 = 0.926$ $\chi^2 = 1.413$ NRMSE = 0.065
Sips	$q_m^S$ (mg/g) = 18.13 $K_S$ (mg/L) <sup>-1/n<sub>S</sub></sup> = 1.598 1/n <sub>S</sub> = 1.404	$R^2 = 0.997$ $\chi^2 = 0.086$ NRMSE = 0.012
Dubinin-Astakhov	$q_{DA(max)}$ (mg/g) = 23.71 $K_{DA}$ ((mol/kJ) <sup>n<sub>DA</sub></sup> ) = 1.23x10 <sup>-07</sup> n <sub>DA</sub> = 3.197	$R^2 = 0.978$ $\chi^2 = 0.4003$ NRMSE = 0.035

When Table 3.4. is examined, the best fitting isotherm model for EE2 adsorption by PhHL is found to be Sips isotherm with high  $R^2$  (0.997) and small  $\chi^2$  (0.086) and NRMSE (0.012). The equilibrium data with the fitted Sips model is given in Figure 3.14.

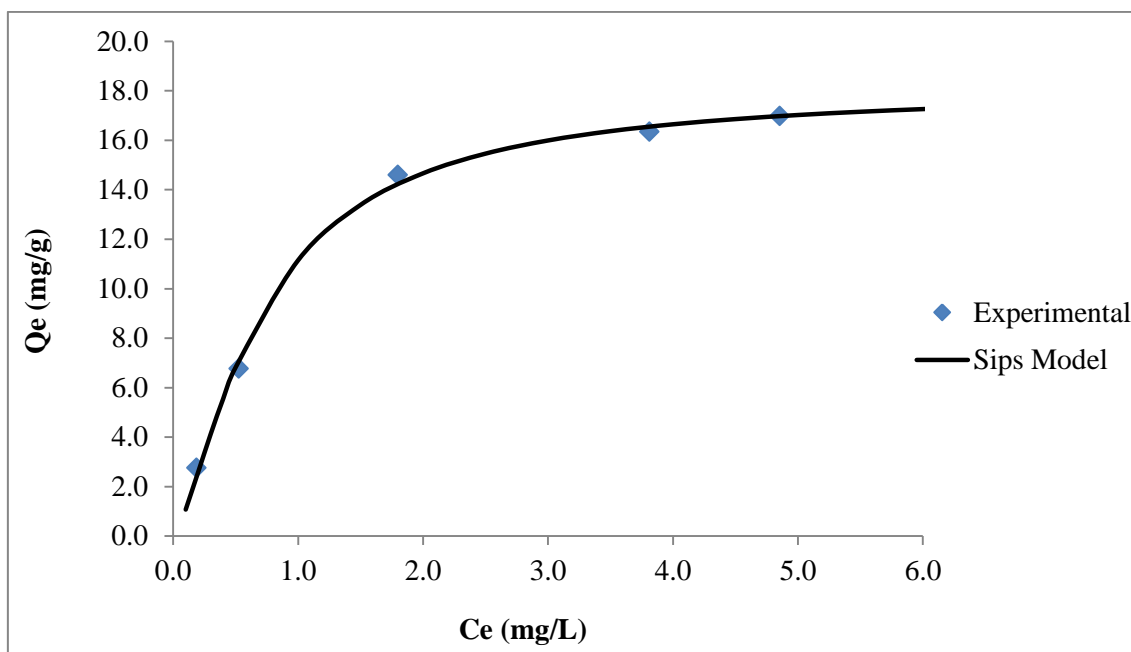


**Figure 3. 14.** Sips isotherm model for EE2 adsorption by PhHL

For both BPA and EE2 adsorption by PhHL, the best fitting isotherm was Sips model which implies that the surface active sites of the PhHL have different affinities for the adsorbate material. This is expected since biosorbents have complex structures, with the binding sites not all identical and there may be interferences between each binding site during biosorption (Hammes, 2000; Liu and Liu, 2008). On the other hand, the Sips heterogeneity constant ( $1/n_s$ ) is close to unity indicating that the isotherm approaches to Langmuir equation and the adsorbent has relatively energetically homogenous binding sites.

The results obtained for EE2 removal in this study are compared with the results from other studies. There are a limited number of adsorbents evaluated for EE2 removal in the literature. These studies are given in Table 3.5. When Table 3.5 is evaluated, there are some high removal amounts such as single-walled carbon nanotubes (209 mg/g), activated carbon (174 mg/g), multi-walled carbon nanotubes (65.34 mg/g), benchmark macroreticular polymeric adsorbent (35.6 mg/g) and aliphatic polyamide (24.8 mg/g). However, the adsorption capacities of the other adsorbents listed in Table 3.5 are lower than that is obtained in this study (18.13 mg/g for PhHL). As a result, PhHL can be considered as a promising adsorbent for EE2 removal from aqueous solutions.

**Table 3.5.** Comparison of EE2 adsorption on PhHL with other materials

<b>Material Used</b>	<b>Maximum adsorption amount</b>	<b>Conditions</b>	<b>Ref.</b>
Phosphonated levan	16.98 mg/g (Experimental) 18.13 mg/g (Sips model)	T = 298 K; pH = 6.2 (solution pH was not adjusted) Adsorbent dose = 0.5 g/L; Ci_EE2 = 1-9 mg/L	<b>This study</b>
Hypersol-macronet polymers and GACs	0.39 $\mu\text{mol/g}$ for MN 250 (hypersol macronet polymer) 0.9 $\mu\text{mol/g}$ for WV-A 1100 (GAC) (Experimental)	T = 298 K; pH = 4 Ci_EE2 = 4 $\mu\text{g/L}$ ; (Different adsorbent doses were used)	(Saha et al., 2010)
GAC	163 $\mu\text{g/g}$ (Experimental)	Influent C_EE2 = 10-15 $\mu\text{g/L}$ (from fixed-bed study)	(De Rudder et al., 2004)
Iron (hydr)oxide modified activated carbon fibers	1.3 mg/g - 1.8 mg/g (Experimental)	pH = 7; Ci_EE2 = 500 $\mu\text{g/L}$	(Hristovski et al., 2009)
Carbon nanomaterials (CNMs)	SWCNT: 209 mg/g MWCNT: 47.4 mg/g Fullerene: 0.139 mg/g AC: 174 mg/g (Experimental)	pH = 7; Ci_EE2 = 0.3-3.3 mg/L Solid/liquid (w/v) ratios: 1:100–1:200 for fullerene; 1:20000–1:120000 for CNMs and AC	(Pan et al., 2010)

(Table 3.5. Continued)

Material Used	Maximum adsorption amount	Conditions	Ref.
Multi-walled carbon nanotubes	For SiO <sub>2</sub> /CNTs (0:1): Q <sub>max_Langmuir</sub> : 65.34 mg/g K <sub>Freundlich</sub> : 493.3 (mg/g)/(mg/L) <sup>1/n</sup> ; n: 1.08 For Al <sub>2</sub> O <sub>3</sub> /CNTs (1:1): Q <sub>max_Langmuir</sub> : 61.95 mg/g K <sub>Freundlich</sub> : 416.3 (mg/g)/(mg/L) <sup>1/n</sup> ; n: 1.05	T = 298 K; pH = 6.3 Adsorbent dose = 50 mg/L; C <sub>EE2</sub> = 0.02 - 0.4 mg/L	(Sun et al., 2015)
SWCNTs	For seawater Q <sub>max_Langmuir</sub> : 35.46 mg/g log K <sub>Freundlich</sub> : 3.39 n <sup>-1</sup> : 0.463 For brackish water Q <sub>max_Langmuir</sub> : 35.71 mg/g log K <sub>Freundlich</sub> : 3.71; n <sup>-1</sup> : 0.347	Adsorbent dose = 0 - 50 mg/L; C <sub>i_EE2</sub> = 1 μM (Ambient temperature)	(Joseph et al., 2011a)
SWCNTs	For landfill leachate Q <sub>max_Langmuir</sub> : 120 mg/g log K <sub>Freundlich</sub> : 4.57; n <sup>-1</sup> : 0.194	Adsorbent dose = 20 - 200 mg/L; C <sub>i_EE2</sub> = 10 μM (Ambient temperature)	(Joseph et al., 2011b)
Black tea leaves waste (TLH) and GAC	2.44 mg/g for TLH 2.97 mg/g for GAC (Langmuir model)	T = 298 K; pH= 3-9 Adsorbent dose = 0.1 - 0.8 g/200 ml; C <sub>EE2</sub> = 2 mg/L	(Ifelebuegu et al., 2015)

(Table 3.5. Continued)

<b>Material Used</b>	<b>Maximum adsorption amount</b>	<b>Conditions</b>	<b>Ref.</b>
AC from from agro-industrial waste	7.88 mg/g (Sips model)	T = 298 K; pH = 6 Adsorbent dose = 1.50 g/L; C <sub>i</sub> _EE2 = 1.00 - 15.0 mg/L	(Rovani et al., 2014)
Aliphatic polyamide (PA612) and benchmark macroporous polymeric adsorbent (Amberlite XAD4)	24.8 mg/g for PA612 35.6 mg/g for Amberlite XAD4 (Langmuir model)	T = 298 K Adsorbent dose = 0.2 g/L; C <sub>i</sub> _EE2 = 150 - 6000 µg/L	(J. Han et al., 2012)
CTAB/MCM-41 composites.	9.5 mg/g (Experimental)	Adsorbent dose = 1 g/L; C <sub>i</sub> _EE2 = 0.5 - 25 mg/L (Room temperature)	(Ribeiro-Santos et al., 2016)
Montmorillonite intercalated with CTA <sup>+</sup>	4.3-8.8 mg/g (Experimental)	T = 298 K; pH = 2 - 10 Adsorbent dose = 1 g/L; C <sub>i</sub> _EE2 = 0 - 25 mg/L	(Burgos et al., 2016)
Activated charcoal	7.47 µg/g (Langmuir model)	T = 298 K; pH = 7 Adsorbent dose = 5 g/L; C <sub>i</sub> _EE2 = 25-100 µg/L	(Kumar and Mohan, 2011)

### 3.3.2. Comparison of the adsorption amounts of BPA and EE2

Among different materials evaluated, the highest adsorption capacities were observed with PhHL for both BPA and EE2. The maximum adsorption amounts obtained for BPA and EE2 were 104.8 mg/g and 16.98 mg/g, respectively. Since the solubility limit of EE2 (9.20 mg/L) is lower than that of BPA (300 mg/L) (Shareef et al., 2006), the adsorption capacities obtained for BPA and EE2 were compared by considering these limits. The equilibrium data for BPA and EE2 for the data points below the initial concentration of 9.20 mg/L are given in Figure 3.15. From this figure, it can be observed that EE2 is adsorbed to a higher extent than BPA. The properties of these materials influencing the extent of the adsorption are discussed below.

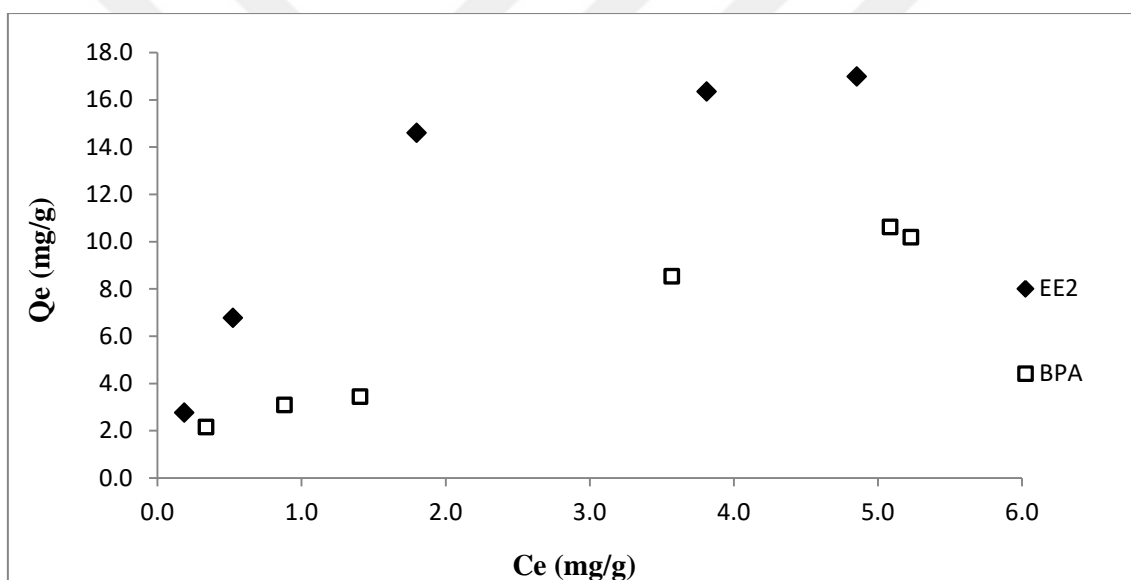


**Figure 3. 15.** Adsorption isotherms of PhHL for BPA and EE2

There are different attributes of the sorbate materials that can influence the adsorption process. Based on previous studies (Calvet, 1989; Cooney, 1998; Reinbold, 1979) these factors are summarized below:

- Molecular size
- Hydrophobicity
- Molecular charge and polarity
- Molecular structure and functional groups

### Effects of molecular size

The structure of BPA and EE2 are given together in Figure 3.16 for comparison. It can be observed that EE2 is a larger molecule than BPA. The maximum molecular size (between the hydroxyl groups of both aromatic rings) of bisphenol A is estimated to be 0.94 nm (9.4 Å) (Kameda et al., 2007) and the maximum size of EE2 molecule is given as 12.137 Å (Karounou, 2004; Saha et al., 2010).

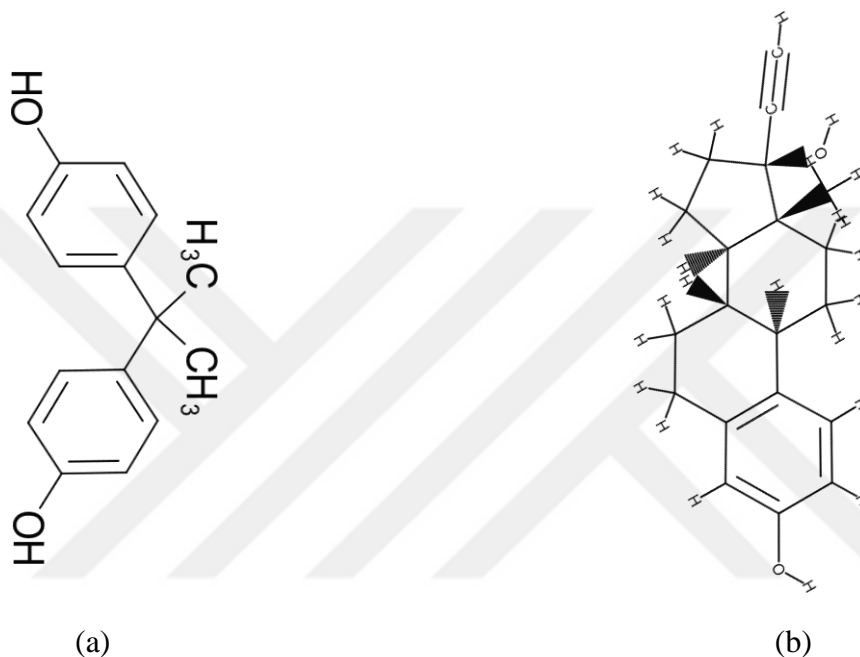


**Figure 3.16.** Comparison of BPA (a) and EE2 (b) molecules

As the size of the organic molecule increases, the adsorption process is usually enhanced especially for homologous series (Cooney, 1998). This generalization is based on Traube's rule which was originally developed for describing the dependence of surface tension on the molecule size (Traube, 1884) and extended to adsorption process (Freundlich and Hatfield, 1926; Holmes and Kelvey, 1928). In general, the larger the molecule to be sorbed, the higher the contribution of molecular interactions to the adsorption potential. Thus, the higher adsorption amount observed for EE2 compared to BPA can be explained by the larger molecular size of EE2.

There is also a limit for the Traube's rule: the pores of the adsorbent may become inaccessible when the molecule size of the sorbate is large enough. In this case, increasing the molecular size may decrease the adsorption capacity (Reinbold, 1979).

For example, higher adsorption amount onto granular activated carbons and Macronet polymers was observed for 17  $\beta$ -estradiol (E2) when compared to EE2. This result was explained by the smaller size of E2 molecule than that of EE2 molecule. It was noted that the extra ethinyl group of EE2 may restrict this molecule from accessing into some of the micropores of the adsorbents due to size exclusion (Karounou, 2004; Saha et al., 2010). On the other hand, the adsorbents used in this study mainly consist of meso and macropores as discussed in SEM results (Section 3.1.1). As a result, the size exclusion is not a problem in this case and larger molecule (EE2) is adsorbed to a higher extent than BPA due to the higher contribution of molecular interactions.

### **Effects of hydrophobicity**

Hydrophobicity is an important molecular property of the sorbate materials. It indicates the preferential migration and accumulation of organic molecules in hydrophobic solvents or on hydrophobic surfaces (Sims et al., 1990). The measures of hydrophobicity include solubility, octanol/water partition coefficient and organic carbon/water partition coefficient. These properties with their relation to the experimental results obtained in this study are briefly discussed below.

The aqueous solubility of BPA (300 mg/L) is higher than that of EE2 (9.20 mg/L). There is generally an inverse relationship between water solubility and adsorption, especially for weakly polar and nonpolar compounds (Calvet, 1989; Carringer et al., 1975; Gerstl and Mingelgrin, 1984). This generalization is valid for the results in this study since higher adsorption potential is observed for EE2 which has lower aqueous solubility than BPA. The reason can be explained by the fact that the solubility reflects the degree of attraction of the solute molecules by the solvent (Cooney, 1998), thus, the solute molecules with higher solubility tend to remain in the aqueous phase.

The octanol/water partition coefficient ( $K_{OW}$ ) is the ratio of the concentration of a compound in octanol to that in water at equilibrium. Generally, there is a correlation between  $K_{OW}$  value of a hydrophobic non-polar organic molecule and its adsorption potential (Byrns, 2001; Dobbs et al., 1989). The materials which have low log  $K_{OW}$  values (<1) are relatively hydrophilic and those which have high log  $K_{OW}$  values (>4) are very hydrophobic (Lyman et al., 1990). Thus, adsorption processes including



hydrophobic interactions are favored for the materials with high log  $K_{OW}$  values. Based on the relation of  $K_{OW}$  value and the accumulation of hydrophobic contaminants in sewage sludge solids, Rogers (1996) suggested the following guide (Rogers, 1996):

**Log  $K_{OW}$  < 2.5:** low sorption potential

**Log  $K_{OW}$  > 2.5 and < 4.0:** medium sorption potential

**Log  $K_{OW}$  > 4.0:** high sorption potential

Log  $K_{OW}$  value of BPA is 3.32 (Hansch et al., 1995) indicating that it has a medium sorption potential and that of EE2 is given as 3.67 (Kuster et al., 2004) and 4.15 (Lai et al., 2000), indicating that it has a medium to high sorption potential. In this study, EE2 with higher log  $K_{OW}$  value is adsorbed to a higher extent than BPA, which is in accordance with the above generalization.

The organic carbon/water partition coefficient ( $K_{OC}$ ) is also an important parameter for the adsorption of organic molecules.  $K_{OC}$  is the ratio of the concentration of the solute in the solid organic carbon phase to the concentration of the solute in the aqueous phase. In the literature, different  $K_{OC}$  values are reported for EDCs since this parameter is dependent on the adsorbent material used for its determination. Ying et al. (2003) reported the  $K_{OC}$  values of BPA and EE2 as 778 ml/g and 4840 ml/g respectively, using aquifer material (Ying et al., 2003). This parameter can be used for the determination of the mobility of organic compounds in soils as shown in Table 3.6.

**Table 3.6.** Mobility classification based on  $K_{OC}$  values (FAO, 2000)

<b><math>K_{OC}</math> (ml/g)</b>	<b>Log <math>K_{OC}</math></b>	<b>Mobility Class</b>
<b>&lt; 10</b>	< 1	Highly Mobile
<b>10-100</b>	1-2	Mobile
<b>100-1,000</b>	2-3	Moderately Mobile
<b>1,000 - 10,000</b>	3-4	Slightly Mobile

<b>10,000 - 100,000</b>	4-5	Hardly Mobile
<b>&gt; 100,000</b>	> 5	Immobile

The  $K_{OC}$  value of BPA (778 ml/g) indicates that it is moderately mobile in soils. The  $K_{OC}$  value of EE2 (4840 ml/g) shows that it is slightly mobile in soils. This parameter also indicates that adsorption of EE2 to organic carbon is expected to be more favorable than that of BPA. Thus, higher adsorption amount obtained for EE2 can also be explained by the higher  $K_{OC}$  value of EE2 when compared to that of BPA.

### **Effects of molecular charge, polarity, structure and functional groups**

Although molecular charge and polarity are important determinants of adsorption process, most EDC molecules are neutral, including BPA and EE2. Their adsorption can take place via the interaction of their functional groups with the surface groups of the adsorbents. BPA has two phenol groups and EE2 has one phenol group which is effective in the pi interaction mechanisms. Moreover, EE2 has an ethynyl group. LaGrega et al. (2010) stated that the unsaturated (double or triple-carbon bond) organic molecules are more easily adsorbed than saturated (single-carbon bond) organic molecules (LaGrega et al., 2010). The effects of these functional groups in the adsorption mechanism and the possible interactions will be further discussed in section 3.3.4.

### **3.3.3. Adsorption kinetics**

Kinetic models may be used to evaluate the performance of the adsorbents for the removal of target EDCs from aqueous solutions. In this study, three well-known kinetic models, pseudo-first order (PFO), pseudo-second order (PSO) and Elovich models are applied to explain the experimental data.

Based on Lagergren's kinetics equation (Lagergren, 1898), pseudo-first order equation is described as follows (Ho and McKay, 1998):

$$q_t = q_e(1 - e^{-k_1t}) \quad (3.2)$$

where,  $q_t$  and  $q_e$  are the amounts of BPA or EE2 adsorbed (mg/g) at time,  $t$  (min) and at equilibrium;  $k_1$  is the rate constant of pseudo-first order equation (1/min).

Pseudo-second order kinetic model (Blanchard et al., 1984; Ho, 2006; Ho et al., 1996) is given in Equation 3.3.

$$q_t = \frac{q_e^2 k_2 t}{1 + q_e k_2 t} \quad (3.3)$$

where,  $q_t$  and  $q_e$  are the amounts of BPA or EE2 adsorbed (mg/g) at time,  $t$  (min) and at equilibrium;  $k_2$  is the rate constant of pseudo-second order equation g/(mg·min).

Another widely used kinetic model is Elovich equation (Equation 3.4), developed by the contributions of different authors (Aharoni and Tompkins, 1970).

$$q_t = \frac{1}{\beta} \ln(1 + \alpha\beta t) \quad (3.4)$$

where,  $q_t$  is the amount of BPA or EE2 adsorbed (mg/g) at time,  $t$  (min);  $\alpha$  and  $\beta$  are constants. The constant  $\alpha$  (mg/(g·min)) can be regarded as the initial sorption rate (Low, 1960; Taylor and Thon, 1952) and  $\beta$  (g/mg) is related to the extent of surface coverage and activation energy for chemisorption (Cheung et al., 2000).

Intraparticle diffusion model (Weber and Morris, 1963) is also commonly used for kinetic modelling of the adsorption data. This model is based on plotting the adsorbed concentration versus the square root of time according to Equation 3.5.

$$q_t = k_{id}\sqrt{t} + C \quad (3.5)$$

However, Schwaab et al. (2017) criticized the use of the square root approach. They explained that this approach is only valid at the beginning of batch adsorption process, when bulk concentration is not significantly decreased and solid can be considered as a semi-infinite diffusion medium (Schwaab et al., 2017). As a result, the square root approach is not used in this study. Schwaab et al. (2017) suggested the use of finite bath approach instead of square root approach. However, the equations suggested for finite bath approach necessitate the inclusion of some predetermined constants (fluid and surface diffusivities, particle radius, density and porosity). Since these constants were not previously determined for the adsorbents used in this study, the finite bath approach suggested by Schwaab et al. (2017) is not used in this study.

### 3.3.3.1. Adsorption kinetics for BPA

The kinetic data obtained for BPA removal by PhHL is shown in Figure 3.17. As can be seen in Figure 3.17, adsorption reaches equilibrium in 360 minutes. The aforementioned kinetic models were tested on the obtained kinetic data. Tran et al. (2017) reported that for the most accurate modelling of kinetic data, adsorption kinetics data collection should be started at an initial time of less than 2 min and finish when the adsorption process reaches equilibrium (Tran et al., 2017). Regarding this concern, during kinetic studies, data collection was started in the first minute and the equilibrium data (the data points corresponding to 1440 and 1500 minutes) were not included in further model fitting efforts.

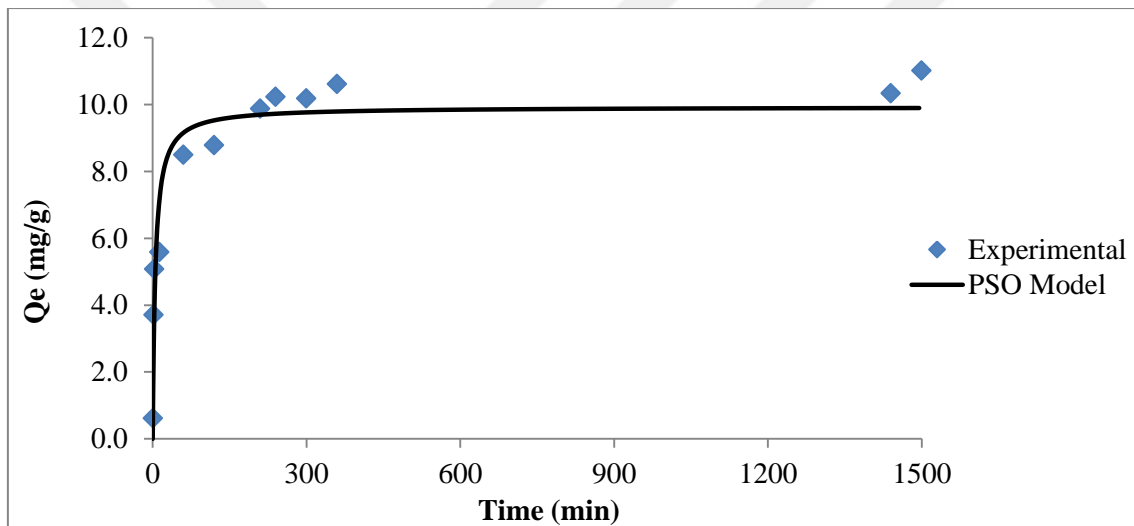


**Figure 3. 17.** Kinetic data and PSO model fit for BPA adsorption by PhHL

The evaluated kinetic models and the calculated model constants with the measure of goodness of fit parameters are given in Table 3.7. According to these results, pseudo-second order (PSO) model best describes the experimental data (low Chi square, high  $R^2$ , and low NRMSE values) with a PSO rate constant of 0.020 g/(mg·min).

**Table 3.7.** Evaluation of kinetic models for BPA adsorption by PhHL

Model	Model Constants	R <sup>2</sup>	χ <sup>2</sup>	NRMSE
PFO	$k_1 = 0.142 \text{ min}^{-1}$	0.854	3.220	0.123
PSO	$k_2 = 0.020 \text{ g}/(\text{mg}\cdot\text{min})$	0.920	2.004	0.091
Elovich	$\alpha = 9.496 \text{ mg}/(\text{g}\cdot\text{min})$ $\beta = 0.789 \text{ g}/\text{mg}$	0.916	2.377	0.093

### 3.3.3.2. Adsorption kinetics for EE2

The kinetic data obtained for BPA removal by PhHL is shown in Figure 3.18. From this figure, the equilibrium time can be determined as 120 minutes.

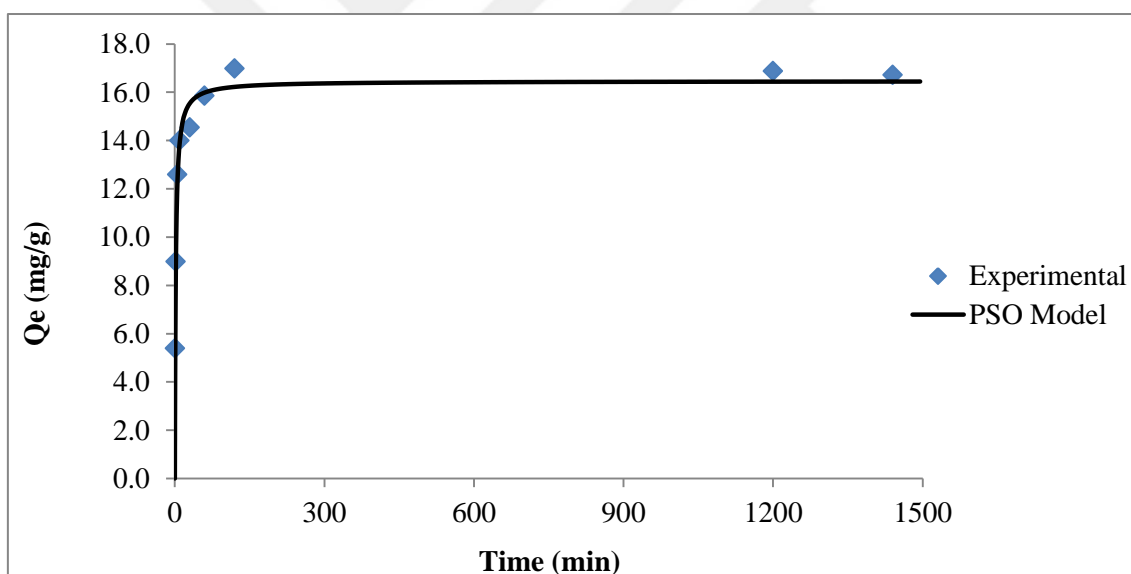


**Figure 3. 18.** Kinetic data and PSO model fit for EE2 adsorption by PhHL

PFO, PSO and Elovich kinetic models were applied to the obtained experimental kinetic data. The results are given in Table 3.8. From Table 3.8, it can be concluded that PSO model best describes the kinetic data with a rate constant ( $k_2$ ) of 0.034 g/(mg·min).

**Table 3.8.** Evaluation of kinetic models for EE2 adsorption by PhHL

<b>Model</b>	<b>Model Constants</b>	<b>R<sup>2</sup></b>	<b>χ<sup>2</sup></b>	<b>NRMSE</b>
<b>PFO</b>	$k_1 = 0.402 \text{ min}^{-1}$	0.944	0.397	0.065
<b>PSO</b>	$k_2 = 0.034 \text{ g}/(\text{mg}\cdot\text{min})$	0.978	0.174	0.040
<b>Elovich</b>	$\alpha = 9.241 \text{ mg}/(\text{g}\cdot\text{min})$ $\beta = 0.335 \text{ g}/\text{mg}$	0.698	12.651	0.180

In this study, both BPA and EE2 adsorption by PhHL were well described by PSO model. Ho and McKay (1999) reported that application of simple kinetic models (e.g. first- or second-order models) to a sorption with solid surfaces which are rarely homogeneous is generally not suitable since the effects of transport phenomena and chemical reactions are often experimentally inseparable (Ho and McKay, 1999). However, the PhHL is a relatively homogenous material as discussed in the Section 3.3.1. Therefore, the kinetic data of this study can be described by the PSO model.

#### **3.3.4. Adsorption mechanism**

There are several possible mechanisms for the adsorption process. Classification of these mechanisms is important to better evaluate complex processes. However, in the literature, there are many different classification schemes for the adsorption mechanisms. In this study, different classifications suggested for the molecular interactions and the adsorption mechanisms (Anslyn and Dougherty, 2006; Crini et al., 2018; Robalds et al., 2016) are evaluated and the main adsorption mechanisms are listed as follows:

- Physisorption:** Van der Waals interactions (forces of orientation, induction and/or dispersion)  
Electrostatic interactions (hydrogen bonding, halogen bonding)  
Pi-interactions

Hydrophobic interactions  
Diffusion into the network of the material

**Chemisorption:** Complexation (including coordination and/or chelation)  
Covalent bonding

**Ion-exchange**

**Microprecipitation**

There is a debate in the literature for the classification of the adsorption mechanisms. For example, Srivastava and Goyal (2010) classified ion exchange as a sub-group of chemisorption (Srivastava and Goyal, 2010). On the other hand, Robalds et al. (2016) classified ion exchange as a separate mechanism (Robalds et al., 2016).

Febrianto et al. (2009) included coordination, complexation and chelation processes among possible mechanisms of biosorption (Febrianto et al., 2009). However, it was noted that the correct statement should be as follows: “complexation (including coordination and/or chelation)” (Robalds et al., 2016).

Crini et al. (2018) classified physisorption to include surface adsorption, van der Waals interactions, hydrogen bond, hydrophobic interactions, diffusion into the network of the material and Yoshida's interaction (Crini et al., 2018). On the other hand, some authors indicate that physisorption results from electrostatic and van der Waals interactions (Davis et al., 2003; Podstawczyk et al., 2014; Robalds et al., 2016). While Crini et al. (2018) classified microprecipitation, surface precipitation and proton displacement as the sub-groups of precipitation mechanism, Robalds et al. (2016) classified only microprecipitation among the main classes of adsorption mechanisms.

Another concern is related to CH- $\pi$  interaction. Nishio et al. (1998) stated that CH- $\pi$  interaction can be the weakest hydrogen bond (Nishio et al., 1998). However, Tsuzuki and Fujii (2008) claimed that the nature and the physical origin of CH/ $\pi$  interaction are significantly different from conventional hydrogen bonds (Tsuzuki and Fujii, 2008).

Moreover, there is a debate on the difficulty of identifying adsorption mechanisms for some new materials (Wilson et al., 2016). Morin-Crini et al. (2018) explained the reason of this difficulty by the fact that adsorption process may involve different interactions

that can occur simultaneously, which makes the interpretation of the results complicated. Each mechanism may play a role of varying importance depending on the type of the materials used and the experimental conditions. Regarding these concerns, determination of the relative importance of each contribution to the adsorption mechanism is stated to be complicated. Furthermore, in recent years different mechanisms have been taken into consideration (e.g. the role of the macromolecular network formed by the cross-linking agent in the case of cross-linked cyclodextrin polymers) and the synthesis process of the adsorbent materials become more important (Morin-Crini et al., 2018).

### **Adsorption mechanism of BPA by PhHL**

According to the kinetic experiments, pseudo-second order (PSO) model was found to best fit the experimental data. Although adsorption processes following PSO kinetics are usually attributed to chemisorption process, in recent studies, it is emphasized that fitting kinetic models is not enough to explain the mechanism of adsorption (Khamizov et al., 2018a, 2018b; Lima et al., 2015; Tran et al., 2017). In order to explain the adsorption mechanism, it is necessary to prove the formation of some chemical bonds using some analytical techniques i.e. FTIR, XPS, Raman spectroscopy, thermogravimetric analysis and thermodynamic data (Lima et al., 2015; Litter et al., 2018). In this study, FTIR and XPS analyses were used to elucidate the adsorption mechanism.

The FTIR spectra of PhHL samples before and after the BPA adsorption are given in Figure 3.19 (a) and (b). For comparison, the FTIR spectrum of the pure BPA is also given (Figure 3.19 (c)). In PhHL spectrum after BPA adsorption, new peaks between 800-1800  $\text{cm}^{-1}$  can be observed which are in accordance with the characteristic peaks of BPA. However, these changes are not intense, indicating that adsorption is weak.



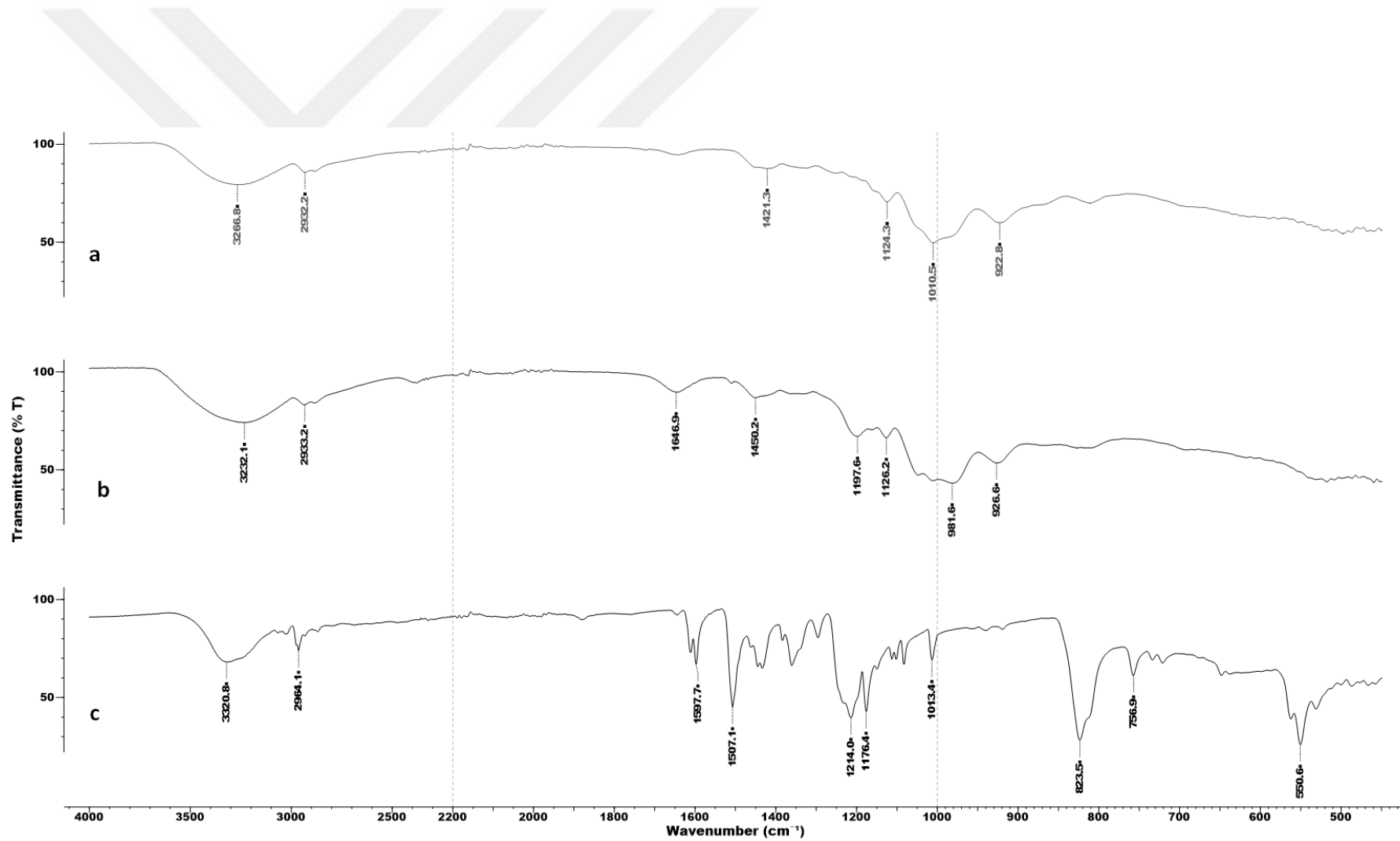


**Figure 3. 19.** FTIR Results of pure PhHL (a), PhHL after BPA adsorption (b), pure BPA (c)

As can also be seen in Figure 3.19, the absorption band corresponding to O–H stretching vibration in the FTIR spectrum of PhHL was widened and shifted from 3266  $\text{cm}^{-1}$  to 3232  $\text{cm}^{-1}$  after BPA adsorption. This change can be explained by the occurrence of the intermolecular OH- $\pi$  bonds (Capelluto, 2013) between the hydroxyl groups of the PhHL and  $\pi$  bonds of BPA, and the intermolecular hydrogen bonds (Kim et al., 2011; Xu et al., 2012) between hydroxyl groups of PhHL and BPA.

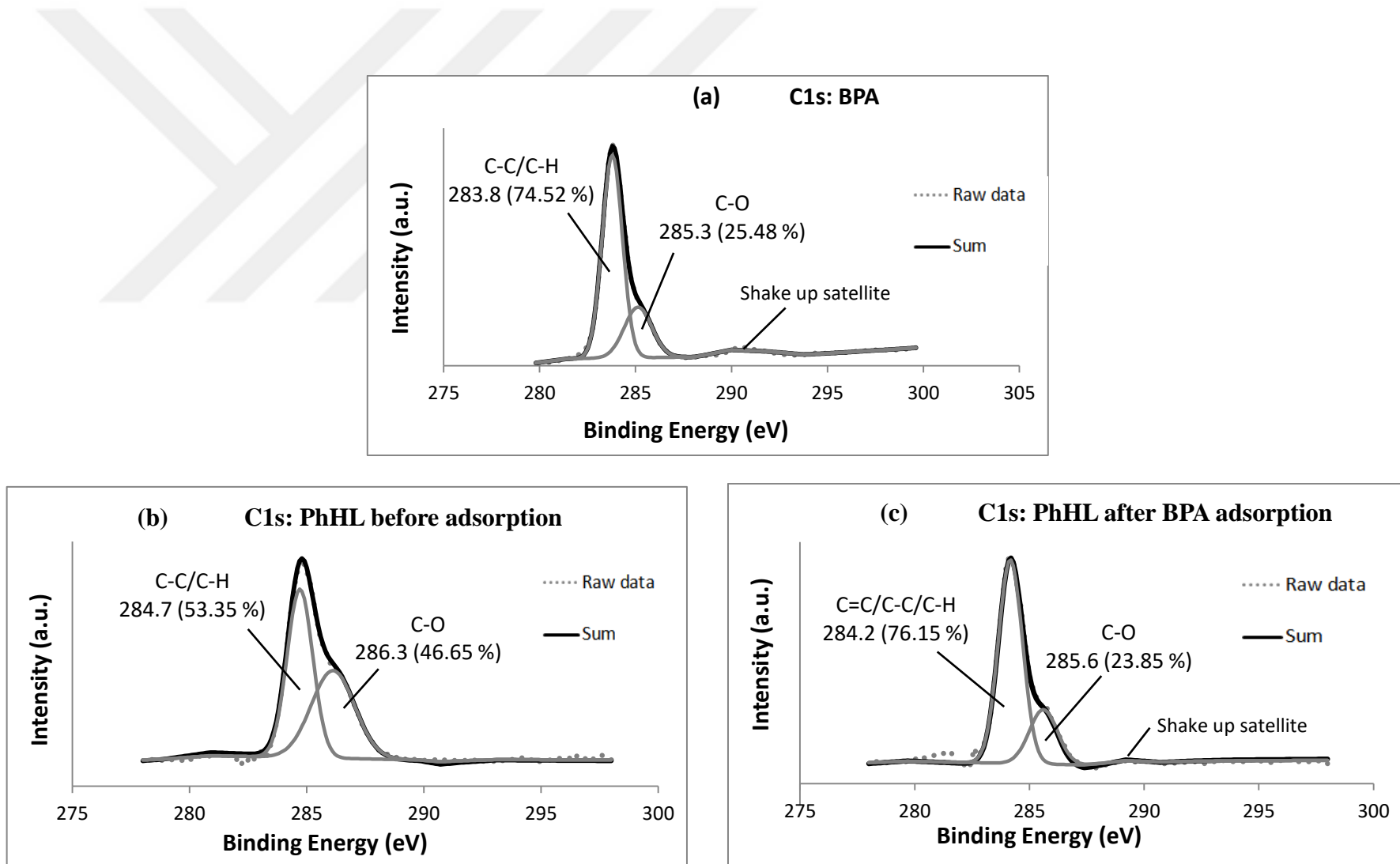
Moreover, the peak associated with C–H bending in PhHL (1421  $\text{cm}^{-1}$ ) is widened and shifted to 1450  $\text{cm}^{-1}$  after BPA adsorption. The aromatic rings in BPA contain the electron-rich  $\pi$  systems which can interact with the partial positive charges on H atoms in CH groups of PhHL (Nishio, 2011; Nishio et al., 1998; Okawa et al., 1982). Therefore, the observed changes in C–H bending band of PhHL is attributed to the possible CH- $\pi$  interactions. Nishio and Hirota (1989) classified the CH- $\pi$  interaction as a weak hydrogen bond occurring between a soft acid and a soft base in reference to the Pearson hard and soft acid base principle (Nishio and Hirota, 1989; Pearson, 1966).

Figure 3.20 shows the XPS spectra of C1s for BPA (a), PhHL before adsorption (b) and PhHL after BPA adsorption (c). In the Figure 3.20 (a), the C1s spectra for BPA could be deconvoluted into two major components at 283.8 and 285.3 eV, which are assigned to C-C/C-H (Kanchi et al., 2018) and C-O (Y. Li et al., 2018) peaks, respectively. In this figure, a shake up satellite at around 291 eV appears which is due to the benzene rings of BPA (Sakai et al., 2009). In the Figure 3.20 (b), the C1s spectra for PhHL before adsorption was deconvoluted into two major components at 284.7 eV (C-C/C-H) and 286.3 eV (C-O).

The XPS spectra of O1s for BPA, PhHL before adsorption and PhHL after BPA adsorption are given in Figure 3.21 (a), (b) and (c), respectively. The O1s spectra of BPA (Figure 3.21 (a)) contains a single peak at 533.1 eV which is assigned to C-OH (Halevy et al., 2017). This result is expected since BPA contains a single type of oxygen bond corresponding to the hydroxyl group attached to the aromatic rings. The O1s spectra of PhHL before the adsorption (Figure 3.21 (b)) was deconvoluted into two peaks: 531.7 eV (C-O-C) and 533.4 eV (C-OH) (Halevy et al., 2017).

The observed changes in the XPS spectra of PhHL after adsorption (Figure 3.20 (c) and 21 (c)) are summarized below and the possible reasons of these changes are explained.

- In the C1s spectrum, the percent area of C-C/C-H peak increased from 53.35% to 76.15% after BPA adsorption. On the other hand, the percent area of C-O peak decreased from 46.65% to 23.85%. This change can be attributed to the interaction of the benzene rings of BPA with the C-H and C-OH groups of PhHL.  
The large surfaces of the benzene rings may cover the H atoms of C-H and C-OH groups of PhHL. Since BPA has a higher carbon to oxygen ratio compared to PhHL, C-C/C-H content of PhHL increases and C-O content decreases after BPA adsorption (Capelluto, 2013).
- The C1s peaks of PhHL were slightly shifted to a lower binding energy after BPA adsorption, which can be explained by the increase in electron cloud density (ECD) due to the electron shift from the pi bonds of BPA benzene rings to PhHL. As a result of the increase in ECD, the C1s electrons of PhHL after BPA adsorption are less strongly attracted by the nucleus. Consequently, the C1s electrons have lower binding energies after adsorption (Wang and Linford, 2015).
- In the C1s spectrum for PhHL, a shake-up satellite peak appears after BPA adsorption. The shake-up satellite peak is due to the resonance in the benzene ring structure, therefore, its presence is indicative of effective adsorption of BPA on PhHL (Sakai et al., 2009).
- In the O1s spectrum, the percent area corresponding to C-O-C peak was 32.07% for PhHL before the adsorption and it slightly decreased to 25.26% after the BPA adsorption. The percent area of the C-OH peak, on the other hand, increased from 67.93% to 74.74%. These changes suggest that the C-O-C content of PhHL decreases and its C-OH content increases after BPA adsorption due to the presence of C-OH groups on BPA molecule.



**Figure 3. 20.** XPS spectra of C1s for BPA (a) PhHL before adsorption (b) PhHL after BPA adsorption (c)

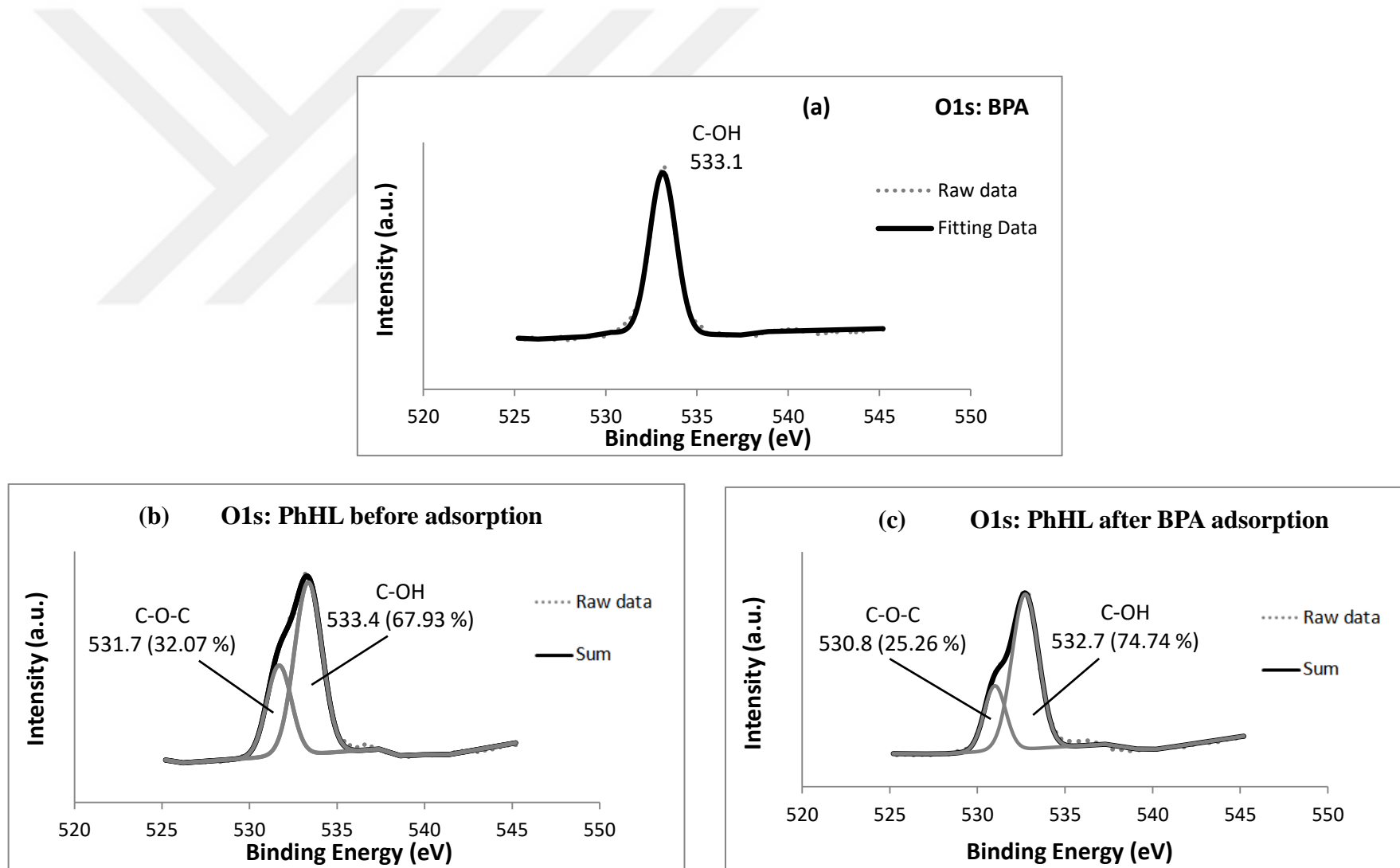


**Figure 3. 21.** XPS spectra of O1s for BPA (a) PhHL before adsorption (b) PhHL after BPA adsorption (c)

### **Adsorption mechanism of EE2 by PhHL**

FTIR spectra of PhHL samples before and after EE2 adsorption and that of pure EE2 are given in Figure 3.22. When the FTIR results of PhHL before and after EE2 adsorption are compared, changes in the peak structures can be observed between 800-1800  $\text{cm}^{-1}$ . Similar to the case of BPA adsorption, these changes are not intense, thus, it can be concluded that the adsorption is weak.

In the Figure 3.22, the absorption band corresponding to O–H stretching vibration in the FTIR spectrum of PhHL was widened and shifted from 3240.8  $\text{cm}^{-1}$  to 3230.2  $\text{cm}^{-1}$  after EE2 adsorption. This change in the O–H stretching vibration band can be attributed to the occurrence of the intermolecular OH- $\pi$  bonds (Capelluto, 2013) between the hydroxyl groups of the PhHL and  $\pi$  bonds of EE2, and the hydrogen bonds (Kim et al., 2011; Xu et al., 2012) formed between the hydroxyl groups of PhHL and EE2.

The peak associated with C–H bending in PhHL at around 1453  $\text{cm}^{-1}$  is changed in shape with decreased intensity after EE2 adsorption. This change in the C–H bending band of PhHL is ascribed to the CH- $\pi$  interactions between the CH groups of PhHL and benzene ring of EE2.

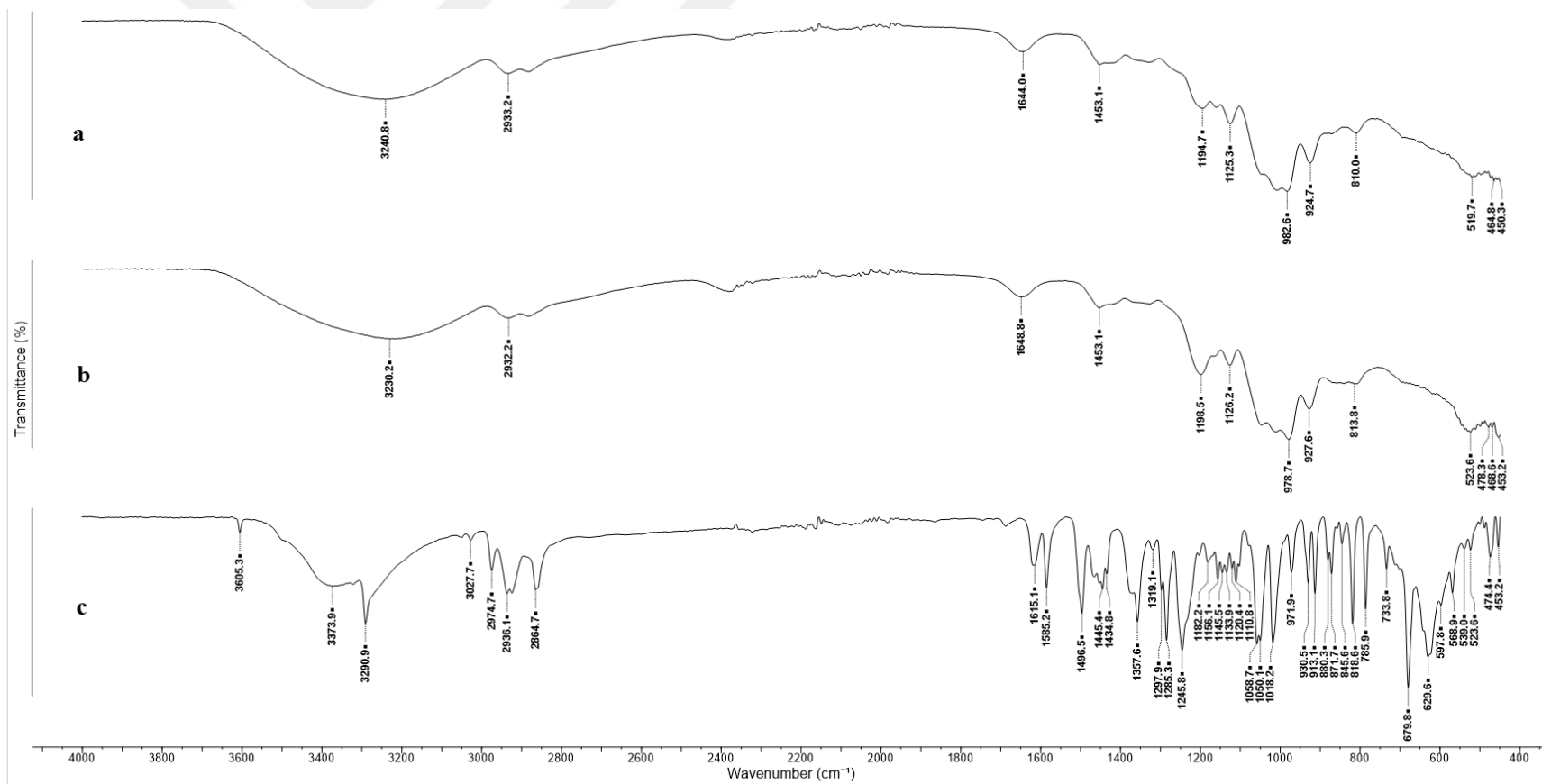


**Figure 3. 22.** FTIR Results of pure PhHL (a) PhHL after EE2 adsorption (b) pure EE2 (c)

The XPS analysis results of C1s spectra for EE2, PhHL before adsorption and PhHL after EE2 adsorption are given in Figure 3.23. The C1s spectra for EE2 (Figure 3.23 (a)) was deconvoluted into two major components at 284.6 and 285.9 eV, which can be assigned to C-C/C-H and C-O peaks, respectively. Moreover, there is a shake-up satellite peak at around 291 eV, which indicates the presence of benzene ring in the EE2 structure (Sakai et al., 2009).

As previously explained for the Figure 3.21 (b), the C1s spectra for PhHL before adsorption was deconvoluted also into two major components (C-C/C-H at 284.7 eV and C-O at 286.3 eV). When the C1s spectra for PhHL before adsorption (Figure 3.23 (b)) and PhHL after EE2 adsorption (Figure 3.23 (c)) are compared, it can be noted that the percent area of C-O peak decreased from 46.65% to 35.29% while that of C-C/C-H peak increased from 53.35% to 64.71% after EE2 adsorption. This result can be explained by the interaction of the benzene ring of EE2 with the C-H and C-OH groups of PhHL. The EE2 molecule has a lower C/O ratio compared to PhHL. Thus, it causes an increase in the C-C/C-H content and a decrease in the C-O content of PhHL upon adsorption. Moreover, after EE2 adsorption a shake-up satellite peak appears in the C1s spectra, which is due to the resonance in the benzene ring structure. This indicates the effective adsorption of EE2 on PhHL (Sakai et al., 2009).

Figure 3.24 shows the O1s spectra for EE2, PhHL before adsorption and PhHL after EE2 adsorption. The O1s spectra for EE2 (Figure 3.24 (a)) contains a single peak at 533.1 eV corresponding to C-OH. The O1s spectra for PhHL before adsorption (Figure 3.24 (b)) was deconvoluted into two peaks: C-O-C (531.7) and C-OH (533.4) (Halevy et al., 2017).

In the O1s spectra for PhHL after EE2 adsorption, the percent area corresponding to C-O-C peak was decreased from 32.07% to 22.99% and that of the C-OH peak increased from 67.93% to 77.01%. These results can be explained by an increase C-OH content and a decrease in the C-O-C content of PhHL upon EE2 adsorption resulting from the presence of C-OH groups on EE2 molecule.

The P2p spectra for PhHL before adsorption and PhHL after EE2 adsorption are given in Figure B1 (Appendix B). When these two spectra are compared, it can be concluded that there is not a significant change in the P2p spectra upon adsorption.



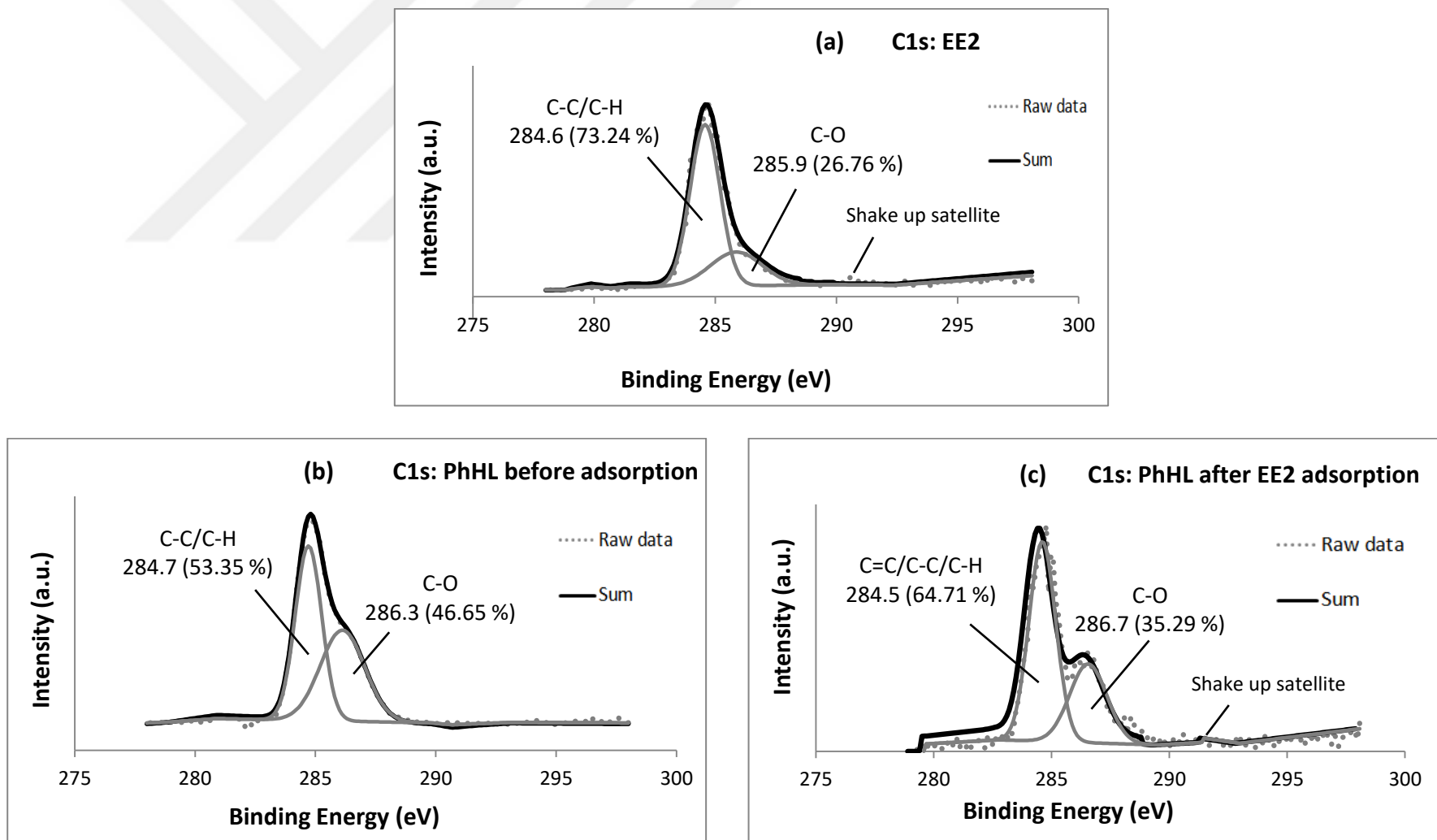
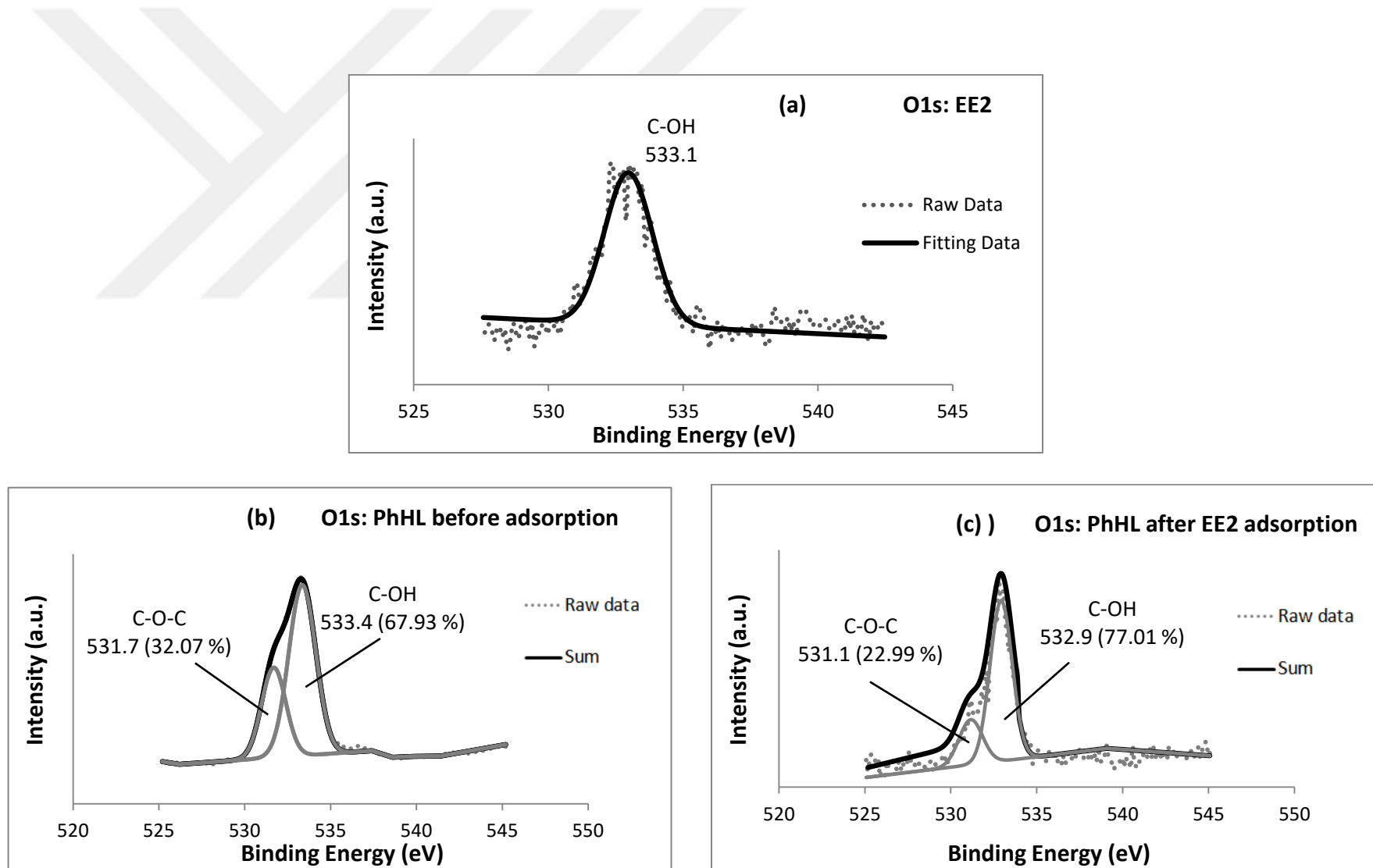


Figure 3. 23. XPS spectra of C1s for EE2 (a) PhHL before adsorption (b) PhHL after EE2 adsorption (c)



**Figure 3. 24.** XPS spectra of O1s for EE2 (a) PhHL before adsorption (b) PhHL after EE2 adsorption (c)

Based on the FTIR and XPS results, the adsorption mechanism of BPA and EE2 by PhHL is estimated to include OH- $\pi$  and CH- $\pi$  interactions. These interactions are explained in detail in the following part.

### **Pi-interactions**

Aromatic compounds contain a circular  $\pi$ -bond where electron density cloud is evenly distributed above and below the ring. This electron density cloud exhibits a partial negative charge. This negatively charged region can interact with positively charged species (Ma and Dougherty, 1997). A simple illustration of the interaction of  $\pi$  system with (C or O)-H groups is given in Figure 3. 25.

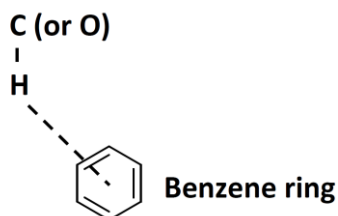


**Figure 3. 25.** Illustration of the  $\pi$  interaction

The ability of aromatic compounds to behave as electron donor in hydrogen bonding was recognized as early as in 1950s (Nishio et al., 1998; Tamres, 1952). Due to the advances in the analytical techniques such as FTIR, nuclear magnetic resonance (NMR) spectroscopy, XPS and XRD, the nature of  $\pi$  interactions was further revealed.  $\pi$  interactions are classified among noncovalent molecular interactions. These interactions involve different types of functional groups such as: cation- $\pi$ , anion- $\pi$ , CH- $\pi$ , OH- $\pi$ , NH- $\pi$  and  $\pi$ - $\pi$  groups.

The magnitude of the energies associated with the  $\pi$  interactions depends on the complexity of the molecules involved in the interaction. The energy range for cation- $\pi$  interaction is given as 2-50 kJ/mol (Nadeau, 2017). For other types of  $\pi$  interactions, the energy range can be given as 4.3-14 kJ/mol, based on different studies (Ran and Wong, 2006; Shibasaki et al., 2006; Sinnokrot et al., 2002). For comparison, the energy ranges of physical (or weak) adsorption and chemical adsorption are given below (Shibasaki et al., 2006):

- Physical (or weak) adsorption: 20–40 kJ/mol
- Chemical adsorption: 100–400 kJ/mol

When the energy ranges given above are compared, the adsorption processes involving pi interactions can be classified as physical (or weak) adsorption.

In this study, according to the FTIR and XPS results, the adsorption mechanism of BPA and EE2 by PhHL is estimated to be based on OH-pi and CH-pi interactions. Although OH-pi and CH-pi interactions are sources of weak attraction (Nishio, 2011; Tsuzuki and Fujii, 2008), this can be an advantage when considering desorption and reuse of PhHL which will be discussed in the section 3.3.5.

The knowledge of the adsorption mechanism may contribute to the design of new and effective adsorbent materials. For example, it is possible to synthesize a novel adsorbent, which contains different functional groups to improve OH-pi and CH-pi interactions with different EDC molecules leading to enhanced adsorption properties.

### **3.3.5. Desorption and reuse studies**

Desorption and reusability is important for large scale use of an adsorbent and its economic feasibility. In this study, desorption and reuse cycles were repeated for three times for BPA and EE2, and the obtained results are given in the following sections.

#### **3.3.5.1. Desorption and reuse studies for BPA**

Initially, the amount of BPA adsorbed per gram of PhHL was 9.82 mg/g, and it was reduced to 7.01 mg/g after the third adsorption desorption cycle. The obtained results for desorption and reuse studies are shown in Figure 3.26. From these results, it can be concluded that the adsorption capacity of PhHL towards BPA decreased by 28.6 % after the third cycle under the given desorption conditions.

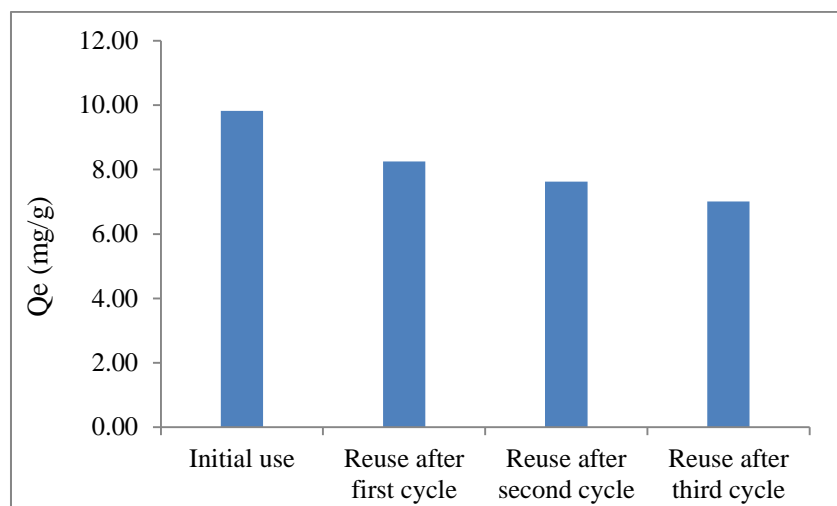


**Figure 3. 26.** Results of reuse studies for BPA adsorption by PhHL

### 3.3.5.2. Desorption and reuse studies for EE2

The results for desorption and reuse studies for EE2 are shown in Figure 3.27. The amount of EE2 adsorbed per unit weight of PhHL decreased from 16.98 mg/g to 11.76 mg/g at the end of the third adsorption desorption cycle, corresponding to a 30.7 % reduction.

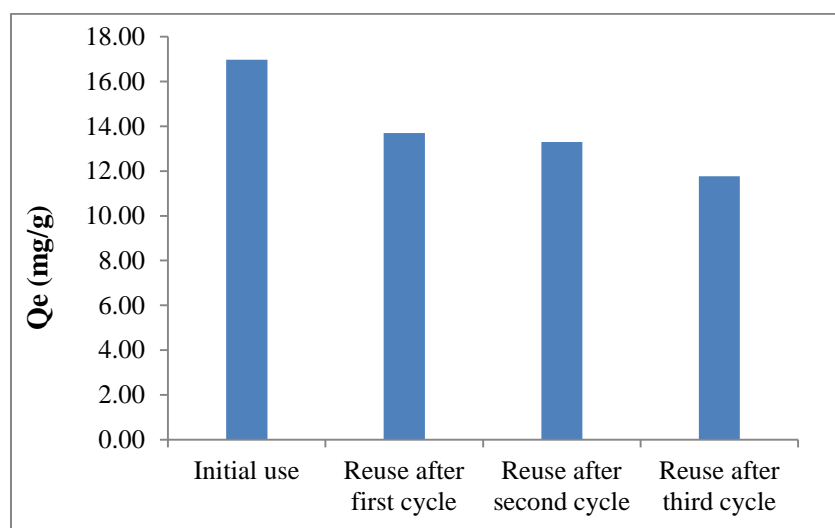


**Figure 3. 27.** Results of reuse studies for EE2 adsorption by PhHL

Desorption and reuse studies indicate that the adsorption capacity of PhHL for both BPA and EE2 decreased significantly after the third cycle. However, FTIR and XPS

spectra of PhHL before and after adsorption suggest the weak interactions between PhHL and adsorbate materials (BPA and EE2), which imply that efficient BPA and EE2 desorption is possible. Therefore, it is expected that if the desorption conditions are improved (e.g. by optimizing ethanol/water mixture volumetric ratio or sonication time), the adsorbed BPA and EE2 will be successfully removed from the surface, thus making most of the sorption sites readily available for adsorption again. Such an effort will be considered in future studies.



## 4. CONCLUSIONS

In this study, adsorptive removal of two common EDCs, BPA and EE2 from aqueous solutions was investigated by using different adsorbents. For this purpose, pure MNP (magnetite), PhHL-MNP composite, chitosan-MNP composite, PhHL and chitosan were used.

The characterization studies including SEM, FTIR and XRD analyses demonstrated that MNP, PhHL, PhHL-MNP composite and chitosan-MNP composite were successfully produced. Moreover, the surface functional groups of the adsorbent materials were assessed by FTIR analyses.

The adsorbent materials were used in the batch adsorption studies. The maximum amounts of BPA adsorbed per unit weight of adsorbents were 21.34, 34.69, 25.02, 104.8 and 43.67 mg/g for pure MNP, PhHL-MNP composite, chitosan-MNP composite, PhHL and chitosan, respectively. The maximum amounts of EE2 adsorbed per unit weight of adsorbents were 5.41, 7.32, 6.01, 16.98 and 8.89 mg/g for pure MNP, PhHL-MNP composite, chitosan-MNP composite, PhHL and chitosan, respectively. As a result, it can be concluded that PhHL has shown the maximum adsorption capacity for both BPA and EE2.

Since PhHL had the highest adsorption capacity for BPA and EE2, its adsorption properties were further investigated. According to the isotherm studies, the maximum adsorption capacity of PhHL was determined by Sips model as 126.6 and 18.13 mg/g for BPA and EE2, respectively. The adsorption capacity of PhHL for EE2 was higher than that for BPA when the comparison was made with respect to the initial adsorbate concentration of 9.2 mg/L (the solubility limit of EE2). The possible reasons of the difference in the adsorption capacities for BPA and EE2 were explained by their molecular properties.

According to the kinetic studies, the adsorption of BPA and EE2 by PhHL followed pseudo-second order kinetics. The second order rate constants were 0.020 and 0.034 g/(mg·min) and the equilibrium times were 360 and 120 min for BPA and EE2, respectively.

The mechanism of adsorption was evaluated by FTIR and XPS studies. For this

purpose, FTIR and XPS analyses of PhHL before adsorption, PhHL after adsorption, pure BPA and pure EE2 were conducted. Based on the results of FTIR and XPS analyses, OH-pi and CH-pi interactions were found to be effective in the adsorption mechanism of BPA and EE2 by PhHL.

Reuse studies demonstrated that the adsorption capacity of PhHL was reduced after the third cycle by 28.6 and 30.7 % for BPA and EE2, respectively.

The obtained results show that EDCs like BPA and EE2 can be effectively removed from aqueous solution by adsorption. Especially, PhHL is a promising adsorbent for the removal of BPA and EE2, with a high adsorption capacity. Moreover, it can be suggested that PhHL can be applied for the adsorptive removal of other EDCs with similar chemical properties to BPA and EE2.

### **Recommendations for future work**

The following research areas can be recommended for further work:

- Conducting the adsorption experiments using real water and wastewater samples which requires the development of a new measurement technique by GC-MS, including pre-concentration and purification steps (i.e. solid phase extraction) followed by derivatization.
- Studying the competitive adsorption of different EDC molecules and determining the influence of various coexisting solutes on the adsorption of EDC molecules.
- Enhancing the reuse potential by the optimizing desorption and reuse conditions.
- Treating the backwash water resulting from desorption and reuse studies.
- Scale up of the adsorption process by using continuous fixed-bed column adsorption and evaluation of the economic feasibility.
- Evaluating the combined application of the adsorption and advanced oxidation processes for the complete destruction of EDCs.
- Synthesizing novel adsorbent materials, which contain different functional groups to improve OH-pi and CH-pi interactions for enhanced adsorption properties.



## REFERENCES

- Abdullah, M.F., Shaw, R., Mukherjee, A., 2016. Paramagnetic Iron Oxide Nanoparticles in Guar-ester for Bisphenol A Removal in Water Environment. *Nanospectrum A Curr. Scenar.* 1, 89.
- Agency, U.S.E.P., 1997. Special report on environmental endocrine disruption: An effects assessment and analysis. Rep. No. EPA/630/R-96/012.
- Aharoni, C., Sparks, D.L., 1991. Kinetics of soil chemical reactions—a theoretical treatment. *Rates soil Chem. Process.* 1–18.
- Aharoni, C., Tompkins, F.C., 1970. Kinetics of adsorption and desorption and the Elovich equation. *Adv. Catal.* 21, 1–49.
- Ahn, Y., Choi, E.J., Kim, E.H., 2003. Superparamagnetic relaxation in cobalt ferrite nanoparticles synthesized from hydroxide carbonate precursors. *Rev. Adv. Mater. Sci.* 5, 477–480.
- Alexander, H.C., Dill, D.C., Smith, L.W., Guiney, P.D., Dorn, P., 1988. Bisphenol A: acute aquatic toxicity. *Environ. Toxicol. Chem.* 7, 19–26.
- Alsbaiee, A., Smith, B.J., Xiao, L., Ling, Y., Helbling, D.E., Dichtel, W.R., 2016. Rapid removal of organic micropollutants from water by a porous  $\beta$ -cyclodextrin polymer. *Nature* 529, 190.
- Anslyn, E. V, Dougherty, D.A., 2006. *Modern physical organic chemistry.* University science books.
- Arampatzidou, A.C., Deliyanni, E.A., 2016. Comparison of activation media and pyrolysis temperature for activated carbons development by pyrolysis of potato peels for effective adsorption of endocrine disruptor bisphenol-A. *J. Colloid Interface Sci.* 466, 101–112.
- Aris, A.Z., Shamsuddin, A.S., Praveena, S.M., 2014. Occurrence of 17 $\alpha$ -ethynylestradiol (EE2) in the environment and effect on exposed biota: a review. *Environ. Int.* 69, 104–119.
- Asad, S.S., 2018. Cytotoxic effect of iron nanoparticles in vitro on some cell lines. *Iraqi J. Cancer Med. Genet.* 10.
- Avsar, G., Agirbasli, D., Agirbasli, M.A., Gunduz, O., Oner, E.T., 2018. Levan based fibrous scaffolds electrospun via co-axial and single-needle techniques for tissue engineering applications. *Carbohydr. Polym.* 193, 316–325.
- Ballesteros-Gomez, A., Ruiz, F.-J., Rubio, S., Perez-Bendito, D., 2007. Determination of bisphenols A and F and their diglycidyl ethers in wastewater and river water by coacervative extraction and liquid chromatography–fluorimetry. *Anal. Chim. Acta* 603, 51–59.
- Barone, J.R., Medynets, M., 2007. Thermally processed levan polymers. *Carbohydr. Polym.* 69, 554–561.
- Baronti, C., Curini, R., D’Ascenzo, G., Di Corcia, A., Gentili, A., Samperi, R., 2000. Monitoring natural and synthetic estrogens at activated sludge sewage treatment plants and in a receiving river water. *Environ. Sci. Technol.* 34, 5059–5066.

- Belfroid, A., van Velzen, M., van der Horst, B., Vethaak, D., 2002. Occurrence of bisphenol A in surface water and uptake in fish: evaluation of field measurements. *Chemosphere* 49, 97–103.
- Bergman, Å., Heindel, J.J., Jobling, S., Kidd, K., Zoeller, T.R., Organization, W.H., 2013. State of the science of endocrine disrupting chemicals 2012: summary for decision-makers.
- Bergmann, C.P., Machado, F.M., 2015. Carbon nanomaterials as adsorbents for environmental and biological applications. Springer.
- Bhatnagar, A., Anastopoulos, I., 2017. Adsorptive removal of bisphenol A (BPA) from aqueous solution: a review. *Chemosphere* 168, 885–902.
- Blanchard, G., Maunay, M., Martin, G., 1984. Removal of heavy metals from waters by means of natural zeolites. *Water Res.* 18, 1501–1507.
- Bogdan, D., 2013. Removal of Bisphenol A from Water using Iron Oxide Adsorbents.
- Boyer, C., Whittaker, M.R., Bulmus, V., Liu, J., Davis, T.P., 2010. The design and utility of polymer-stabilized iron-oxide nanoparticles for nanomedicine applications. *NPG Asia Mater.* 2, 23.
- Bui, X.T., Vo, T.P.T., Ngo, H.H., Guo, W.S., Nguyen, T.T., 2016. Multicriteria assessment of advanced treatment technologies for micropollutants removal at large-scale applications. *Sci. Total Environ.* 563, 1050–1067.
- Burgos, A.E., Ribeiro-Santos, T.A., Lago, R.M., 2016. Adsorption of the harmful hormone ethinyl estradiol inside hydrophobic cavities of CTA<sup>+</sup> intercalated montmorillonite. *Water Sci. Technol.* 74, 663–671.
- Buyisch, H.J., 1999. Bisphenols (Bishydroxyaryllkanes). *Ind. Org. Chem.* 6, 3768–3774.
- Byrns, G., 2001. The fate of xenobiotic organic compounds in wastewater treatment plants. *Water Res.* 35, 2523–2533.
- Calvet, R., 1989. Adsorption of organic chemicals in soils. *Environ. Health Perspect.* 83, 145–177.
- Can, Z.S., Fırlak, M., Kerç, A., Evcimen, S., 2014. Evaluation of different wastewater treatment techniques in three WWTPs in Istanbul for the removal of selected EDCs in liquid phase. *Environ. Monit. Assess.* 186, 525–539.
- Capelluto, D.G.S., 2013. Lipid-mediated protein signaling. Springer.
- Careghini, A., Mastorgio, A.F., Saponaro, S., Sezenna, E., 2015. Bisphenol A, nonylphenols, benzophenones, and benzotriazoles in soils, groundwater, surface water, sediments, and food: a review. *Environ. Sci. Pollut. Res.* 22, 5711–5741.
- Carringer, R.D., Weber, J.B., Monaco, T.J., 1975. Adsorption-desorption of selected pesticides by organic matter and montmorillonite. *J. Agric. Food Chem.* 23, 568–572.
- Cartinella, J.L., Cath, T.Y., Flynn, M.T., Miller, G.C., Hunter, K.W., Childress, A.E., 2006. Removal of natural steroid hormones from wastewater using membrane contactor processes. *Environ. Sci. Technol.* 40, 7381–7386.
- Chang, H.-S., Choo, K.-H., Lee, B., Choi, S.-J., 2009. The methods of identification,

- analysis, and removal of endocrine disrupting compounds (EDCs) in water. *J. Hazard. Mater.* 172, 1–12.
- Chen, T.-S., Chen, T.-C., Yeh, K.-J.C., Chao, H.-R., Liaw, E.-T., Hsieh, C.-Y., Chen, K.-C., Hsieh, L.-T., Yeh, Y.-L., 2010. High estrogen concentrations in receiving river discharge from a concentrated livestock feedlot. *Sci. Total Environ.* 408, 3223–3230.
- Cheung, C.W., Porter, J.F., McKay, G., 2000. Sorption kinetics for the removal of copper and zinc from effluents using bone char. *Sep. Purif. Technol.* 19, 55–64.
- Choi, S., Dong Yoo, S., Lee, B., 2004. Toxicological Characteristics of Endocrine-Disrupting Chemicals: Developmental Toxicity, Carcinogenicity, and Mutagenicity, *Journal of toxicology and environmental health. Part B, Critical reviews.* <https://doi.org/10.1080/10937400490253229>
- Clara, M., Strenn, B., Gans, O., Martinez, E., Kreuzinger, N., Kroiss, H., 2005. Removal of selected pharmaceuticals, fragrances and endocrine disrupting compounds in a membrane bioreactor and conventional wastewater treatment plants. *Water Res.* 39, 4797–4807.
- Clara, M., Strenn, B., Saracevic, E., Kreuzinger, N., 2004. Adsorption of bisphenol-A, 17 $\beta$ -estradiol and 17 $\alpha$ -ethinylestradiol to sewage sludge. *Chemosphere* 56, 843–851.
- Cooney, D.O., 1998. Adsorption design for wastewater treatment. CRC press.
- Corchero, J.L., Villaverde, A., 2009. Biomedical applications of distally controlled magnetic nanoparticles. *Trends Biotechnol.* 27, 468–476.
- Corrales, J., Kristofco, L.A., Steele, W.B., Yates, B.S., Breed, C.S., Williams, E.S., Brooks, B.W., 2015. Global assessment of bisphenol A in the environment: review and analysis of its occurrence and bioaccumulation. *Dose-Response* 13, 1559325815598308.
- Costa, R.R., Neto, A.I., Calgeris, I., Correia, C.R., Pinho, A.C.M., Fonseca, J., Öner, E.T., Mano, J.F., 2013. Adhesive nanostructured multilayer films using a bacterial exopolysaccharide for biomedical applications. *J. Mater. Chem. B* 1, 2367–2374.
- Crini, G., Lichtfouse, E., Wilson, L.D., Morin-Crini, N., 2018. Conventional and non-conventional adsorbents for wastewater treatment. *Environ. Chem. Lett.* 1–19.
- Damstra, T., Barlow, S., Bergman, A., Kavlock, R., Van Der Kraak, G., 2002. Global assessment of the state-of-the-science of endocrine disruptors. Geneva World Heal. Organ.
- Davis, T.A., Volesky, B., Mucci, A., 2003. A review of the biochemistry of heavy metal biosorption by brown algae. *Water Res.* 37, 4311–4330.
- De Cazes, M., Abejón, R., Belleville, M.-P., Sanchez-Marcano, J., 2014. Membrane bioprocesses for pharmaceutical micropollutant removal from waters. *Membranes (Basel)*. 4, 692–729.
- De Mes, T., Zeeman, G., Lettinga, G., 2005. Occurrence and fate of estrone, 17 $\beta$ -estradiol and 17 $\alpha$ -ethinylestradiol in STPs for domestic wastewater. *Rev. Environ. Sci. bio/technology* 4, 275.
- De Rudder, J., Van de Wiele, T., Dhooge, W., Comhaire, F., Verstraete, W., 2004. Advanced water treatment with manganese oxide for the removal of 17 $\alpha$ -

- ethynylestradiol (EE2). *Water Res.* 38, 184–192.
- de Souza, Í.F.T., Petri, D.F.S., 2018.  $\beta$ -Cyclodextrin hydroxypropyl methylcellulose hydrogels for bisphenol A adsorption. *J. Mol. Liq.* 266, 640–648.
- Deblonde, T., Cossu-Leguille, C., Hartemann, P., 2011. Emerging pollutants in wastewater: a review of the literature. *Int. J. Hyg. Environ. Health* 214, 442–448.
- Dehghani, M.H., Ghadermazi, M., Bhatnagar, A., Sadighara, P., Jahed-Khaniki, G., Heibati, B., McKay, G., 2016. Adsorptive removal of endocrine disrupting bisphenol A from aqueous solution using chitosan. *J. Environ. Chem. Eng.* 4, 2647–2655.
- Delgado, L.F., Charles, P., Glucina, K., Morlay, C., 2012. The removal of endocrine disrupting compounds, pharmaceutically activated compounds and cyanobacterial toxins during drinking water preparation using activated carbon—a review. *Sci. Total Environ.* 435, 509–525.
- Dobbs, R.A., Wang, L., Govind, R., 1989. Sorption of toxic organic compounds on wastewater solids: correlation with fundamental properties. *Environ. Sci. Technol.* 23, 1092–1097.
- Dorn, P.B., Chou, C.-S., Gentempo, J.J., 1987. Degradation of bisphenol A in natural waters. *Chemosphere* 16, 1501–1507.
- Dubinin, M.M., Astakhov, V.A., 1971. Development of the concepts of volume filling of micropores in the adsorption of gases and vapors by microporous adsorbents. *Russ. Chem. Bull.* 20, 3–7.
- Elliott, D.W., Zhang, W.-X., 2001. Field assessment of nanoscale bimetallic particles for groundwater treatment. *Environ. Sci. Technol.* 35, 4922–4926.
- Erkorkmaz, B.A., Kırtel, O., Duru, Ö.A., Öner, E.T., 2018. Development of a cost-effective production process for *Halomonas levan*. *Bioprocess Biosyst. Eng.* 1–13.
- Everett, D.H., 1972. Manual of symbols and terminology for physicochemical quantities and units, appendix II: Definitions, terminology and symbols in colloid and surface chemistry. *Pure Appl. Chem.* 31, 577–638.
- FAO, A.S.C., 2000. A Reference Manual. FAO, Rome.
- Febrianto, J., Kosasih, A.N., Sunarso, J., Ju, Y.-H., Indraswati, N., Ismadji, S., 2009. Equilibrium and kinetic studies in adsorption of heavy metals using biosorbent: a summary of recent studies. *J. Hazard. Mater.* 162, 616–645.
- Fernandez, M.P., Ikononou, M.G., Buchanan, I., 2007. An assessment of estrogenic organic contaminants in Canadian wastewaters. *Sci. Total Environ.* 373, 250–269.
- Fierascu, R.C., Dinu-Pirvu, C.E., Fierascu, I., Tarmure, V., Stanica, N., Nicolae, C.-A., Somoghi, R., Trica, B., Anuta, V., 2018. Inorganic/organic core-shell magnetic materials for removal of endocrine disrupting pharmaceuticals from water. *Farmacia* 66, 316–322.
- Focazio, M.J., Kolpin, D.W., Barnes, K.K., Furlong, E.T., Meyer, M.T., Zaugg, S.D., Barber, L.B., Thurman, M.E., 2008. A national reconnaissance for pharmaceuticals and other organic wastewater contaminants in the United States—II) Untreated drinking water sources. *Sci. Total Environ.* 402, 201–216.

- Freundlich, H., 1907. Über die adsorption in lösungen. *Zeitschrift für Phys. Chemie* 57, 385–470.
- Freundlich, H., Hatfield, H.S., 1926. *Colloid and capillary chemistry*. Methuen And Co. Ltd; London.
- Fromme, H., Kuchler, T., Otto, T., Pilz, K., Müller, J., Wenzel, A., 2002. Occurrence of phthalates and bisphenol A and F in the environment. *Water Res.* 36, 1429–1438.
- Fukazawa, H., Watanabe, M., Shiraishi, F., Shiraishi, H., Shiozawa, T., Matsushita, H., Terao, Y., 2002. Formation of chlorinated derivatives of bisphenol A in waste paper recycling plants and their estrogenic activities. *J. Heal. Sci.* 48, 242–249.
- Gerstl, Z., Mingelgrin, U., 1984. Sorption of organic substances by soils and sediments. *J. Environ. Sci. Heal. Part B* 19, 297–312.
- Ghijsen, R.T., Hoogenboezem, W., 2000. Endocrine disrupting compounds in the Rhine and Meuse basin: occurrence in surface, process and drinking water.
- Ghoochian, M., Panahi, H.A., Sobhanardakani, S., Taghavi, L., Hassani, A.H., 2018. Synthesis and application of Fe<sub>3</sub>O<sub>4</sub>/SiO<sub>2</sub>/thermosensitive/PAMAM-CS nanoparticles as a novel adsorbent for removal of tamoxifen from water samples. *Microchem. J.*
- Ghosh, S., Badruddoza, A.Z.M., Hidajat, K., Uddin, M.S., 2013. Adsorptive removal of emerging contaminants from water using superparamagnetic Fe<sub>3</sub>O<sub>4</sub> nanoparticles bearing aminated  $\beta$ -cyclodextrin. *J. Environ. Chem. Eng.* 1, 122–130.
- Godby, N., Conklin, A., 2017. Comparing adsorption of bisphenol A and similar compounds in aqueous solution by syringe filters. *Adsorpt. Sci. Technol.* 35, 153–161.
- Gomes, T.D., Caridade, S.G., Sousa, M.P., Azevedo, S., Kandur, M.Y., Öner, E.T., Alves, N.M., Mano, J.F., 2018. Adhesive free-standing multilayer films containing sulfated levan for biomedical applications. *Acta Biomater.* 69, 183–195.
- Gómez, M.J., Bueno, M.J.M., Lacorte, S., Fernández-Alba, A.R., Agüera, A., 2007. Pilot survey monitoring pharmaceuticals and related compounds in a sewage treatment plant located on the Mediterranean coast. *Chemosphere* 66, 993–1002.
- Gore, A.C., Chappell, V.A., Fenton, S.E., Flaws, J.A., Nadal, A., Prins, G.S., Toppari, J., Zoeller, R.T., 2015. EDC-2: The Endocrine Society's Second Scientific Statement on Endocrine-Disrupting Chemicals. *Endocr. Rev.* 36, E1–E150.
- Gray, G.M., Cohen, J.T., Cunha, G., Hughes, C., McConnell, E.E., Rhomberg, L., Sipes, I.G., Mattison, D., 2004. Weight of the Evidence Evaluation of Low-Dose Reproductive and Developmental Effects of Bisphenol A. *Hum. Ecol. Risk Assess. An Int. J.* 10, 875–921. <https://doi.org/10.1080/10807030490513883>
- Guibal, E., 2005. Heterogeneous catalysis on chitosan-based materials: a review. *Prog. Polym. Sci.* 30, 71–109.
- Guo, L., Liang, Y., Chen, X., Xu, W., Wu, K., Wei, H., Xiong, Y., 2016. Effective Removal of Tetracycline from Aqueous Solution by Organic Acid-Coated Magnetic Nanoparticles. *J. Nanosci. Nanotechnol.* 16, 2218–2226.
- Gupta, V.K., Agarwal, S., Sadegh, H., Ali, G.A.M., Bharti, A.K., Makhlof, A.S.H., 2017. Facile route synthesis of novel graphene oxide- $\beta$ -cyclodextrin nanocomposite and its application as adsorbent for removal of toxic bisphenol A from the aqueous phase. *J.*

Mol. Liq. 237, 466–472.

Hai, F.I., Tessmer, K., Nguyen, L.N., Kang, J., Price, W.E., Nghiem, L.D., 2011. Removal of micropollutants by membrane bioreactor under temperature variation. *J. Memb. Sci.* 383, 144–151.

Halevy, S., Bochlin, Y., Kadosh, Y., Kaplan, A., Avraham, H., Nissim, A., Hamo, R. Ben, Ohaion-Raz, T., Korin, E., Bettelheim, A., 2017. Graphene Oxide Sheets Combine into Conductive Coatings by Direct Oxidative Electropolymerization. *Sci. Rep.* 7, 4987.

Hammes, G.G., 2000. *Thermodynamics and kinetics for the biological sciences*. Wiley-Interscience New York.

Han, J., Qiu, W., Meng, S., Gao, W., 2012. Removal of ethinylestradiol (EE2) from water via adsorption on aliphatic polyamides. *Water Res.* 46, 5715–5724.

Han, W., Luo, L., Zhang, S., 2012. Adsorption of bisphenol A on lignin: effects of solution chemistry. *Int. J. Environ. Sci. Technol.* 9, 543–548.

Han, Y.W., 1990. Microbial levan, in: *Advances in Applied Microbiology*. Elsevier, pp. 171–194.

Hansch, C., Leo, A., Hoekman, D., Livingstone, D.J., 1995. *Exploring QSAR: hydrophobic, electronic, and steric constants*. American Chemical Society Washington, DC.

Hao, Y., Wang, Z., Gou, J., Wang, Z., 2015. Kinetics and thermodynamics of diquat removal from water using magnetic graphene oxide nanocomposite. *Can. J. Chem. Eng.* 93, 1713–1720.

Ho, Y.-S., 2006. Review of second-order models for adsorption systems. *J. Hazard. Mater.* 136, 681–689.

Ho, Y.-S., McKay, G., 1999. Pseudo-second order model for sorption processes. *Process Biochem.* 34, 451–465.

Ho, Y.S., McKay, G., 1998. A comparison of chemisorption kinetic models applied to pollutant removal on various sorbents. *Process Saf. Environ. Prot.* 76, 332–340.

Ho, Y.S., Wase, D.A.J., Forster, C.F., 1996. Kinetic studies of competitive heavy metal adsorption by sphagnum moss peat. *Environ. Technol.* 17, 71–77.

Holmes, H.N., Kelvey, J.B.M., 1928. The Reversal of Traube's Rule of Adsorption. *J. Phys. Chem.* 32, 1522–1523.

Hristovski, K.D., Nguyen, H., Westerhoff, P.K., 2009. Removal of arsenate and 17 $\alpha$ -ethinyl estradiol (EE2) by iron (hydr) oxide modified activated carbon fibers. *J. Environ. Sci. Heal. Part A* 44, 354–361.

Huang, D., Tang, Z., Peng, Z., Lai, C., Zeng, G., Zhang, C., Xu, P., Cheng, M., Wan, J., Wang, R., 2017. Fabrication of water-compatible molecularly imprinted polymer based on  $\beta$ -cyclodextrin modified magnetic chitosan and its application for selective removal of bisphenol A from aqueous solution. *J. Taiwan Inst. Chem. Eng.* 77, 113–121.

Huang, W., Hu, Y., Li, Y., Zhou, Y., Niu, D., Lei, Z., Zhang, Z., 2018. Citric acid-crosslinked  $\beta$ -cyclodextrin for simultaneous removal of bisphenol A, methylene blue and copper: the roles of cavity and surface functional groups. *J. Taiwan Inst. Chem.*

Eng. 82, 189–197.

Hurwitz, A.R., Liu T, S., 1977. Determination of aqueous solubility and pKa values of estrogens. *J. Pharm. Sci.* 66, 624–627.

Hyeon, T., 2003. Chemical synthesis of magnetic nanoparticles. *Chem. Commun.* 927–934.

Ifelebuegu, A.O., Ukpebor, J.E., Obidiegwu, C.C., Kwofi, B.C., 2015. Comparative potential of black tea leaves waste to granular activated carbon in adsorption of endocrine disrupting compounds from aqueous solution. *Glob. J. Environ. Sci. Manag.* 1, 205–214.

Inglezakis, V.J., 2007. Solubility-normalized Dubinin–Astakhov adsorption isotherm for ion-exchange systems. *Microporous mesoporous Mater.* 103, 72–81.

Inoue, K., Baba, Y., Yoshizuka, K., 1993. Adsorption of metal ions on chitosan and crosslinked copper (II)-complexed chitosan. *Bull. Chem. Soc. Jpn.* 66, 2915–2921.

Janex-Habibi, M.-L., Huyard, A., Esperanza, M., Bruchet, A., 2009. Reduction of endocrine disruptor emissions in the environment: The benefit of wastewater treatment. *Water Res.* 43, 1565–1576.

Jardim, W.F., Moraes, S.G., Takiyama, M.M.K., 1997. Photocatalytic degradation of aromatic chlorinated compounds using TiO<sub>2</sub>: toxicity of intermediates. *Water Res.* 31, 1728–1732.

Jathore, N.R., Bule, M. V, Tilay, A. V, Annature, U.S., 2012. Microbial levan from *Pseudomonas fluorescens*: Characterization and medium optimization for enhanced production. *Food Sci. Biotechnol.* 21, 1045–1053.

Jerden Jr, J.L., Sinha, A.K., 2006. Geochemical coupling of uranium and phosphorous in soils overlying an unmined uranium deposit: Coles Hill, Virginia. *J. Geochemical Explor.* 91, 56–70.

Jin, Z., Wang, X., Sun, Y., Ai, Y., Wang, X., 2015. Adsorption of 4-n-nonylphenol and bisphenol-A on magnetic reduced graphene oxides: a combined experimental and theoretical studies. *Environ. Sci. Technol.* 49, 9168–9175.

Joseph, L., Heo, J., Park, Y.-G., Flora, J.R. V, Yoon, Y., 2011a. Adsorption of bisphenol A and 17 $\alpha$ -ethinyl estradiol on single walled carbon nanotubes from seawater and brackish water. *Desalination* 281, 68–74.

Joseph, L., Zaib, Q., Khan, I.A., Berge, N.D., Park, Y.-G., Saleh, N.B., Yoon, Y., 2011b. Removal of bisphenol A and 17 $\alpha$ -ethinyl estradiol from landfill leachate using single-walled carbon nanotubes. *Water Res.* 45, 4056–4068.

Joss, A., Keller, E., Alder, A.C., Göbel, A., Mc Ardell, C.S., Ternes, T., Siegrist, H., 2005. Removal of pharmaceuticals and fragrances in biological wastewater treatment. *Water Res.* 39, 3139–3152.

Jung, C., Son, A., Her, N., Zoh, K.-D., Cho, J., Yoon, Y., 2015. Removal of endocrine disrupting compounds, pharmaceuticals, and personal care products in water using carbon nanotubes: A review. *J. Ind. Eng. Chem.* 27, 1–11.

Kameda, T., Saito, M., Umetsu, Y., 2007. Uptake of bisphenol A from aqueous solution by Mg–Al-layered double hydroxides intercalated with 2-naphthalene sulfonate and 2,

6-naphthalene disulfonate. *Mater. Trans.* 48, 2225–2229.

Kanchi, S., Ahmed, S., Sabela, M.I., Hussain, C.M., 2018. *Nanomaterials: Biomedical, Environmental, and Engineering Applications*. John Wiley & Sons.

Kang, J.-H., Aasi, D., Katayama, Y., 2007. Bisphenol A in the aquatic environment and its endocrine-disruptive effects on aquatic organisms. *Crit. Rev. Toxicol.* 37, 607–625.

Karounou, E., 2004. Removal of endocrine disruptors by activated carbons and Hypersol-Macronet hypercrosslinked polymeric adsorbents.

Khamizov, R.K., Sveshnikova, D.A., Kucherova, A.E., Sinyaeva, L.A., 2018a. Kinetic Models of Batch Sorption in a Limited Volume. *Russ. J. Phys. Chem. A* 92, 1782–1789.

Khamizov, R.K., Sveshnikova, D.A., Kucherova, A.E., Sinyaeva, L.A., 2018b. Kinetic Model of Batch Sorption Processes: Comparing Calculated and Experimental Data. *Russ. J. Phys. Chem. A* 92, 2032–2038.

Khatibikamal, V., Panahi, H.A., Torabian, A., Baghdadi, M., 2019. Optimized poly (amidoamine) coated magnetic nanoparticles as adsorbent for the removal of nonylphenol from water. *Microchem. J.* 145, 508–516.

Kim, Y.-H., Lee, B., Choo, K.-H., Choi, S.-J., 2011. Selective adsorption of bisphenol A by organic–inorganic hybrid mesoporous silicas. *Microporous Mater.* 138, 184–190.

Kitamura, S., Suzuki, T., Sanoh, S., Kohta, R., Jinno, N., Sugihara, K., Yoshihara, S., Fujimoto, N., Watanabe, H., Ohta, S., 2005. Comparative study of the endocrine-disrupting activity of bisphenol A and 19 related compounds. *Toxicol. Sci.* 84, 249–259.

Kleineidam, S., Schüth, C., Grathwohl, P., 2002. Solubility-normalized combined adsorption-partitioning sorption isotherms for organic pollutants. *Environ. Sci. Technol.* 36, 4689–4697.

Kolpin, D.W., Furlong, E.T., Meyer, M.T., Thurman, E.M., Zaugg, S.D., Barber, L.B., Buxton, H.T., 2002. Pharmaceuticals, hormones, and other organic wastewater contaminants in US streams, 1999– 2000: A national reconnaissance. *Environ. Sci. Technol.* 36, 1202–1211.

Kono, H., Onishi, K., Nakamura, T., 2013. Characterization and bisphenol A adsorption capacity of  $\beta$ -cyclodextrin–carboxymethylcellulose-based hydrogels. *Carbohydr. Polym.* 98, 784–792.

Kraus, A., Jainae, K., Unob, F., Sukpirom, N., 2009. Synthesis of MPTS-modified cobalt ferrite nanoparticles and their adsorption properties in relation to Au (III). *J. Colloid Interface Sci.* 338, 359–365.

Kruithof, J.C., Kamp, P.C., Martijn, B.J., 2007. UV/H<sub>2</sub>O<sub>2</sub> treatment: a practical solution for organic contaminant control and primary disinfection. *Ozone Sci. Eng.* 29, 273–280.

Kuch, H.M., Ballschmiter, K., 2001. Determination of endocrine-disrupting phenolic compounds and estrogens in surface and drinking water by HRGC–(NCI)– MS in the picogram per liter range. *Environ. Sci. Technol.* 35, 3201–3206.

Kumar, A.K., Mohan, S.V., 2011. Endocrine disruptive synthetic estrogen (17 $\alpha$ -ethynylestradiol) removal from aqueous phase through batch and column sorption



studies: Mechanistic and kinetic analysis. *Desalination* 276, 66–74.

Kuster, M., de Alda, M.J.L., Barceló, D., 2004. Analysis and distribution of estrogens and progestogens in sewage sludge, soils and sediments. *TrAC Trends Anal. Chem.* 23, 790–798.

Lagergren, S., 1898. Zur theorie der sogenannten adsorption gelöster stoffe. *K. Sven. vetenskapsakademiens. Handl.* 24, 1–39.

LaGrega, M.D., Buckingham, P.L., Evans, J.C., 2010. Hazardous waste management. Waveland Press.

Lai, K.M., Johnson, K.L., Scrimshaw, M.D., Lester, J.N., 2000. Binding of waterborne steroid estrogens to solid phases in river and estuarine systems. *Environ. Sci. Technol.* 34, 3890–3894.

Länge, R., Hutchinson, T.H., Croudace, C.P., Siegmund, F., Schweinfurth, H., Hampe, P., Panter, G.H., Sumpter, J.P., 2001. Effects of the synthetic estrogen 17 $\alpha$ -ethinylestradiol on the life-cycle of the fathead minnow (*Pimephales promelas*). *Environ. Toxicol. Chem.* 20, 1216–1227.

Langmuir, I., 1918. The adsorption of gases on plane surfaces of glass, mica and platinum. *J. Am. Chem. Soc.* 40, 1361–1403.

Larcher, S., Delbès, G., Robaire, B., Yargeau, V., 2012. Degradation of 17 $\alpha$ -ethinylestradiol by ozonation—Identification of the by-products and assessment of their estrogenicity and toxicity. *Environ. Int.* 39, 66–72.

Lee, C.O., Howe, K.J., Thomson, B.M., 2009. State of knowledge of pharmaceutical, personal care product, and endocrine disrupting compound removal during municipal wastewater treatment. *New Mex. Environ. Dep.* 1–55.

Lee, H.-B., Peart, T.E., 2000. Determination of bisphenol A in sewage effluent and sludge by solid-phase and supercritical fluid extraction and gas chromatography/mass spectrometry. *J. AOAC Int.* 83, 290–297.

Lee, H.K., Pak, Y., 2018. Persistent Organic Pollutants, Mitochondrial Dysfunction, and Metabolic Syndrome, in: *Mitochondrial Dysfunction Caused by Drugs and Environmental Toxicants*. pp. 691–707. <https://doi.org/10.1002/9781119329725.ch44>

Lee, J.H., Kwak, S.-Y., 2018. Rapid Adsorption of Bisphenol A from Wastewater by  $\beta$ -Cyclodextrin-Functionalized Mesoporous Magnetic Clusters. *Appl. Surf. Sci.*

Li, S., Gong, Y., Yang, Y., He, C., Hu, L., Zhu, L., Sun, L., Shu, D., 2015. Recyclable CNTs/Fe<sub>3</sub>O<sub>4</sub> magnetic nanocomposites as adsorbents to remove bisphenol A from water and their regeneration. *Chem. Eng. J.* 260, 231–239.

Li, X., Zhou, M., Jia, J., Ma, J., Jia, Q., 2018. Design of a hyper-crosslinked  $\beta$ -cyclodextrin porous polymer for highly efficient removal toward bisphenol a from water. *Sep. Purif. Technol.* 195, 130–137.

Li, Y., Zhang, J., Liu, H., 2018. Removal of chloramphenicol from aqueous solution using low-cost activated carbon prepared from *Typha orientalis*. *Water* 10, 351.

Li, Z., Gondal, M.A., Yamani, Z.H., 2014. Preparation of magnetic separable CoFe<sub>2</sub>O<sub>4</sub>/PAC composite and the adsorption of bisphenol A from aqueous solution. *J. Saudi Chem. Soc.* 18, 208–213.

- Libbrecht, W., Vandaele, K., De Buysser, K., Verberckmoes, A., Thybaut, J.W., Poelman, H., De Clercq, J., Van Der Voort, P., 2015. Tuning the pore geometry of ordered mesoporous carbons for enhanced adsorption of bisphenol-A. *Materials (Basel)*. 8, 1652–1665.
- Lima, É.C., Adebayo, M.A., Machado, F.M., 2015. Kinetic and equilibrium models of adsorption, in: *Carbon Nanomaterials as Adsorbents for Environmental and Biological Applications*. Springer, pp. 33–69.
- Litter, M.I., Quici, N., Meichtry, M., 2018. *Iron Nanomaterials for Water and Soil Treatment*. CRC Press.
- Liu, G., Ma, J., Li, X., Qin, Q., 2009. Adsorption of bisphenol A from aqueous solution onto activated carbons with different modification treatments. *J. Hazard. Mater.* 164, 1275–1280.
- Liu, L., Luo, X.-B., Ding, L., Luo, S.-L., 2018. APPLICATION OF NANOTECHNOLOGY IN THE REMOVAL OF HEAVY METAL FROM WATER. *Nanomater. Remov. Pollut. Resour. Reutil.* 83.
- Liu, X., Hu, Y., Huang, J., Wei, C., 2016. Detailed characteristics of adsorption of bisphenol A by highly hydrophobic MCM-41 mesoporous molecular sieves. *Res. Chem. Intermed.* 42, 7169–7183.
- Liu, Y., Liu, Y.-J., 2008. Biosorption isotherms, kinetics and thermodynamics. *Sep. Purif. Technol.* 61, 229–242.
- Lopez, J.A., González, F., Bonilla, F.A., Zambrano, G., Gómez, M.E., 2010. Synthesis and characterization of Fe<sub>3</sub>O<sub>4</sub> magnetic nanofluid. *Rev. Latinoam. Metal. y Mater.* 30, 60–66.
- Low, M.J.D., 1960. Kinetics of chemisorption of gases on solids. *Chem. Rev.* 60, 267–312.
- Lyman, W.J., Reehl, W.F., Rosenblatt, D.H., 1990. *Handbook of chemical property estimation methods: environmental behavior of organic compounds*.
- Ma, J.C., Dougherty, D.A., 1997. The cation– $\pi$  interaction. *Chem. Rev.* 97, 1303–1324.
- Maciel, J.C., Andrad, P.L., Neri, D.F.M., Carvalho Jr, L.B., Cardoso, C.A., Calazans, G.M.T., Aguiar, J.A., Silva, M.P.C., 2012. Preparation and characterization of magnetic levan particles as matrix for trypsin immobilization. *J. Magn. Mater.* 324, 1312–1316.
- Manandhar, S., Vidhate, S., D'Souza, N., 2009. Water soluble levan polysaccharide biopolymer electrospun fibers. *Carbohydr. Polym.* 78, 794–798.
- Marwick, C., 1999. Hormonally active agents throughout the environment. *JAMA* 282, 722.
- Mauricio, R., Diniz, M., Petrovic, M., Amaral, L., Peres, I., Barcelo, D., Santana, F., 2006. A characterization of selected endocrine disruptor compounds in a Portuguese wastewater treatment plant. *Environ. Monit. Assess.* 118, 75–87.
- Miah, M., Iqbal, Z., Lai, E.P.C., 2015. Comparative Binding of Endocrine Disrupting Compounds and Pharmaceuticals with Polydopamine-and Polypyrrole-coated Magnetic

- Nanoparticles. *CLEAN–Soil, Air, Water* 43, 173–181.
- Michałowicz, J., 2014. Bisphenol A–sources, toxicity and biotransformation. *Environ. Toxicol. Pharmacol.* 37, 738–758.
- Miyagawa, S., Sato, T., Iguchi, T., 2016. Subchapter 101C. Bisphenol A. <https://doi.org/10.1016/B978-0-12-801028-0.00241-5>
- Mohammed, L., Gomaa, H.G., Ragab, D., Zhu, J., 2017. Magnetic nanoparticles for environmental and biomedical applications: A review. *Particuology* 30, 1–14.
- Monier, M., Ayad, D.M., Wei, Y., Sarhan, A.A., 2010. Preparation and characterization of magnetic chelating resin based on chitosan for adsorption of Cu (II), Co (II), and Ni (II) ions. *React. Funct. Polym.* 70, 257–266.
- Morin-Crini, N., Winterton, P., Fourmentin, S., Wilson, L.D., Fenyvesi, É., Crini, G., 2018. Water-insoluble  $\beta$ -cyclodextrin–epichlorohydrin polymers for removal of pollutants from aqueous solutions by sorption processes using batch studies: A review of inclusion mechanisms. *Prog. Polym. Sci.* 78, 1–23.
- Mousavi, S.V., Bozorgian, A., Mokhtari, N., Gabris, M.A., Nodeh, H.R., Ibrahim, W.A.W., 2019. A novel cyanopropylsilane-functionalized titanium oxide magnetic nanoparticle for the adsorption of nickel and lead ions from industrial wastewater: Equilibrium, kinetic and thermodynamic studies. *Microchem. J.* 145, 914–920.
- Nadeau, J.L., 2017. Introduction to experimental biophysics: biological methods for physical scientists. CRC Press.
- Nethaji, S., Sivasamy, A., 2017. Graphene oxide coated with porous iron oxide ribbons for 2, 4-Dichlorophenoxyacetic acid (2, 4-D) removal. *Ecotoxicol. Environ. Saf.* 138, 292–297.
- Nishio, M., 2011. The CH/ $\pi$  hydrogen bond in chemistry. Conformation, supramolecules, optical resolution and interactions involving carbohydrates. *Phys. Chem. Chem. Phys.* 13, 13873–13900.
- Nishio, M., Hirota, M., 1989. CH/ $\pi$  interaction: Implications in organic chemistry. *Tetrahedron* 45, 7201–7245.
- Nishio, M., Hirota, M., Umezawa, Y., 1998. The CH/ $\pi$  interaction: evidence, nature, and consequences. John Wiley & Sons.
- Obeid, L., El Kolli, N., Talbot, D., Welschbillig, M., Bée, A., 2015. Influence of a cationic surfactant on adsorption of p-nitrophenol by a magsorbent based on magnetic alginate beads. *J. Colloid Interface Sci.* 457, 218–224.
- Okawa, H., Ueda, K., Kida, S., 1982. Noncovalent interactions in metal complexes. 3. Stereoselectivity caused by interligand, hydrophobic CH...  $\pi$ . interaction in 1-l-menthoxy-3-benzoylacetato complexes. *Inorg. Chem.* 21, 1594–1598.
- Öner, E.T., Hernández, L., Combie, J., 2016. Review of levan polysaccharide: from a century of past experiences to future prospects. *Biotechnol. Adv.* 34, 827–844.
- Pan, B., Sun, K., Xing, B., 2010. Adsorption kinetics of 17 $\alpha$ -ethinyl estradiol and bisphenol A on carbon nanomaterials. II. Concentration-dependence. *J. Soils Sediments* 10, 845–854.

- Pankhurst, Q.A., Thanh, N.T.K., Jones, S.K., Dobson, J., 2009. Progress in applications of magnetic nanoparticles in biomedicine. *J. Phys. D. Appl. Phys.* 42, 224001.
- Park, H.-S., Koduru, J.R., Choo, K.-H., Lee, B., 2015. Activated carbons impregnated with iron oxide nanoparticles for enhanced removal of bisphenol A and natural organic matter. *J. Hazard. Mater.* 286, 315–324.
- Patel, H., Vashi, R.T., 2015. Characterization and treatment of textile wastewater. Elsevier.
- Paula Alves da Silva, A., de Oliveira, C.D., Quirino, A., Danilo Morais da Silva, F., Saraiva, R., Santos Silva-Cavalcanti, J., 2018. Endocrine Disruptors in Aquatic Environment: Effects and Consequences on the Biodiversity of Fish and Amphibian Species, *Aquatic Science and Technology*. <https://doi.org/10.5296/ast.v6i1.12565>
- Pearson, R.G., 1966. Acids and bases. *Science* (80- ). 151, 172–177.
- Perez, P., Pulgar, R., Olea-Serrano, F., Villalobos, M., Rivas, A., Metzler, M., Pedraza, V., Olea, N., 1998. The estrogenicity of bisphenol A-related diphenylalkanes with various substituents at the central carbon and the hydroxy groups. *Environ. Health Perspect.* 106, 167.
- Philip, J., Shima, P.D., Raj, B., 2008. Nanofluid with tunable thermal properties. *Appl. Phys. Lett.* 92, 43108.
- Phillips, B., Harrison, P., 1999. Overview of the endocrine disrupters issue. *Issues Environ. Sci. Technol.* 12, 1–26.
- Pickering, A.D., Sumpter, J.P., 2003. Peer Reviewed: Comprehending endocrine disruptors in aquatic environments.
- Piferrer, F., Donaldson, E.M., 1992. The comparative effectiveness of the natural and a synthetic estrogen for the direct feminization of chinook salmon (*Oncorhynchus tshawytscha*). *Aquaculture* 106, 183–193.
- Podstawczyk, D., Witek-Krowiak, A., Chojnacka, K., Sadowski, Z., 2014. Biosorption of malachite green by eggshells: mechanism identification and process optimization. *Bioresour. Technol.* 160, 161–165.
- Purdum, C.E., Hardiman, P.A., Bye, V.V.J., Eno, N.C., Tyler, C.R., Sumpter, J.P., 1994. Estrogenic effects of effluents from sewage treatment works. *Chem. Ecol.* 8, 275–285.
- Ragavan, K. V, Rastogi, N.K., 2017.  $\beta$ -Cyclodextrin capped graphene-magnetite nanocomposite for selective adsorption of Bisphenol-A. *Carbohydr. Polym.* 168, 129–137.
- Rakshit, S., Sarkar, D., Elzinga, E.J., Punamiya, P., Datta, R., 2013. Mechanisms of ciprofloxacin removal by nano-sized magnetite. *J. Hazard. Mater.* 246, 221–226.
- Ran, J., Wong, M.W., 2006. Saturated hydrocarbon– benzene complexes: theoretical study of cooperative CH/ $\pi$  interactions. *J. Phys. Chem. A* 110, 9702–9709.
- Rao, K.S.V.K., Rao, K.M., Kumar, P.V.N., Chung, I.-D., 2010. Novel chitosan-based pH sensitive micro-networks for the controlled release of 5-fluorouracil.
- Reinbold, K.A., 1979. Adsorption of energy-related organic pollutants: a literature

review. Environmental Research Laboratory, Office of Research and Development, US ....

Ribeiro-Santos, T.A., Henriques, F.F., Villarroel-Rocha, J., de Castro, M.C.M., Magalhães, W.F., Windmüller, D., Sapag, K., Lago, R.M., Araujo, M.H., 2016. Hydrophobic channels produced by micelle-structured CTAB inside MCM-41 mesopores: a unique trap for the hazardous hormone ethinyl estradiol. *Chem. Eng. J.* 283, 1203–1209.

Rivera-Utrilla, J., Ocampo-Perez, R., Sanchez-Polo, M., Lopez-Penalver, J.J., Gomez-Pacheco, C. V, 2018. Removal of Tetracyclines from Water by Adsorption/Bioadsorption and Advanced Oxidation Processes. A Short Review. *Curr. Org. Chem.* 22, 1005–1021.

Robalds, A., Naja, G.M., Klavins, M., 2016. Highlighting inconsistencies regarding metal biosorption. *J. Hazard. Mater.* 304, 553–556.

Rogers, H.R., 1996. Sources, behaviour and fate of organic contaminants during sewage treatment and in sewage sludges. *Sci. Total Environ.* 185, 3–26. [https://doi.org/https://doi.org/10.1016/0048-9697\(96\)05039-5](https://doi.org/https://doi.org/10.1016/0048-9697(96)05039-5)

Rouquerol, J., Rouquerol, F., Llewellyn, P., Maurin, G., Sing, K.S.W., 2013. Adsorption by powders and porous solids: principles, methodology and applications. Academic press.

Rovani, S., Censi, M.T., Pedrotti Jr, S.L., Lima, É.C., Cataluña, R., Fernandes, A.N., 2014. Development of a new adsorbent from agro-industrial waste and its potential use in endocrine disruptor compound removal. *J. Hazard. Mater.* 271, 311–320.

Rubin, B.S., 2011. Bisphenol A: an endocrine disruptor with widespread exposure and multiple effects. *J. Steroid Biochem. Mol. Biol.* 127, 27–34.

Ruthven, D.M., 1984. Principles of adsorption and adsorption processes. John Wiley & Sons.

Saha, B., Karounou, E., Streat, M., 2010. Removal of 17 $\beta$ -oestradiol and 17 $\alpha$ -ethinyl oestradiol from water by activated carbons and hypercrosslinked polymeric phases. *React. Funct. Polym.* 70, 531–544.

Sakai, Y., Iijima, Y., Takaishi, R., Asakawa, D., Hiraoka, K., 2009. X-ray photoelectron spectroscopy analysis of organic materials etched by charged water droplet impact. *J. Vac. Sci. Technol. A Vacuum, Surfaces, Film.* 27, 743–747.

Sam, S., Kucukasik, F., Yenigun, O., Nicolaus, B., Oner, E.T., Yukselen, M.A., 2011. Flocculating performances of exopolysaccharides produced by a halophilic bacterial strain cultivated on agro-industrial waste. *Bioresour. Technol.* 102, 1788–1794.

Scherrer, P., 1918. Estimation of the size and internal structure of colloidal particles by means of röntgen. *Nachr. Ges. Wiss. Göttingen* 2, 96–100.

Schulz, M., Fussnegger, B., Bodmeier, R., 2011. Influence of adsorbents in transdermal matrix patches on the release and the physical state of ethinyl estradiol and levonorgestrel. *Eur. J. Pharm. Biopharm.* 77, 240–248.

Schwaab, M., Steffani, E., Barbosa-Coutinho, E., Júnior, J.B.S., 2017. Critical analysis of adsorption/diffusion modelling as a function of time square root. *Chem. Eng. Sci.*

173, 179–186.

Shamim, N., Hong, L., Hidajat, K., Uddin, M.S., 2007. Thermosensitive polymer (N-isopropylacrylamide) coated nanomagnetic particles: preparation and characterization. *Colloids surfaces b biointerfaces* 55, 51–58.

Shareef, A., Angove, M.J., Wells, J.D., Johnson, B.B., 2006. Aqueous solubilities of estrone, 17 $\beta$ -estradiol, 17 $\alpha$ -ethynylestradiol, and bisphenol A. *J. Chem. Eng. Data* 51, 879–881.

Sharma, V.K., Anquandah, G.A.K., Yngard, R.A., Kim, H., Fekete, J., Bouzek, K., Ray, A.K., Golovko, D., 2009. Nonylphenol, octylphenol, and bisphenol-A in the aquatic environment: a review on occurrence, fate, and treatment. *J. Environ. Sci. Heal. Part A* 44, 423–442.

Shen, H.-Y., Chen, Z.-X., Li, Z.-H., Hu, M.-Q., Dong, X.-Y., Xia, Q.-H., 2015. Controlled synthesis of 2, 4, 6-trichlorophenol-imprinted amino-functionalized nano-Fe<sub>3</sub>O<sub>4</sub>-polymer magnetic composite for highly selective adsorption. *Colloids Surfaces A Physicochem. Eng. Asp.* 481, 439–450.

Sherlala, A.I.A., Raman, A.A.A., Bello, M.M., Asghar, A., 2018. A review of the applications of organo-functionalized magnetic graphene oxide nanocomposites for heavy metal adsorption. *Chemosphere* 193, 1004–1017.

Shibasaki, K., Fujii, A., Mikami, N., Tsuzuki, S., 2006. Magnitude of the CH/ $\pi$  interaction in the gas phase: experimental and theoretical determination of the accurate interaction energy in benzene-methane. *J. Phys. Chem. A* 110, 4397–4404.

Sims, J.L., Sims, R.C., Matthews, J.E., 1990. Approach to bioremediation of contaminated soil. *Hazard. waste Hazard. Mater.* 7, 117–149.

Şimşek, S., Ulusoy, H.İ., 2018. Synthesis of a Useful and Economic Polymeric Material for Effective Removal of Bisphenol A. *J. Polym. Environ.* 26, 1605–1612.

Sinha, A., Jana, N.R., 2013. Graphene-Based Composite with  $\gamma$ -Fe<sub>2</sub>O<sub>3</sub> Nanoparticle for the High-Performance Removal of Endocrine-Disrupting Compounds from Water. *Chem. Asian J.* 8, 786–791.

Sinha, V.R., Singla, A.K., Wadhawan, S., Kaushik, R., Kumria, R., Bansal, K., Dhawan, S., 2004. Chitosan microspheres as a potential carrier for drugs. *Int. J. Pharm.* 274, 1–33.

Sinnokrot, M.O., Valeev, E.F., Sherrill, C.D., 2002. Estimates of the ab initio limit for  $\pi$ - $\pi$  interactions: The benzene dimer. *J. Am. Chem. Soc.* 124, 10887–10893.

Sips, R., 1948. On the structure of a catalyst surface. *J. Chem. Phys.* 16, 490–495.

Snyder, S.A., Westerhoff, P., Yoon, Y., Sedlak, D.L., 2003. Pharmaceuticals, personal care products, and endocrine disruptors in water: implications for the water industry. *Environ. Eng. Sci.* 20, 449–469.

Srivastava, S., Goyal, P., 2010. Novel biomaterials: decontamination of toxic metals from wastewater. Springer Science & Business Media.

Stackelberg, P.E., Gibs, J., Furlong, E.T., Meyer, M.T., Zaugg, S.D., Lippincott, R.L., 2007. Efficiency of conventional drinking-water-treatment processes in removal of pharmaceuticals and other organic compounds. *Sci. Total Environ.* 377, 255–272.

- Staples, C.A., Dome, P.B., Klecka, G.M., Oblock, S.T., Harris, L.R., 1998. A review of the environmental fate, effects, and exposures of bisphenol A. *Chemosphere* 36, 2149–2173.
- Steinmetz, R., Brown, N.G., Allen, D.L., Bigsby, R.M., Ben-Jonathan, N., 1997. The environmental estrogen bisphenol A stimulates prolactin release in vitro and in vivo. *Endocrinology* 138, 1780–1786.
- Street, M., Angelini, S., Bernasconi, S., Burgio, E., Cassio, A., Catellani, C., Cirillo, F., Deodati, A., Fabbri, E., Fanos, V., 2018. Current knowledge on endocrine disrupting chemicals (EDCs) from animal biology to humans, from pregnancy to adulthood: highlights from a national italian meeting. *Int. J. Mol. Sci.* 19, 1647.
- Su, C., 2017. Environmental implications and applications of engineered nanoscale magnetite and its hybrid nanocomposites: A review of recent literature. *J. Hazard. Mater.* 322, 48–84.
- Sun, W., Zhang, C., Xu, N., Ni, J., 2015. Effect of inorganic nanoparticles on 17 $\beta$ -estradiol and 17 $\alpha$ -ethynylestradiol adsorption by multi-walled carbon nanotubes. *Environ. Pollut.* 205, 111–120.
- Tamres, M., 1952. Aromatic compounds as donor molecules in hydrogen bonding1. *J. Am. Chem. Soc.* 74, 3375–3378.
- Taylor, H.A., Thon, N., 1952. Kinetics of Chemisorption1. *J. Am. Chem. Soc.* 74, 4169–4173.
- Ternes, T.A., Andersen, H., Gilberg, D., Bonerz, M., 2002. Determination of estrogens in sludge and sediments by liquid extraction and GC/MS/MS. *Anal. Chem.* 74, 3498–3504.
- Ternes, T.A., Stumpf, M., Mueller, J., Haberer, K., Wilken, R.-D., Servos, M., 1999. Behavior and occurrence of estrogens in municipal sewage treatment plants—I. Investigations in Germany, Canada and Brazil. *Sci. Total Environ.* 225, 81–90.
- Thorpe, K.L., Gross-Sorokin, M., Johnson, I., Brighty, G., Tyler, C.R., 2005. An assessment of the model of concentration addition for predicting the estrogenic activity of chemical mixtures in wastewater treatment works effluents. *Environ. Health Perspect.* 114, 90–97.
- Tran, H.N., You, S.-J., Hosseini-Bandegharai, A., Chao, H.-P., 2017. Mistakes and inconsistencies regarding adsorption of contaminants from aqueous solutions: a critical review. *Water Res.* 120, 88–116.
- Traube, J., 1884. Capillaritätserscheinungen in Beziehung zur Constitution und zum Molekulargewicht. *Berichte der Dtsch. Chem. Gesellschaft* 17, 2294–2316.
- Tsuzuki, S., Fujii, A., 2008. Nature and physical origin of CH/ $\pi$  interaction: significant difference from conventional hydrogen bonds. *Phys. Chem. Chem. Phys.* 10, 2584–2594.
- Uruse, T., Miyashita, K., 2003. Factors affecting the concentration of bisphenol A in leachates from solid waste disposal sites and its fate in treatment processes. *J. Mater. cycles waste Manag.* 5, 77–82.
- Vangijzegem, T., Stanicki, D., Laurent, S., 2019. Magnetic iron oxide nanoparticles for

- drug delivery: applications and characteristics. *Expert Opin. Drug Deliv.*
- Velicu, M., Suri, R., 2009. Presence of steroid hormones and antibiotics in surface water of agricultural, suburban and mixed-use areas. *Environ. Monit. Assess.* 154, 349–359.
- Velmurugan, N., Kumar, G.G., Han, S.S., Nahm, K.S., Lee, Y.S., 2009. Synthesis and characterization of potential fungicidal silver nano-sized particles and chitosan membrane containing silver particles.
- Verma, S., Gupta, A.K., Mittal, N., 2015. GC-MS Analysis of *Bruchus pisorum* Extract to Analyze the Presence of Semichemical Components. *Int. J. Curr. Microbiol. App. Sci* 4, 474–478.
- vom Saal, F.S., Hughes, C., 2005. An extensive new literature concerning low-dose effects of bisphenol A shows the need for a new risk assessment. *Environ. Health Perspect.* 113, 926–933. <https://doi.org/10.1289/ehp.7713>
- Wang, H., Linford, M.R., 2015. X-ray Photoelectron Spectroscopy and Auger Electron Spectroscopy: Comparison and Basic Principles. *Vac. Technol. Coat.*
- Wang, M., Liu, P., Wang, Y., Zhou, D., Ma, C., Zhang, D., Zhan, J., 2015. Core-shell superparamagnetic Fe<sub>3</sub>O<sub>4</sub>@ β-CD composites for host-guest adsorption of polychlorinated biphenyls (PCBs). *J. Colloid Interface Sci.* 447, 1–7.
- Weber, W.J., Morris, J.C., 1963. Kinetics of adsorption on carbon from solution. *J. Sanit. Eng. Div.* 89, 31–60.
- Weber, W.J., Smith, E.H., 1987. Simulation and design models for adsorption processes. *Environ. Sci. Technol.* 21, 1040–1050.
- Wilson, L.D., Mohamed, M.H., McMartin, D.W., 2016. The Role of Inclusion Binding Contributions for β-Cyclodextrin Polymers Cross-Linked with Divinyl Sulfone?—A Comment on Morales-Sanfrutos et al. Entitled “Divinyl Sulfone Cross-Linked Cyclodextrin-Based Polymeric Materials: Synthesis and Applications as S. Molecules 21, 93.
- Wise, A., O’Brien, K., Woodruff, T., 2010. Are oral contraceptives a significant contributor to the estrogenicity of drinking water? *Environ. Sci. Technol.* 45, 51–60.
- Wu, F.-C., Tseng, R.-L., Juang, R.-S., 2001. Enhanced abilities of highly swollen bellen chitosads for color removal and tyrosinase immobilization. *J. Hazard. Mater.* 81, 167–177.
- Wu, W., Wu, Z., Yu, T., Jiang, C., Kim, W.-S., 2015. Recent progress on magnetic iron oxide nanoparticles: synthesis, surface functional strategies and biomedical applications. *Sci. Technol. Adv. Mater.* 16, 23501. <https://doi.org/10.1088/1468-6996/16/2/023501>
- Xu, J., Wang, L., Zhu, Y., 2012. Decontamination of bisphenol A from aqueous solution by graphene adsorption. *Langmuir* 28, 8418–8425.
- Yadav, M., Rhee, K.Y., Park, S.J., Hui, D., 2014. Mechanical properties of Fe<sub>3</sub>O<sub>4</sub>/GO/chitosan composites. *Compos. Part B Eng.* 66, 89–96.
- Ying, G.-G., Kookana, R.S., Dillon, P., 2003. Sorption and degradation of selected five endocrine disrupting chemicals in aquifer material. *Water Res.* 37, 3785–3791.
- Ying, G.-G., Kookana, R.S., Ru, Y.-J., 2002. Occurrence and fate of hormone steroids



in the environment. *Environ. Int.* 28, 545–551.

Ying, G., Kookana, R., Waite, T.D., 2004. Endocrine disrupting chemicals (EDCs) and pharmaceuticals and personal care products (PPCPs) in reclaimed water in Australia.

Yoon, S.U., Mahanty, B., Kim, C.G., 2016. Preparation of superparamagnetic iron oxide nanoparticles and evaluation of their adsorption capacity toward carbamazepine and diatrizoate. *Desalin. Water Treat.* 57, 7789–7800.

Yu, X., Li, L., Zhang, J., Shen, Z., Zhu, C., Wang, P., Jiang, X., 2016. Structural analysis of macromolecular levan produced by *Bacillus megaterium* GJT321 based on enzymatic method. *Int. J. Biol. Macromol.* 93, 1080–1089.

Yu, Z., Xiao, B., Huang, W., Peng, P., 2004. Sorption of steroid estrogens to soils and sediments. *Environ. Toxicol. Chem. An Int. J.* 23, 531–539.

Zhang, B., Li, Y., Wu, T., Sun, D., Chen, W., Zhou, X., 2018. Magnetic iron oxide/graphene oxide nanocomposites: Formation and interaction mechanism for efficient removal of methylene blue and p-tert-butylphenol from aqueous solution. *Mater. Chem. Phys.* 205, 240–252.

Zhang, G., Niu, A., Peng, S., Jiang, M., Tu, Y., Li, M., Wu, C., 2001. Formation of novel polymeric nanoparticles. *Acc. Chem. Res.* 34, 249–256.

Zhou, L., Ji, L., Ma, P.-C., Shao, Y., Zhang, H., Gao, W., Li, Y., 2014. Development of carbon nanotubes/CoFe<sub>2</sub>O<sub>4</sub> magnetic hybrid material for removal of tetrabromobisphenol A and Pb (II). *J. Hazard. Mater.* 265, 104–114.

Zhou, M., Wu, Y., Qiao, J., Zhang, J., McDonald, A., Li, G., Li, F., 2013. The removal of bisphenol A from aqueous solutions by MIL-53 (Al) and mesostructured MIL-53 (Al). *J. Colloid Interface Sci.* 405, 157–163.

Zhou, Y., Hu, Y., Huang, W., Cheng, G., Cui, C., Lu, J., 2018. A novel amphoteric  $\beta$ -cyclodextrin-based adsorbent for simultaneous removal of cationic/anionic dyes and bisphenol A. *Chem. Eng. J.* 341, 47–57.

Zogorski, J.S., Faust, S.D., Haas Jr, J.H., 1976. The kinetics of adsorption of phenols by granular activated carbon. *J. Colloid Interface Sci.* 55, 329–341.

## APPENDIX A. Comparison of FTIR results for PhHL and pure levan

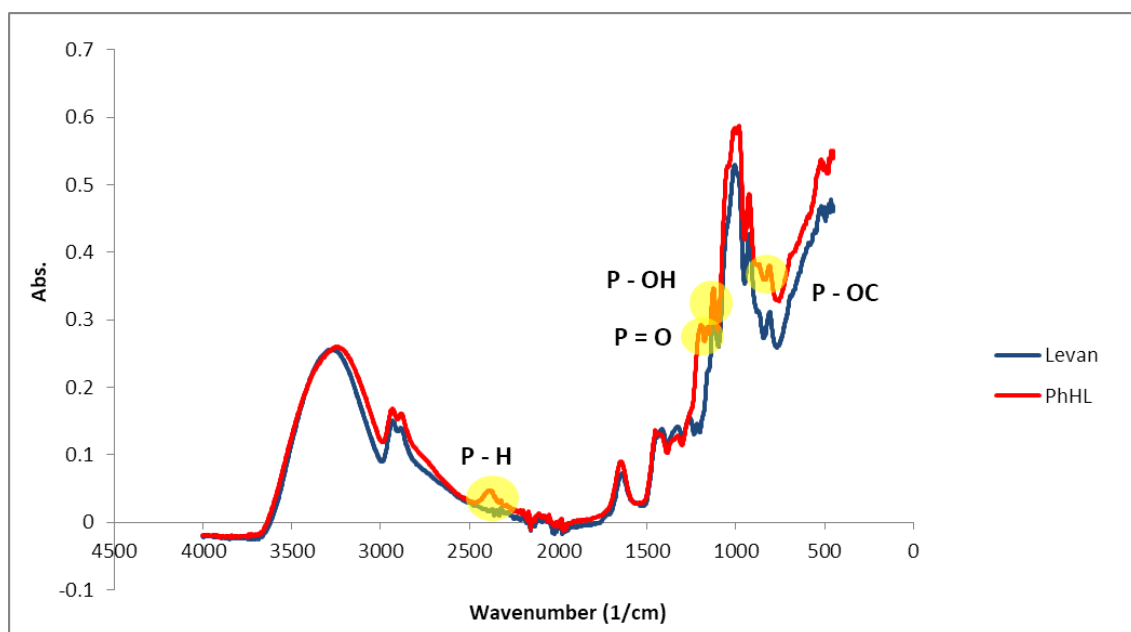


**Figure A.1.** Comparison of FTIR results for PhHL and pure levan

## APPENDIX B. XPS spectra of P2p

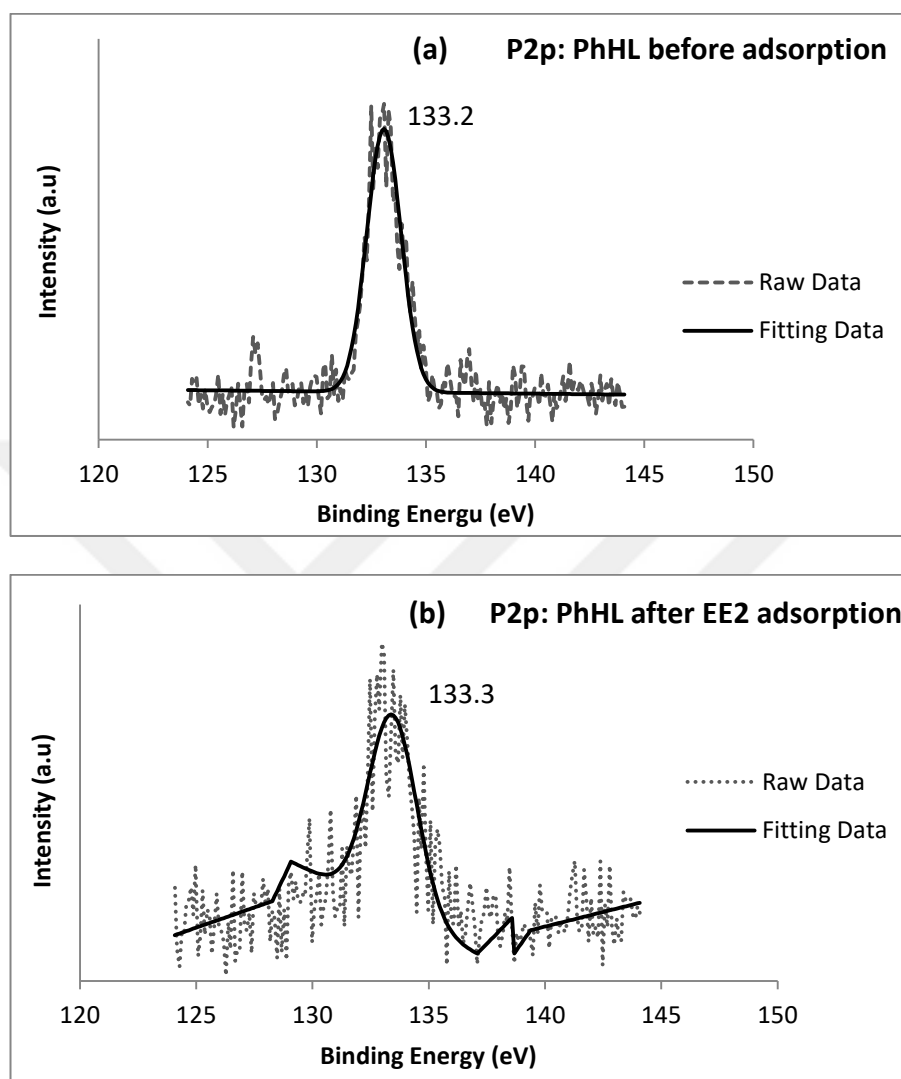


**Figure B.1.** XPS spectra of P2p for (a) PhHL before adsorption  
(b) PhHL after EE2 adsorption

## ÖZGEÇMİŞ

### **Gül Gülenay Haciosmanoğlu**

Marmara Üniversitesi, Mühendislik Fakültesi,

Çevre Mühendisliği Bölümü, MB552

Göztepe 34722, İstanbul

Telefon : +90 216 348 02 92 (1266)

Faks : +90 216 348 13 69

E-posta: [gulenay.haciosmanoglu@marmara.edu.tr](mailto:gulenay.haciosmanoglu@marmara.edu.tr)

### **Eğitim**

Doktora : Çevre Teknolojisi, Marmara Üniversitesi, 2019.

Yüksek Lisans : Çevre Teknolojisi, Boğaziçi Üniversitesi, 2010.

Lisans : Çevre Mühendisliği, Marmara Üniversitesi, 2017.

Lisans : Gıda Mühendisliği, Orta Doğu Teknik Üniversitesi, 2004

### **Mesleki Deneyim**

2012 - : Araştırma Görevlisi

Çevre Mühendisliği Bölümü, Marmara Üniversitesi

2011 - 2012 : Araştırma Görevlisi,

Çevre Mühendisliği Bölümü, Konya Üniversitesi

2004 - 2011 : Mühendis

Gıda, Tarım ve Hayvancılık Bakanlığı

### **Tezler**

#### **Doktora Tezi**

G. Gülenay Haciosmanoğlu “Adsorption of Endocrine Disrupting Compounds by Magnetic Nanoparticles” Doktora Tezi, Marmara Üniversitesi, Fen Bilimleri Enstitüsü, Çevre Teknolojisi Anabilim Dalı, 2019. Danışman: Prof. Dr. Zehra Semra Can.

## Yüksek Lisans Tezi

G. Gülenay Hacıosmanoğlu “Pretreatment of Wastewater Sludge by Pulsed Electric Field Application at Different pH Conditions” Yüksek Lisans Tezi, Boğaziçi Üniversitesi, Çevre Bilimleri Enstitüsü, Çevre Teknolojisi Anabilim Dalı, 2010. Danışman: Prof. Dr. Ayşen Erdinçler.

## Projeler

Farklı Biyosorbentler ile Sucul Ortamlardan Bisfenol A Giderimi, Marmara Üniversitesi BAP Projesi, FEN-B-120418-0163 (Araştırmacı) Nisan 2018- Nisan 2020.

Manyetik Nanoparçacıklar Kullanılarak Endokrin Bozucu Maddelerin Adsorpsiyon Yoluyla Giderilmesi, Marmara Üniversitesi BAP Projesi, FEN-C-DRP-110117-0022 (Araştırmacı) Ocak 2017- Ocak 2019.

Sıfır Değerlikli Demir Nanoparçacık (nZVI) ve nZVI/Fullerene Nanokompoziti ile Nonilfenol ve Oktilfenol Gideriminin Araştırılması, TÜBİTAK, 114Y431 (Bursiyer) Aralık 2014-Aralık 2016.

Üniversitelerin Sürdürülebilir Geleceğinin İnşası için PESTLE Analizi, Marmara Üniversitesi BAPKO Projesi, SOS-B-100615-0290 (Araştırmacı) Haziran 2015- Haziran 2016.

Levan Biyopolimeri ile Kaplanmış Manyetik Nanoparçacık Sentezlenmesi ve Cu(II) Adsorpsiyon Özelliklerinin İncelenmesi, Marmara Üniversitesi, BAP Projesi, Proje No: FEN-A-100713-0321 (Araştırmacı) Temmuz 2013- Temmuz 2016.

Pretreatment of Wastewater Sludge by Pulsed Electric Field Application at Different pH Conditions, Boğaziçi Üniversitesi, BAP Projesi, Proje No:07Y102, (Araştırmacı) Mart 2007- Mart 2010.

## Yayınlar

### Hakemli Dergiler/Uluslararası

Hacıosmanoğlu, G. G., Doğruel, T., Genc, S., Toksoy-Oner, E., Can, Z. S. 2019. Adsorptive Removal of Bisphenol A from Aqueous Solutions Using Phosphonated Levan. *Journal of Hazardous Materials* (in press).

Tohme, S., Haciosmanođlu, G. G., Erođlu, M. S., Kasavi, C., Gen, S., Can, Z. S., Toksoy-Oner, E. 2018. Halomonas smyrnensis as a cell factory for co-production of PHB and levan. *International Journal of Biological Macromolecules*. 118, 1238-1246.

Yassin, O., Can, Z. S., Haciosmanoglu, G. G., Toksoy-Oner, E., Genc, S. 2018. Copper Removal From Ammoniacal Spent Etchant by Using Magnetic Nanoparticles. *Environmental Research and Technology*, 1 (1), 38-42.

### **Hakemli Konferans ve Sempozyum Bildirileri/Uluslararası**

Haciosmanođlu, G. G., Yücesoy-Özkan, Z., Can, Z. S., Gen, S., Soyer, E., Pehlivanoglu-Mantas, E., Erdim, E. 2018. Removal of nonylphenol and octylphenol from aqueous solutions by a novel nano-composite (ZVI/Fullerene). 3<sup>rd</sup> EWaS (Efficient Water Systems) International Conference, Lefkada/Yunanistan, 27.06.2018-30.06.2018 (proceedings CD).

Haciosmanođlu, G. G., Gen, S., Can, Z. S. 2017. Use of Chitosan Coated Magnetic Nanoparticles as an Adsorbent for Bisphenol A. 13<sup>th</sup> Nanoscience and Nanotechnology Conference, Antalya, 22.10.2017-25.10.2017, (proceedings CD).

Haciosmanođlu, G. G., Yücesoy, Z., Soyer, E., Gen, S., Can, Z. S., Erdim, E. 2017. Removal of Industrial Xenoestrogens by Using Zero Valent Iron Nanoparticles. International Conference on Civil and Environmental Engineering, Nevşehir, 08.05.2017-10.05.2017, (proceedings CD).

Yassin, Ö. A., Haciosmanođlu, G. G., Gen, S., Toksoy Oner, E., Can, Z. S. 2016. Copper Removal from Ammoniacal Spent Etchant Using Magnetic Nanoparticles. EurAsia Waste Management Symposium, İstanbul, 02.05.2016-04.05.2016, (proceedings CD).

### **Araştırma Konuları**

Mikrokirlleticilerin Analizi ve Giderim Yöntemleri

Çevre Nanoteknolojisi

Adsorpsiyon ve İleri Oksidasyon Prosesleri  
Çevre Mühendisliğinde QSPR Uygulamaları

## Üyelikler

International Water Association (IWA)  
Çevre Mühendisleri Odası

## Asistanlığı Yapılan Dersler

CHEM 101 General Chemistry I  
CHEM 102 General Chemistry II  
CSE 123 Introduction to Computing  
ENVE 201 Environmental Engineering Chemistry I  
ENVE 202 Environmental Engineering Chemistry II  
ENVE 204 Engineering Hydraulics  
ENVE 205 Environmental Engineering Hydrology  
MATH 259 Numerical Methods  
ENVE 262 Basic Fluid Mechanics  
ENVE 411 Water Engineering Design  
ENVE 420 Industrial Pollution Control  
ENVE 422 Wastewater Engineering Design

## Yabancı Dil

İngilizce: 91 (Elektronik Yabancı Dil Sınavı, Ekim 2017)  
Fransızca: 85 (Kamu Personeli Dil Sınavı, Kasım 2005)